AD653769

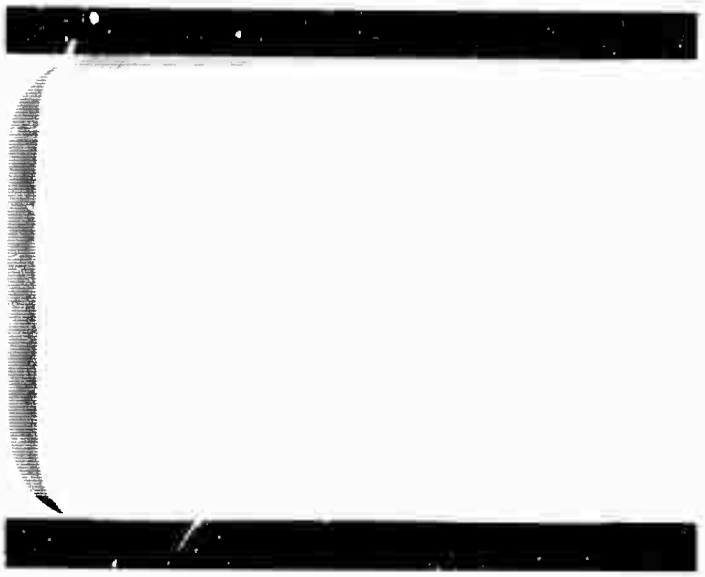

GENERAL DYNAMICS
Convair Division

DISCLAIMER NOTICE

THIS DOCUMENT IS THE BEST QUALITY AVAILABLE.

COPY FURNISHED CONTAINED A SIGNIFICANT NUMBER OF PAGES WHICH DO NOT REPRODUCE LEGIBLY.

GD/C-DRE65-023

HIGH ALTITUDE ROCKET PLUME STRUCTURE

Final Repo

Office of Naval Research

Contract No. Nonr 4747(00)

ARPA Order No. 562

September 1965

This research is part of Project DEFENDER sponsored by the Advanced Research Projects Agency, Department of Defense, and the Office of Naval Research.

GENERAL DYNAMICS
CONVAIR DIVISION

FOREWORD

This report describes research carried out under Contract No. Nonr 4747(00) during the period December 1964 to June 1965. The investigation includes a numerical analysis of the neutral gas structure of ionospheric rocket plumes including diffusive effects and a principally analytic study of the ion and electron distribution. The program for the numerical evaluation of the neutral plume structure had been under development previously under Contract AF19(628)-4360, ARPA Order No. 363 and this was continued concurrently with the present study. Although it is not really possible to isolate the two efforts, the present study has been principally concerned with the incorporation of diffusive effects and with the evaluation of the effects of the geomagnetic field on the ion distribution.

Because no description of the numerical procedure is presently available, we give, in this report, a fairly detailed description of both the inviscid and viscous calculations. Much of the work on the neutral flow structure will be reported subsequently under Contracts No. AF19(628)-3269 and AF19(628)-4360.

Personnel who have spent an appreciable fraction of their time on this study include J. R. Barthel, J. J. Brainerd, R. S. Janda, M. S. Schoonover, and J. A. L. Thomson. The Project Scientist is J. A. L. Thomson. The technical monitor is Morton Cooper, Fluid Dynamics, Office of Naval Research.

Figures II-1 to II-9 are classified Confidential and are submitted as a separate addendum to this report: GD/C-DBE65-025 (Addendum).

ABSTRACT

A calculation of the flow field in the vicinity of a liquid-fueled rocket travelling through the ionosphere is described. A finite difference program is used to obtain both inviscid and viscous approximations to the exhaust and air flow field. The subsonic nose region is treated by an approximate procedure. Viscous effects are included in the so-called merged layer regime. The viscous effects are treated by a modification of a procedure used by Cheng for the nose region of a blunt body in hypersonic, low Reynolds number flow. Numerical calculations of the neutral flow field in the viscous layer approximation are presented for the flow at 180 km.

The influence of the geomagnetic field on the motion of the ions is significant at altitudes above about 150 km. Simplified geometries are used to study the ion motion. At low altitudes (below about 150 km) the ions move with the neutrals. At high altitudes (above 250 km) the ions are more or less constrained by the geomagnetic field to a one-dimensional motion along the field lines except in a region relatively close to the missile where the density is sufficiently high to sweep the ions across the field lines. The model of the high altitude ion motion is essentially that proposed previously by Lighthill (1960). The mechanisms describing the motion of the ions across the field lines are examined in various limiting cases.

TABLE OF CONTENTS

BLANK PAGE

I. Introduction

At high altitudes the static pressure of the exhaust gases at the exit plane of a rocket engine nozzle is considerably greater than that of the ambient atmosphere. The exhaust gases therefore expand greatly upon leaving the nozzle. This expansion and the resulting interaction with the atmosphere results in the characteristic high-altitude missile "plume".

As the vehicle and plume move through the atmosphere, the ambient medium is displaced in much the same way that it would be by a solid body having the shape and dimensions of the plume. The disturbance of the external medium and particularly of the ambient electrons by the passage of the rocket, is the principal object of the investigation described here.

If viscous effects were negligible, it would be possible to describe the external flow exactly as that around a solid body having the same size and shape as the plume. However, the plume size and shape are not known a priori, and must be described by a method which treats both the internal and external flow in considerable detail. The inclusion of transport effects makes the flow near the exhaust-air boundary considerably different from the flow about a solid body, since finite tangential velocities at the boundary and diffusion across the boundary must be considered in the case of the plume at high altitudes.

The altitude range of interest in the present study is 100 to 300 KM. The following generalizations about the exhaust-ambient flow field apply in this altitude range:

1) The free stream is supersonic ($M \geq 4$), partially dissociated, and weakly ionized.

2) The flow field is time-dependent due to atmospheric stratification and vehicle acceleration.

3) The flow field may not be axially symmetric for non-vertical trajectories due to atmospheric stratification.

4) The Reynolds and Knudsen numbers lie in ranges where viscous and mixing effects are important, especially in the nose region and along the plume boundary.

5) The ion-neutral and ion-ion mean free paths are large enough that the geomagnetic field may strongly perturb the ion and electron density profiles.

6) The mean free path is large compared with missile dimensions, so that the relative disturbance of the free stream by the missile itself is small.

The approach we use to determine the neutral flow field is discussed in detail in Section IV. In general the approach is to use finite difference procedures to obtain numerical solutions of the appropriate inviscid and viscous equations of motion. Inviscid calculations of the air and jet flow are carried out first. Some features of the plume, such as the overall size and shape, appear to be quite well described by the inviscid equations. Significant viscous effects are confined more to the detailed form of the density and temperature distributions. A brief preliminary discussion of the magnitude and importance of the viscous effects is given in Section II-4.

Since the cyclotron frequencies of the ions and electrons in earth's magnetic field may be large compared to the collision frequencies, the geomagnetic field is expected to have a significant influence on the ion motion. The ionization level, however, is sufficiently low that the motion of the neutral particles is essentially unaffected by the presence of the

ions. The neutral flow field, therefore, may be evaluated without regard to the magnetic field. The ion motion may be evaluated subsequently, treating the motion of the neutral gas as known. Most of the analysis in the present study is directed towards establishing a model for the ion motion that may be used to evaluate the electron distribution in the neighborhood of the vehicle. The major uncertainty lies in the determination of the ion motion across the magnetic field lines. Inhomogeneities in the ambient ionosphere, asymmetrical ion and neutral flow distributions, the finite time dependence of the neutral flow may all enhance the rate of diffusion of ions across the field. The motion of the ions is studied in a number of limiting cases in Section V. A summary description of the ion motion is given in Section III and of the neutral motion in Section II.

BLANK PAGE

II. SUMMARY OF PRESENT METHOD USED FOR CALCULATING THE NEUTRAL FLOW

II-1. General Description

The high altitude plume may be divided into three regions: the undisturbed air and jet streams and the interaction region (see Figure II-1a. The inner boundary of the interaction region represents the greatest penetration into the plume of the influence of the external environment. This inner limit of the interaction region is the jet shock. Inside of this shock the jet flow is identical to the flow into a vacuum. In the interaction region the exhaust gas flow is separated from the perturbed air flow by a slip surface (when diffusion is negligible). The outer boundary of the interaction region is the air shock. At high altitudes, where much of the interaction region is thin compared to the overall flow field dimensions, it is convenient to think of the undisturbed jet flow and the undisturbed air flow as two equivalent regions separated by the interaction layer. These undisturbed flows may be determined independently (the jet flow by evaluating the expansion into a vacuum) and then used as boundary conditions for a calculation of the interaction region. In this approach the important characteristic dimensions during the calculation are those of the interaction region itself rather than the less appropriate (and often very different) radial dimension of the jet.

In the present calculation the interaction region is analyzed in various approximations: first, strictly inviscid flow and second, flow with viscous effects included in the so-called thin layer approximation. The supersonic portion of the inviscid flow is computed "exactly" using finite difference techniques. At low altitudes the air shock is attached to the nozzle edge (neglecting perturbing influences of the vehicle) and the air flow is entirely supersonic (described by hyperbolic equations). At sufficiently high altitudes the air shock detaches, creating a subsonic region (described by elliptic equations) at the bow of the plume. In addition to exhibiting the usual problems associated with the numerical calculation of elliptic regions this portion of the flow is difficult to define for other reasons. First, Figure II-1b indicates that, at high altitudes, the nose region will be merged (i.e., at no point in the flow is the inviscid approximation useful). Some treatments of such a region are available[1,2]

but it is not clear that sophisticated treatment is appropriate at present. Since most of the exhaust flow is directed backwards only a small mass fraction of the total exhaust flow determines the structure of the nose region. This flow may therefore be strongly influenced by the boundary layer within the nozzle and by the additional minor mass flows associated with the normal operation of a missile: vernier engine exhausts, gas generator exhausts, etc. Thus, a detailed analysis of this region that ignores these effects may not be warranted.

Because of the small mass flows involved, it is expected that this region will not have a major influence on the downstream flow. Thus, relatively crude approximate techniques provide an adequate description of the subsonic region. The procedures used for this purpose are outlined in SectionIV-2. Calculations of the inviscid flow at altitudes up to 180 km indicate that the inviscid approximations of the exhaust plumes of typical upper stage vehicles have relatively sharp noses at all altitudes. Although the turning angle of the flow at the nozzle lip increases monotonically with increasing altitude and may appreciably exceed 90° for some nozzles at very high altitudes, the jet-air boundary inclination decreases rapidly with increasing distance from the nozzle for the first several tens of nozzle diameters. For the 50:1 engine (shown in Figure II-10) at 180 km altitude, less than one per cent of the air flow intercepted by the maximum cross sectional area of the exhaust plume enters the air shock layer at points where the boundary inclination exceeds 45°. Under these conditions we expect rather small detachment distances and small subsonic regions (see Figure II-7).

Nozzle boundary layers, gas generator discharges, and vernier engine mass flows, in addition to the general merged layer effects in the subsonic region, all have a tendency to make the nose of the plume more blunt. A rough estimate of the importance of these mass flows and of the assumptions made in the calculation of the subsonic region may be obtained as follows: The peripheral mass flows typically constitute one to three per cent of the total exhaust gas mass flow. In Figure II-7, we have indicated the positions along the jet shock at which various fractions (e) of the total exhaust gas flow have been entrained by the jet shock layer. We expect that the location and structure of the shock layers in the region close to

the nose, where less than five per cent of the total flow has been entrained, will deviate appreciably from those of the actual vehicle because of the neglect of these minor mass flows. Far downstream, the shock layer structure will be less affected. In Figures II-12 and II-13 we have indicated, at the dividing streamline, the annular width (Δ_e) which contains five per cent of the exhaust mass flow. In the downstream region it is apparent that this width is small compared to the total width of the mixing region (as would be expected for a merged jet shock layer). Here, we expect that the major structure of the flow will not be strongly affected by these minor mass flows.

In Figures II-11, 12, 13, we also indicate the annular widths (Δ_a) required to contain a mass flux of air equal to that which passes through the subsonic and transonic region ($M \leq 1$). In the present numerical calculations, diffusion in this region is not accounted for. This will cause appreciable errors down to a point where the air mass flux in the mixing region considerably exceeds that passing through this nose region. Reference to these figures indicates that the effects of neglecting the diffusion in the subsonic and transonic regions will not introduce much error in the evaluation of most of the downstream flow (for this particular nozzle and at these high altitudes). In other words, even though the collision frequency and the diffusion rate in the subsonic region are sufficiently high to result in a completely merged nose shock layer, the amount of mass involved is small compared to the total amount of air mixed with exhaust gases throughout much of the flow field. When the additional peripheral mass flows are included or when smaller area ratio nozzles are considered, the plume tends to become more blunt-nosed. This will increase the size and importance of the diffusive phenomena occurring in the subsonic region. At present, we do not have any quantitative estimates of how important these effects will be for configurations markedly different from the rather specific one considered here.

II-2 Results of the Present Calculations of the Neutral Flow

In Figures II-2 to II-8 we show the results of inviscid calculations of the shock locations and the contours of constant air density* at three altitudes (100, 135, and 180 km)†. The two lower altitudes had been calculated previously and correspond to the flow resulting from the 25:1 nozzle labeled #1 in Figure II-10. The flow at 180 km altitude was evaluated for a different nozzle (labeled "50:1-Nonuniform" in Figure II-10). However, the jet mass flow angular distributions are similar for the two nozzles and little difference is expected between them. In Figure II-9, we show the shock locations and air density contours at 180 km evaluated in the viscous layer approximation. Reference to this figure shows that there is surprisingly little change in the shock locations resulting from the effects of diffusion. In Figures II-11 to II-15 we show radial distributions of density, pressure and temperature on three different orthogonal surfaces at 180 km (labeled 1, 2, and 3 in Figure II-2). In Figures II-16 and II-17, we show temperature and density histories along two streamlines (a and b in Figure II-1). A number of qualitative conclusions may be drawn from an examination of these figures:

(1) Strong transverse gradients in both pressure and density exist across the jet and air shock layers.

(2) In the inviscid approximation, the density in the jet layer is very much higher than in the air layer although the pressure is lower. There is a slight entropy layer in the air flow along the boundary but it is not marked.

(3) In the viscous layer approximation, the jet shock layer appears merged throughout the flow. The width of the mixing layer is comparable to the width of the air shock layer only near the bow of the plume.

---

*At low altitudes, the electron density distribution may be assumed proportional to the air density.

†Figures II-2 to II-9 are presented in an addendum to this report (GD/C-DBF65-023(Addendum)).

(4) The effects of diffusion have surprisingly little influence on the air density profile although the exhaust gas profile is markedly changed. This observation suggests a model of the process which imagines the jet as a cold solid body whose surface is evaporating.

(5) The cooling effect of the exhaust gases in the mixing layer largely eliminates the high temperature entropy layer.

(6) The pressure gradients at the jet and air shocks are sufficiently large that the shock profiles are not properly matched to the interior flow. A more accurate treatment would have to include the effects of shock curvature on the shock profiles.

(7) The nose of the plume is relatively sharp and the subsonic region small.

(8) The Mach disc formed by the reflection of the jet shock from the axis is small compared to the overall jet dimensions.

A preliminary attempt to evaluate the far field motion at high altitudes has been carried out in the small disturbance approximation. In this approximation only radial motions are considered important and the problem is reduced to obtaining an equivalent one-dimensional unsteady solution of the Navier-Stokes equations. The numerical calculation procedure used is similar in the type of approximations made to that used for the two-dimensional flow.* Results have been obtained for one very high altitude case (290 km for a typical sustainer mass flow) and these are shown in Figures II-18 to II-21.

---

*This case is a limiting case ($M_\infty \to \infty$) of the two-dimensional steady flow and could be calculated with that numerical program. This limit results in several simplifications in the analysis and a separate program was written.

The present results have been calculated for specific vehicles at specific altitudes. For these highly under expanded jets the results may be scaled to other altitudes, velocities and mass flows under certain conditions. The high altitude scaling laws are discussed, in part, in References 3 and 4. Three different cases may be distinguished. In order of decreasing generality they are: the near field inviscid flow when the free stream is hypersonic, the overall inviscid flow, and the flow field when viscous effects are important. All of the scaling laws depend on the fact that, at these high altitudes, the undisturbed flow is source-like ($\rho \sim f(\varphi)\, r^{-2}$) and the jet shock may be considered very strong at almost all points in the flow.

a) The inviscid near field when $M_\infty \gg 1$.

In this case the bow portion of the flow field has a characteristic dimension $\bar{R}$ given by

$$\bar{R} = \sqrt{\dot{m}\, V_J/\rho_\infty V_\infty^2}$$

where $\dot{m}$ is the rocket exhaust mass flow, V_J its limiting velocity ($V_J = \sqrt{2h_c}$ where h_c is the stagnation enthalpy per gram), and ρ_∞ and V_∞ the free stream properties. When the flow structure is evaluated in terms of the dimensionless coordinate $(r/\bar{R},\ x/\bar{R})$, the shape of the flow field is independent of altitude, velocity and mass flow and depends only on the angular distribution of the vacuum flow $\left(f(\varphi)\right)$ and the specific heat ratios of the jet and air streams. Here the jet and air densities and enthalpies may be represented in the universal forms

$$\rho_a = \rho_\infty\, f_1\left(\vec{r}/\bar{R};\ \gamma_a,\ \gamma_j,\ f(\varphi)\right)$$

$$h_a = V_\infty^2 \, f_2\left(\vec{r}/\bar{R};\ \gamma_a,\ \gamma_j,\ f(\varphi)\right)$$

$$\rho_j = \left(\frac{V_a}{V_J}\right)^2 \rho_a \, f_3\left(\vec{r}/\bar{R};\ \gamma_a,\ \gamma_j,\ f(\varphi)\right)$$

$$h_j = V_j^2 \, f_4\left(\vec{r}/\bar{R},\ \gamma_a,\ \gamma_j,\ f(\varphi)\right)$$

b) The inviscid flow for finite values of M_∞

The scaling law just discussed applies to that portion in the plume where the air shock may be considered strong. Far downstream the air shock deviates appreciably from this limit. For the flow field at 180 km nowhere in the flow is this condition adequately satisfied. In this case the flow structure also depends explicitly on the value of the free stream Mach number M_∞. It is expected that this second scaling law will be useful at most ionospheric altitudes for correlating phenomena such as size and shape that do not depend on the detailed structure of the shock layers.

c) The flow with viscous effects

When phenomena which depend on the detailed shock layer structure are to be considered, the effects of diffusion may be important. Here, in addition to the free stream Mach number M_∞, the flow structure may be scaled from one altitude to another only if the velocity ratio V_J/V_∞ and the Knudsen number $\left(\text{proportional to } \sqrt{\dot{m}\, V_J\, \rho_\infty/V_\infty^2}\right)$ are kept constant.

II-3. Method Used for Evaluating the Inviscid Flow Field in the Present Study

A finite difference approximation of the inviscid equations of motion is used to evaluate the supersonic portion of the flow field. In this numerical calculation the equations of motion are expressed in a curvilinear coordinate system composed of the streamlines and the associated orthogonal surfaces (potential surfaces in irrotational flow). Of the four differential equations of motion for two-dimensional steady inviscid flow, three may be integrated directly to give the mass, total enthalpy and entropy conservation equations. These integrated equations plus the differential form of the lateral momentum equation (which determines the streamline curvature) are used to evaluate the flow. Data are evaluated on successive orthogonal surfaces.

The streamline coordinate system was chosen for the finite difference formulation for several reasons. First, in the limiting case of very large Mach number, where characteristics programs have difficulty because the characteristics often do not intersect in a diverging flow unless the mesh spacing is very small, the streamtube procedure reduces to the condition that the streamline curvature is zero and the solution is obtained trivially. Second, by using the integrated conservation equations, it can be assured that these are rigorously satisfied no matter what mesh spacing is used. Third, because we are following fluid elements, chemical reactions or internal relaxations may be easily incorporated. Also slip lines are treated without difficulty. Fourth, because of the marching procedure used, lateral diffusion, heat and momentum transfer can be included without excessive difficulty in the thin layer approximation.

In the formulation of the finite difference procedure, an effort has been made to retain a physically meaningful interpretation even when the mesh sizes are sufficiently large that the relation between derivatives and finite differences is somewhat obscure. For this purpose a streamline or Lagrangian coordinate systems offers several advantages over an Eulerian coordinate system for the evaluation of hypersonic flow fields even though it is often more complex and less efficient in terms of computing time per mesh point. For example, in the computation of the inviscid flow, the integrated forms of the continuity, parallel momentum and energy equations are used so that these are rigorously satisfied no matter how large a step size is used. Truncation errors are limited to the lateral momentum equation:

$$\frac{\partial \varphi}{\partial s} = - \frac{1}{\rho u^2} \frac{\partial p}{\partial y} \tag{1}$$

This equation for the streamline curvature is treated as follows: Each streamtube is characterized by pressure p and a gas velocity $|u|$. These are related to the streamtube area by the integral energy, momentum and mass relations. The curvature $\left(\frac{\partial \varphi}{\partial s} \right)_{12}$ of the streamline separating the adjacent streamtubes 1 and 2 is evaluated from the relation

$$\left(\frac{\partial \varphi}{\partial s} \right)_{12} = - \frac{4\pi}{\dot{m}_1 u_1 + \dot{m}_2 u_2} \left(r_2 p_2 - r_1 p_1 \right) \tag{2}$$

where r_2 and r_1 are the radii of the midpoints of the two streamtubes measured along a surface orthogonal to the streamlines, and $\dot{m}_1$ and $\dot{m}_2$ the (constant) mass flows in these tubes. Thus reasonably accurate evaluations of the flow can be obtained even when the values of the various flow quantities

vary considerably from tube to tube. This is particularly useful in the high altitude jet shock layer, where the total pressure may vary by orders of magnitude and the density by a factor of 5 to 10 across the shock layer while the curvature and flow velocity are virtually constant. For this case Eq. (2) would give accurate results even if the entire shock layer were represented as one tube. Since the computation time is inversely proportional to the square of the tube width and appreciable computing times are involved, even on the 7090, it is important to make the mesh size as large as possible.

In the present calculations relatively simple marching procedures have been used (at present the method is essentially second order Runge-Kutta). Thus truncation errors can arise when flow variations parallel to the streamline are large. Although the procedures can be readily improved to be considerably more accurate (i.e., fourth order Runge-Kutta) the longitudinal flow variations generally encountered are usually quite small compared to the marching rate permitted by the stability of the difference scheme so that the present calculations appear to be stability limited rather than accuracy limited.

An attempt has been made to incorporate the lateral diffusion into the calculation in a manner similar to the centrifugal momentum transport. Here more difficulties are encountered. The diffusion effects are incorporated by evaluating diffusion fluxes of heat, momentum and specie at the surface of each streamtube. Truncation errors enter into relation between the fluxes and the differences of enthalpy, velocity and concentration in adjacent streamtubes. However, the calculation is arranged so that gain of

heat, momentum or specie by one tube are exactly balanced by losses in adjacent tubes. Thus, so long as the longitudinal variations of the flow quantities are small compared to the stepping rate, most of the truncation errors can be thought as being equivalent to using slightly erroneous effective diffusion coefficients.

Since the missile is accelerating and the atmosphere is not uniform the actual plume expansion is not a steady phenomenon. However, the exhaust-air velocity difference far downstream, where this time dependence is expected to have a significant effect, is smaller than the missile velocity. Thus an approximate account of this effect for a vertical trajectory may be obtained by assuming that the flow disturbance at a given altitude is the same as that for a rocket moving through a uniform atmosphere at constant velocity. Here the values of the density and missile velocity must be taken equal to those corresponding to the altitude of interest. (This is really equivalent to a small disturbance approximation far from the vehicle.)

Because of atmospheric stratification, the disturbance created by a vehicle traveling on a non-vertical trajectory will not be axially symmetric. An approximate account of this effect may be obtained if it can be assumed that the azimuthal flow velocities are negligible. In this approximation the flow distribution at a given azimuthal angle will be the same as that in an "equivalent axisymmetric flow" in which the atmospheric density variation with radial displacement is assumed to be the same as that in the real atmosphere in the given azimuthal direction. In other words, for a horizontal trajectory, the stream density and Mach number are assumed to vary

with radial displacement. For an exponential atmosphere the "equivalent axisymmetric free stream" should have a density which varies with radial displacement from the axis according to

$$\rho_\infty(r) \sim \rho_o e^{-r\cos\theta/H}$$

where θ is the azimuthal angle of interest, H the local scale height and ρ_o the local ambient atmospheric density on the plume axis. Since the finite difference formalism is the same for uniform as for nonuniform external flows this method is easily implemented.

II-4. Method Used for Evaluating the Viscous Flow Field

Probstein and Kemp [5] classify different types of viscous flows into seven regimes: boundary layer, vorticity interaction, viscous layer, incipient merged layer, fully merged layer, first order collision theory and free molecular flow regimes. In the first three regimes the shock is treated as a discontinuity obeying the classical Rankine-Hugoniot relations. In the fourth (incipient merged layer) the shock structure has to be included. Here suggested treatments are either to use the complete Navier-Stokes equations to describe both the shock profile and the viscous interior as one continuous pattern, or to treat the shock as a discontinuity and modify the Hugoniot relations so that the tangential shear stress and the enthalpy flux conducted into the shock are properly accounted for. Cheng has used this latter approach successfully to treat the hypersonic blunt body problem.[2]

In treating rarefied gas flows a very useful approximation that is often introduced is the so-called thin layer assumption. Basically the assumption says that, in the coordinate system chosen to evaluate the solution, the viscous stresses and heat conduction are determined by the velocity and enthalpy gradients in a direction known a priori, such as parallel to one of the coordinate axes. In many applications, such as the blunt body shock layer or the hypersonic slender body flow in the small disturbance approximation, this may be satisfied if the shock radius of curvature is much greater than the lateral dimensions of the flow. It is expected that this condition applies to the interaction region of the plume as long as the free stream Mach number is sufficiently high.

We have incorporated viscous effects into the numerical calculation using the thin layer approximation. Using this approach in the incipient

merged layer regime, Cheng has developed an elegant treatment of the hypersonic blunt-body problem at low densities.[2] The same sophistication of solution is presently possible for the high altitude jet. A complete evaluation of the jet flow field would proceed as follows:* first, the flow is evaluated in the inviscid approximation, where the supersonic region is treated exactly and the subsonic region approximately. Second, viscous and heat transport terms are included in the viscous layer approximation for the supersonic flow (i.e., the shocks are still treated as discontinuous and obey the classical Hugoniot relations). The third step is to treat the supersonic flow assuming it is merged. Here Cheng's two-layer approach is appropriate. This amounts to replacing the Hugoniot relations by modified forms which allow the stagnation enthalpy and the tangential velocity to vary through the shock. At the same time the shock profile itself (shock transition zone) may be treated independently in the thin layer approximation. Here the shock is assumed to be locally approximated by a plane shock whose profile may be evaluated by a direct integration of the one-dimensional Navier-Stokes equations, using the local conditions evaluated at the edge of the merged layer as initial conditions. This profile is then "tacked" on to the merged layer calculations. This is essentially the approximation in which Cheng treats the blunt-body problem. The equations are detailed in Section IV-3a,b,c.

Up to this point an approximate inviscid description of the subsonic region such as that detailed in Section IV-2c is used.

The logical fourth step in this procedure would be to use Cheng's method to evaluate the subsonic and transonic region. The only difference from Cheng's

*During the present study, calculations have been carried out only in the first two approximations.

procedure would be that instead of a solid boundary for the innermost streamline, a boundary condition would have to be used which would join the elliptic air region to the hyperbolic jet region. A merged layer calculation would be used for the flow inside this dividing streamline. Diffusion of heat, momentum and species across the dividing streamline would be allowed for. The equations and method for this step are detailed in Section IV-3d.

During the present study it was found that the centrifugal pressure gradients across both the jet and the air shock layer were large (see Fig. II-15) throughout most of the flow. Except for a small region near the nose of the plume the pressure gradient in the air shock layer at 180 km altitude is not very much smaller in absolute value than the peak gradient within the shock transition zone itself (Figs. II-11, 12 and 13). Consequently it is expected that the curvature of the shock front will have an appreciable influence on the shock profile and it will be necessary to include this effect in order to get a consistent fully merged layer calculation. A self consistent procedure has not yet been formulated for this purpose. Because the shock layer tangential shear stress and the stagnation enthalpy flux are relatively small near the shock interface, except near the nose of the plume where the deflection angles are large, it is expected that the influence of the shock curvature (really of the curvature of the streamlines behind the shock) on the shock profile will be the dominant source of differences between a viscous layer calculation and a truly merged layer calculation. Expressed in other words, the difficulty is that, in the air shock transition zone, the streamline curvature and pressure gradient are of opposite sign to those in the shock layer and a plane shock approximation results in a discontinuity in these quantities. In practice this means that

the peak pressure, density and streamline deflection calculated for a plane shock will not be achieved in the actual flow. The detailed calculations to date have been limited to the viscous layer approximation. The density contours shown in Figures II-3 to 8 in the neighborhood of the shock interface were determined by fairing the shock layer profile smoothly into a shock transition zone profile calculated assuming zero shock curvature.

For the jet shock this difficulty is less apparent since the curvatures in the transition zone and in the shock layer have the same sign. In this case, it would be consistent to locate the shock interface at the point in the shock transition profile where the streamline curvature matched the value in the shock layer. However, the viscous layer calculations carried out during this study have not included this sophistication and it has been assumed that the normal pressure and density jumps were achieved across the shock. The errors induced are expected to be relatively small, perhaps equivalent to a shift in the position of the interaction layer by an amount somewhat less than the width of the shock transition zone.

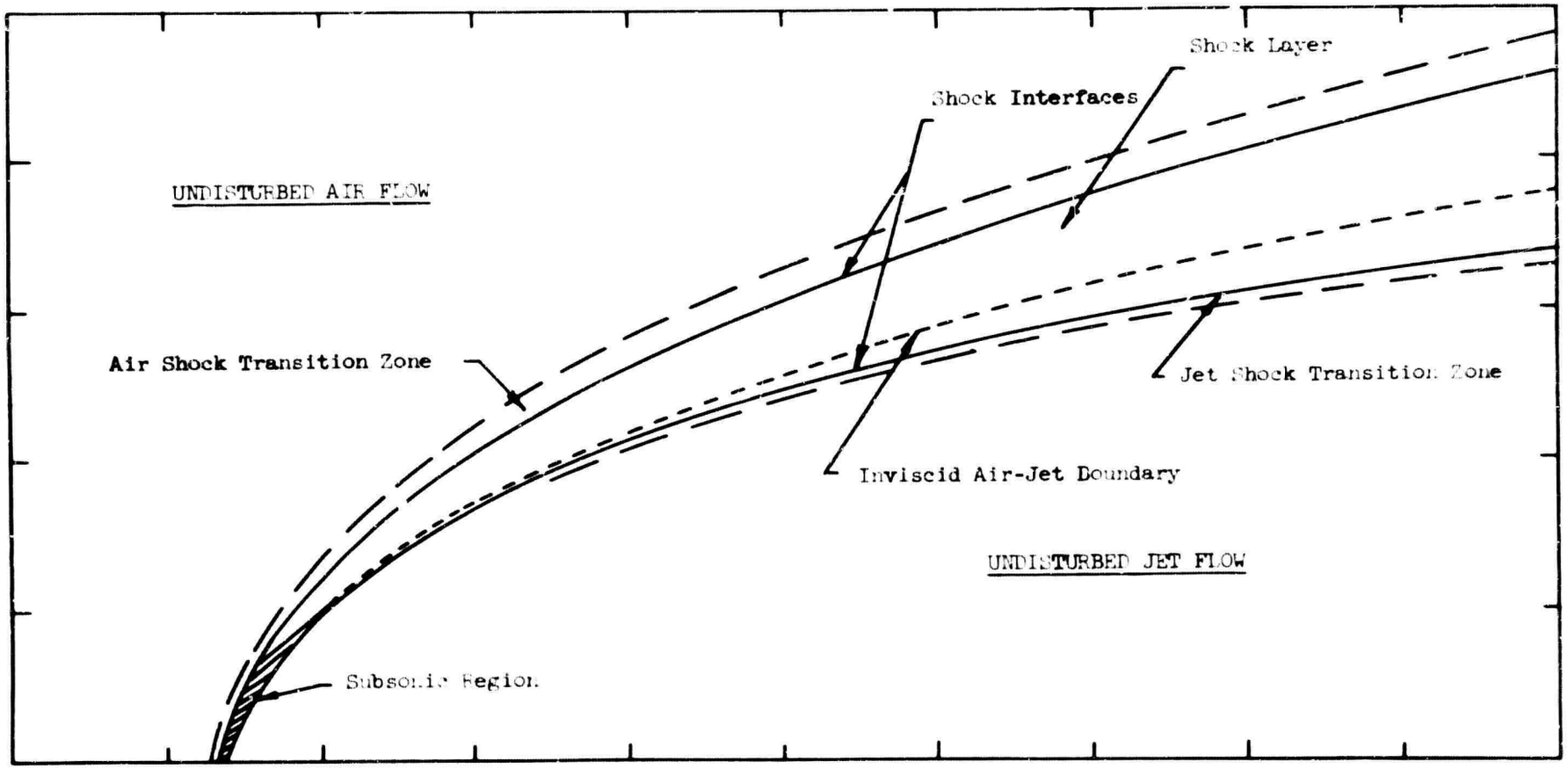

FIG. [illegible]. FLOW FIELD GEOMETRY

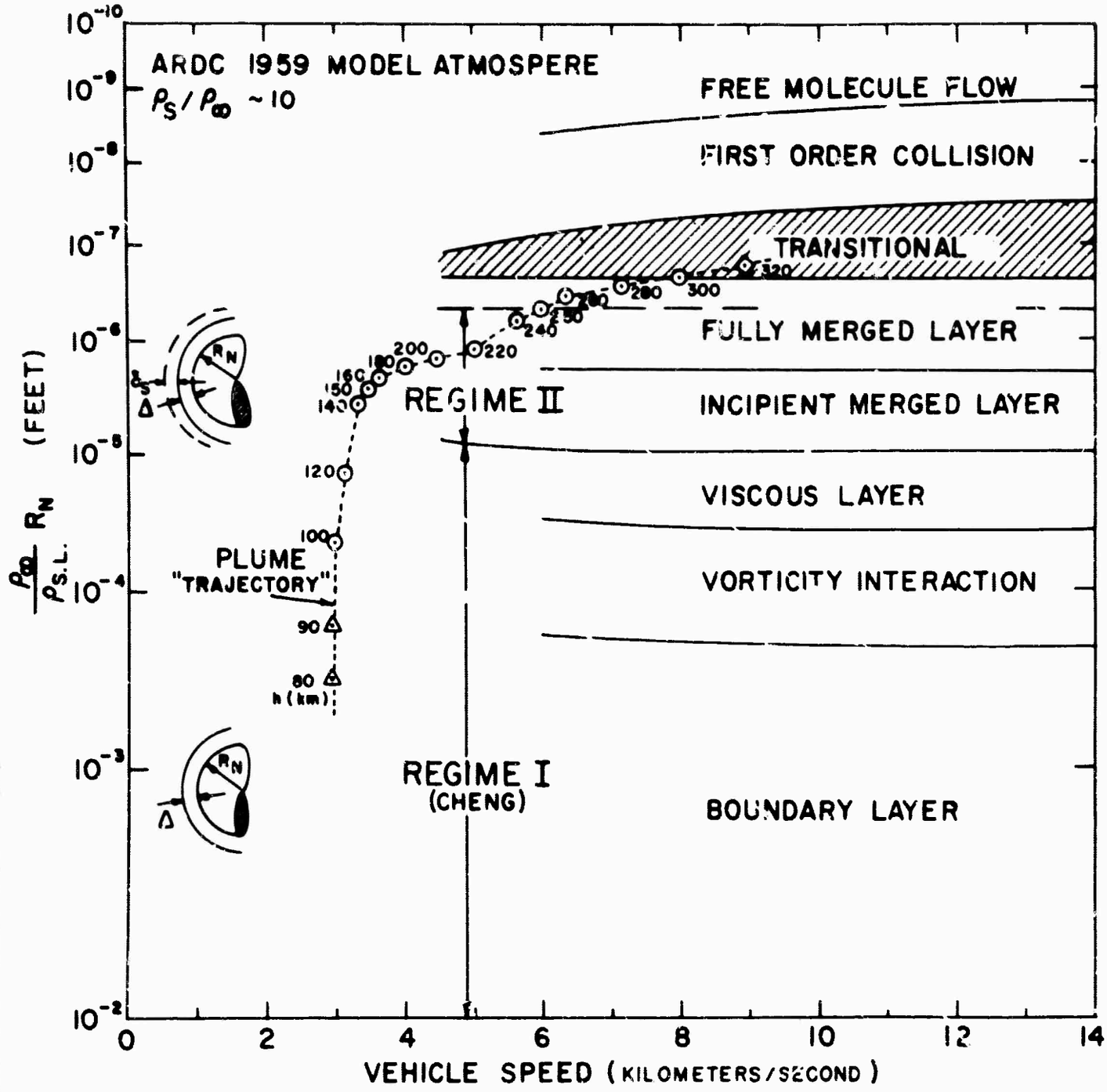

FIG. II-1b, PLUME "TRAJECTORY" IN RELATION TO THE LOW DENSITY VISCOUS REGIMES AS DEFINED BY PROBSTEIN AND BY CHENG (REF. 2).

Figures II-2 to II-9 appear in an addendum to this report - GD C-DBE65-023 (Addendum).

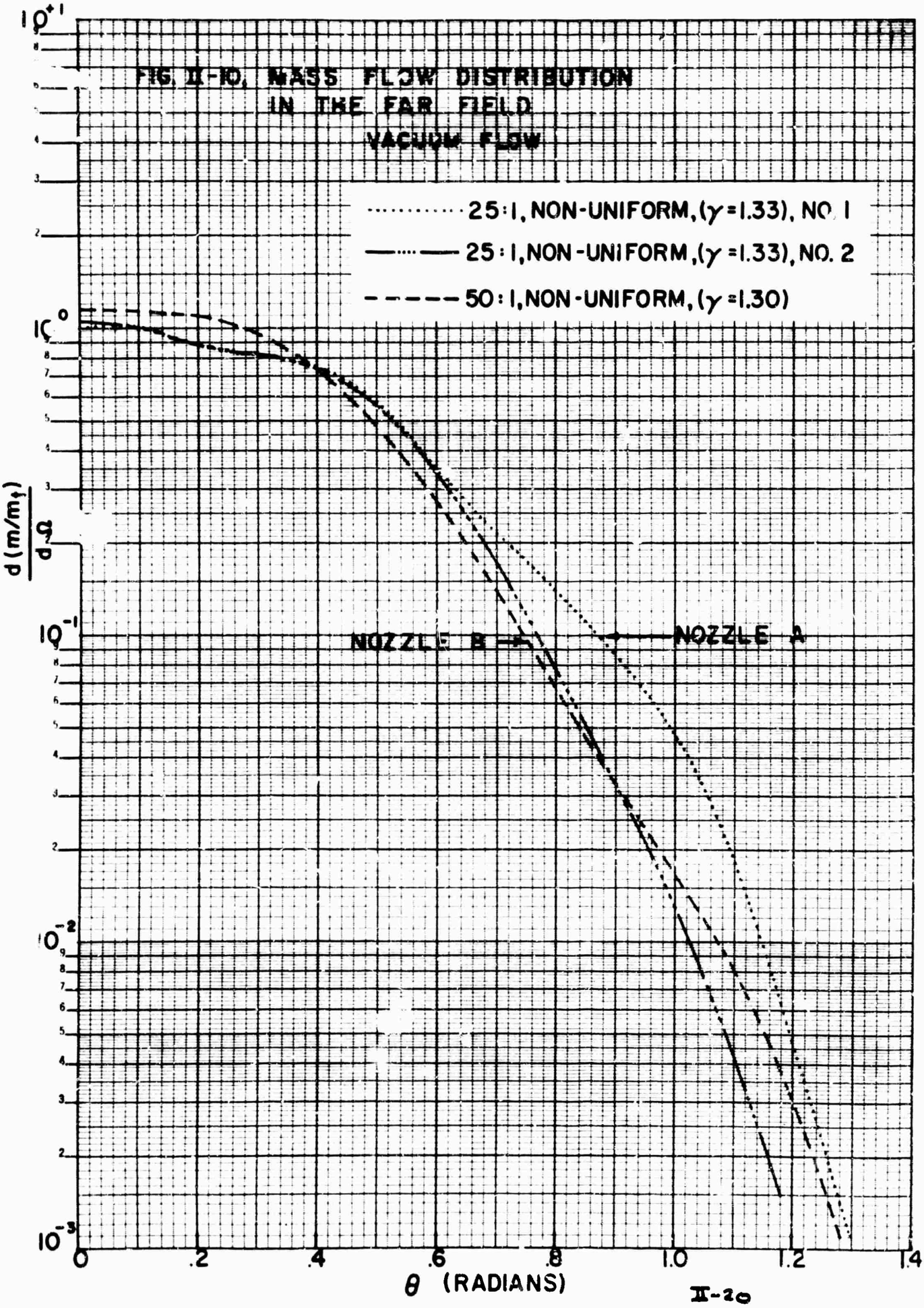
FIG. II-10, MASS FLOW DISTRIBUTION
IN THE FAR FIELD
VACUUM FLOW
25:1, NON-UNIFORM, (γ=1.33), NO. 1
25:1, NON-UNIFORM, (γ=1.33), NO. 2
50:1, NON-UNIFORM, (γ=1.30)
NOZZLE B
NOZZLE A
d(m/m†)/dΩ
θ (RADIANS)
0
.2
.4
.6
.8
1.0
1.2
1.4

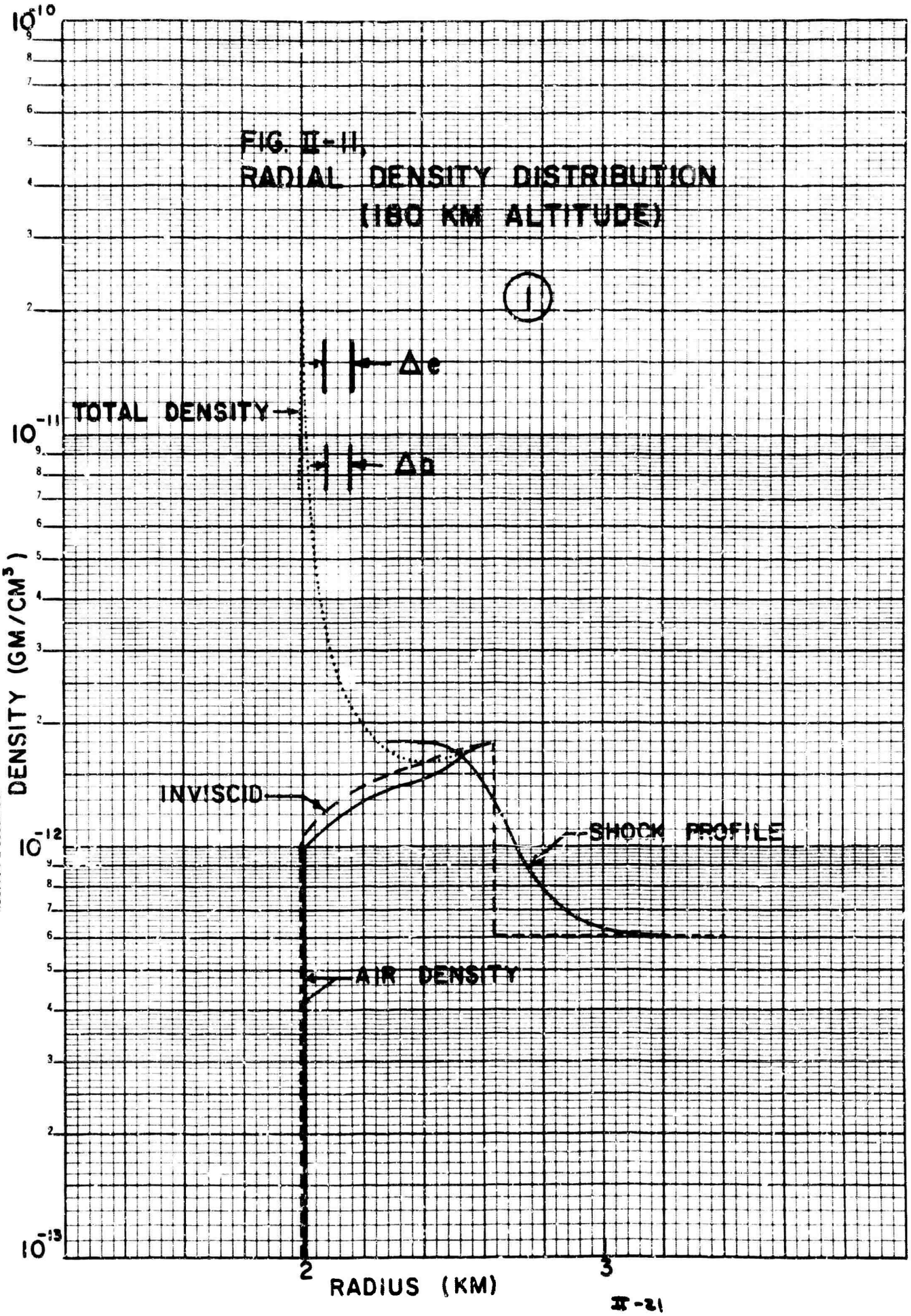
FIG. II-11,
RADIAL DENSITY DISTRIBUTION
(180 KM ALTITUDE)
1
Δe
TOTAL DENSITY
Δb
INVISCID
SHOCK PROFILE
AIR DENSITY
DENSITY (GM/CM³)
RADIUS (KM)
10⁻¹⁰
10⁻¹¹
10⁻¹²
10⁻¹³
2
3

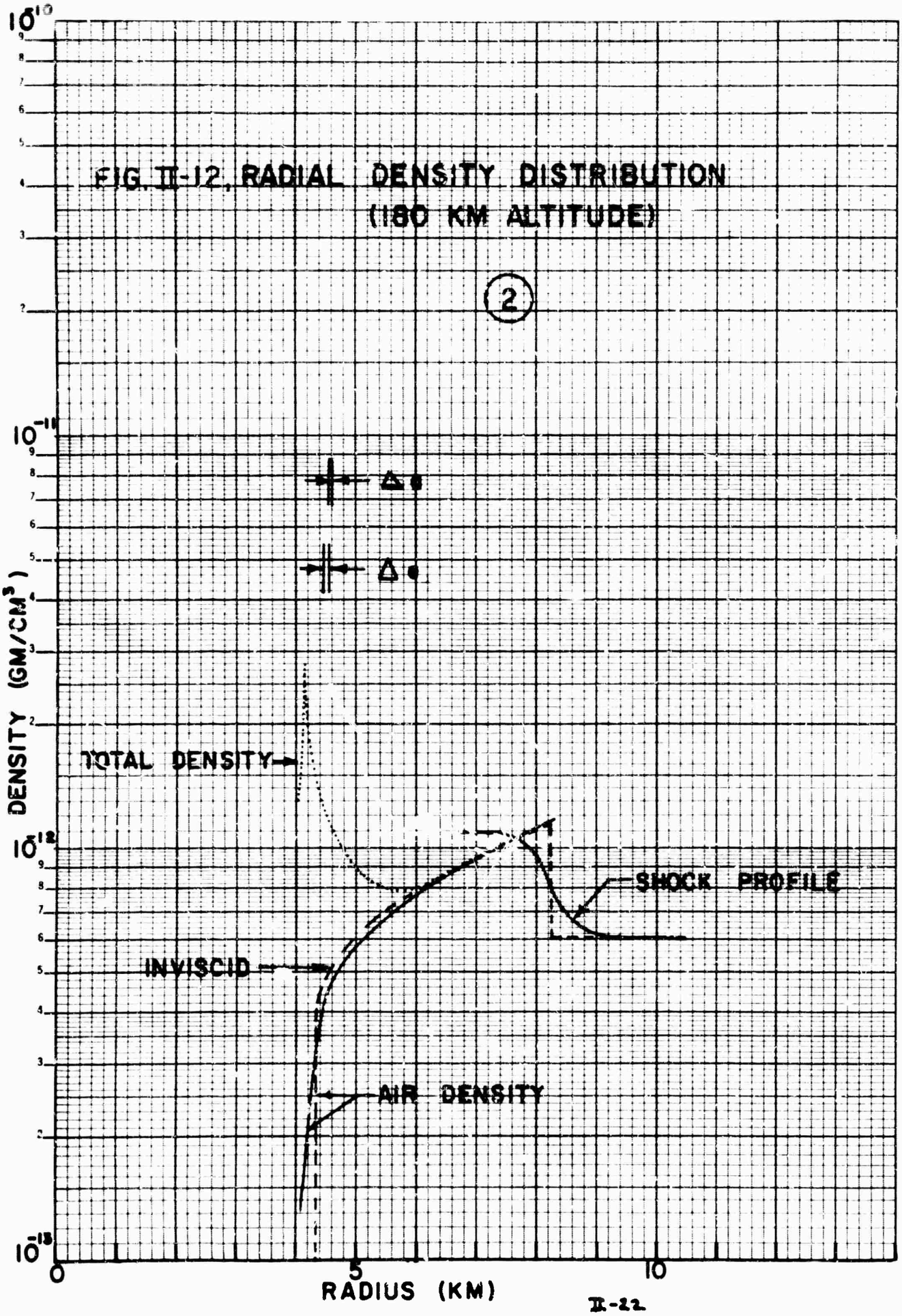
FIG. II-12. RADIAL DENSITY DISTRIBUTION
(180 KM ALTITUDE)
2
DENSITY (GM/CM³)
TOTAL DENSITY
SHOCK PROFILE
INVISCID
AIR DENSITY
RADIUS (KM)
0
5
10

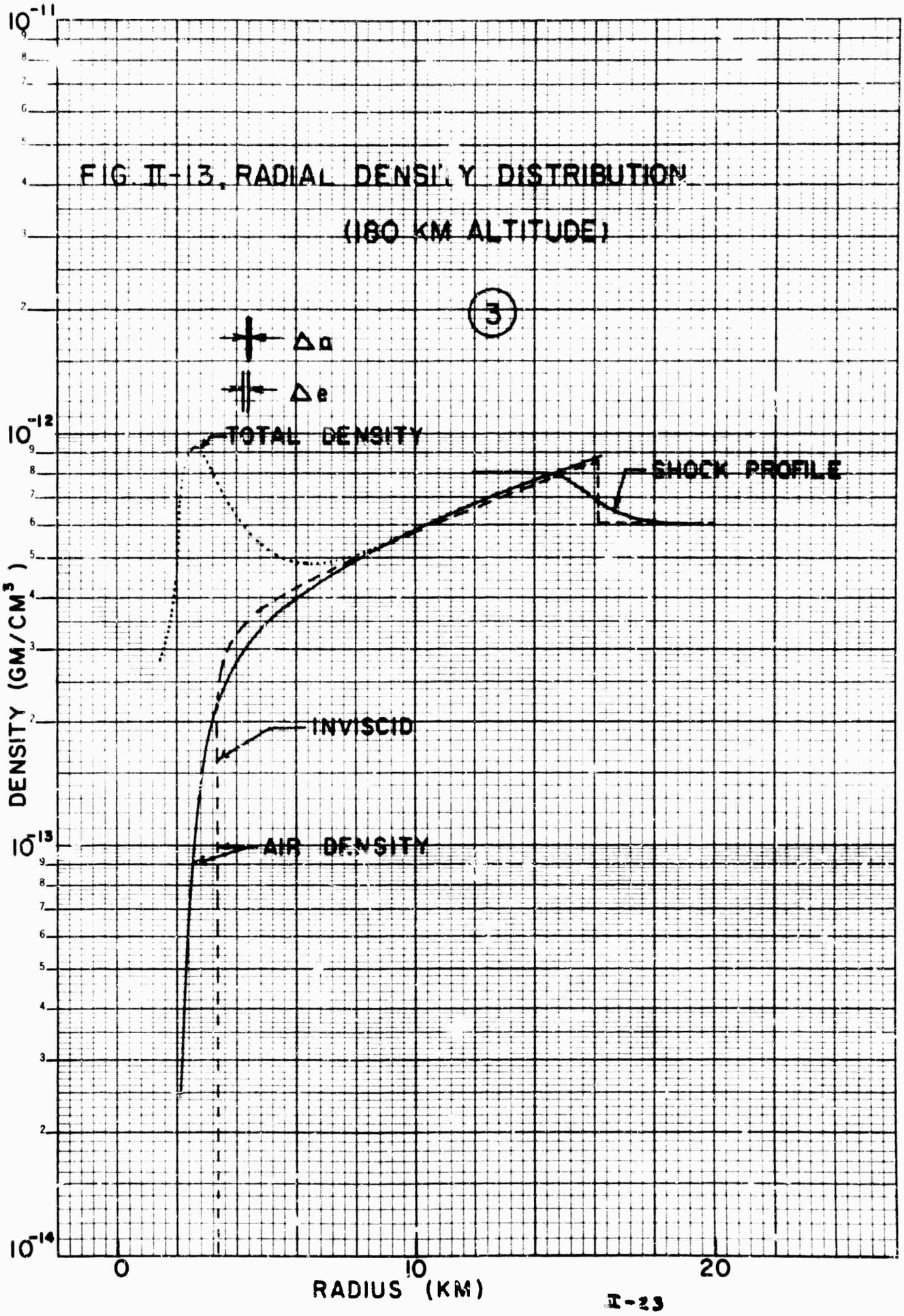

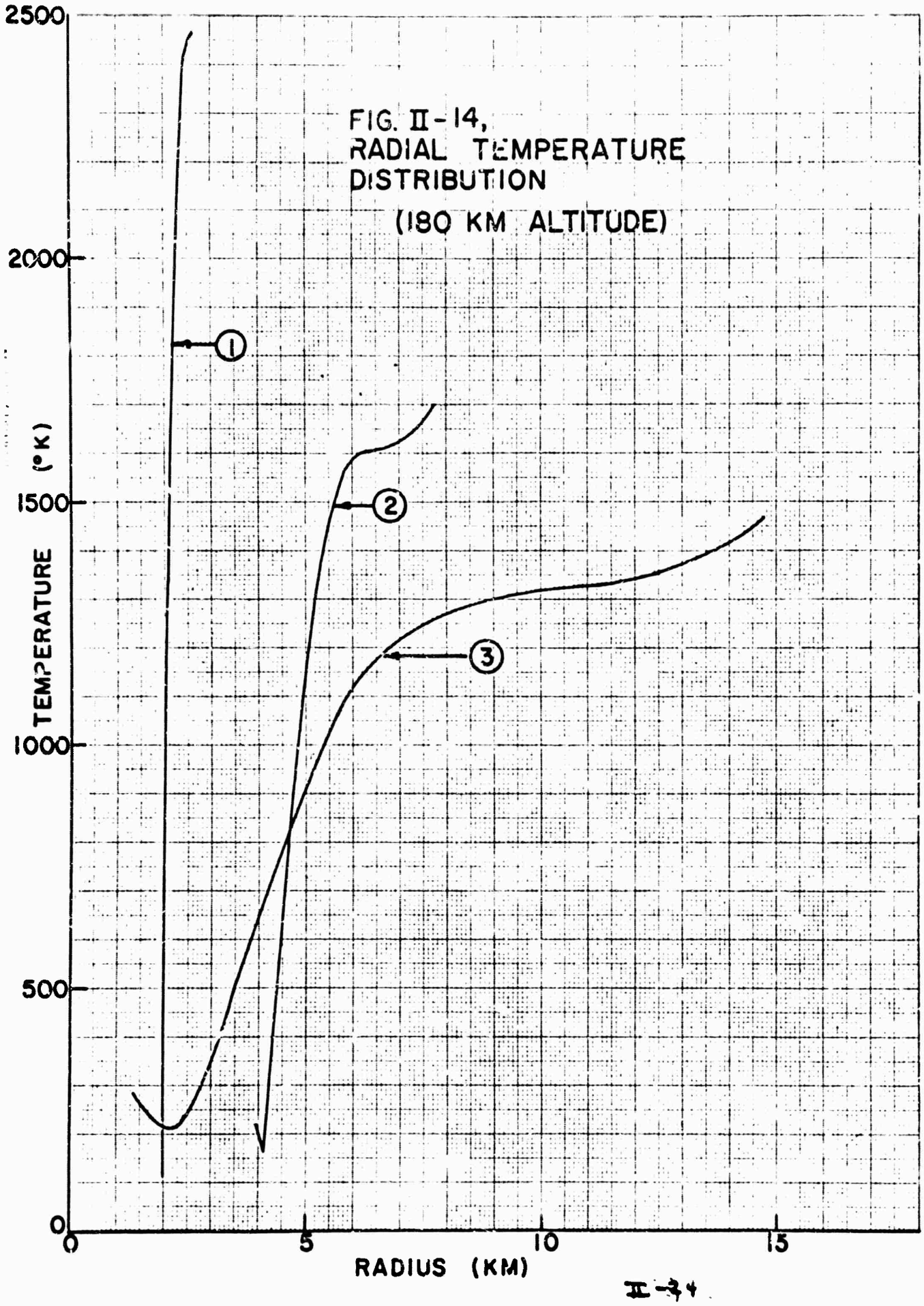

FIG. II-14,
RADIAL TEMPERATURE
DISTRIBUTION
(180 KM ALTITUDE)

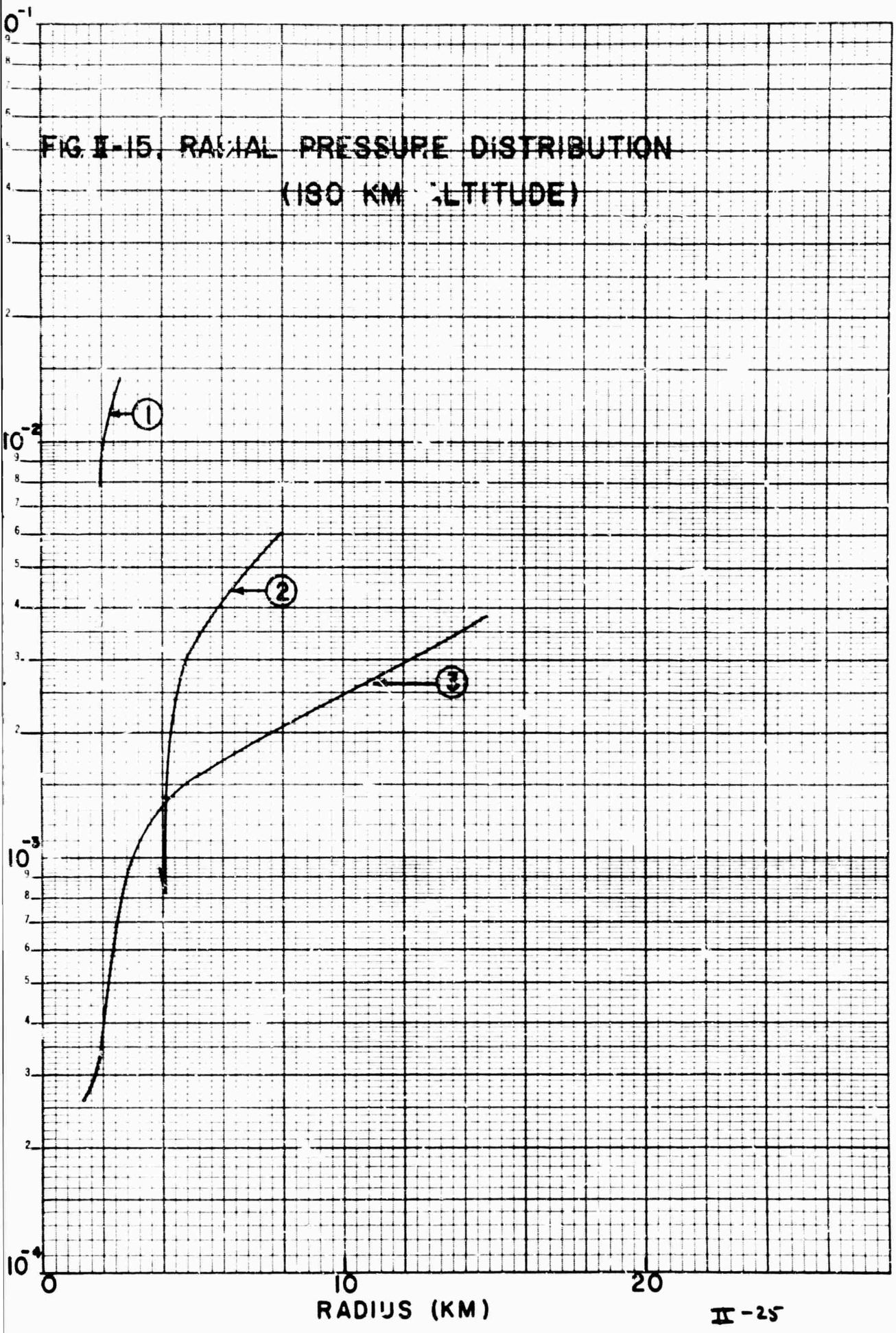
FIG II-15, RADIAL PRESSURE DISTRIBUTION
(180 KM ALTITUDE)
10^{-1}
10^{-2}
10^{-3}
10^{-4}
1
2
3
0
10
20
RADIUS (KM)

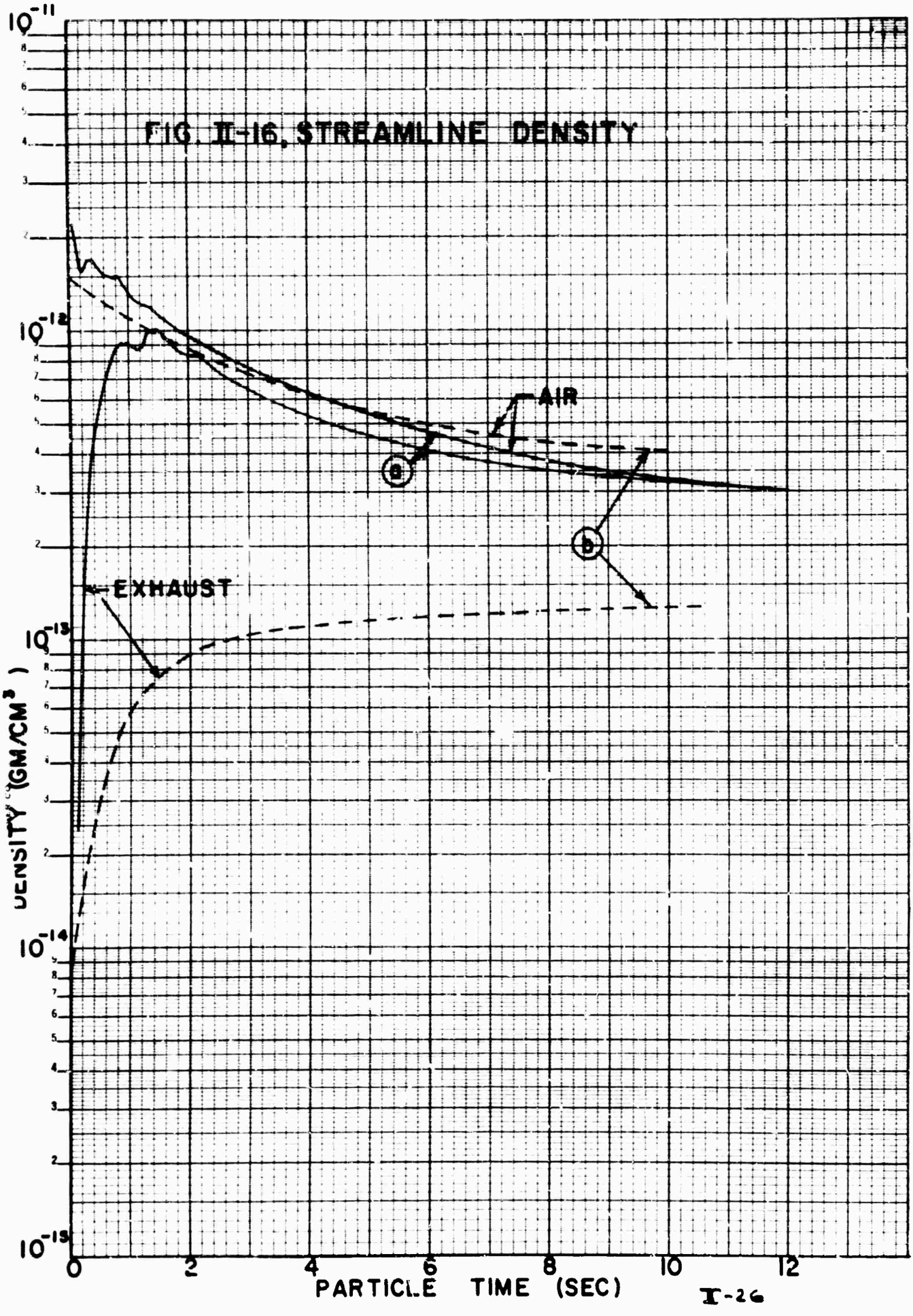
FIG. II-16, STREAMLINE DENSITY
AIR
EXHAUST
a
b
DENSITY (GM/CM³)
PARTICLE TIME (SEC)
10⁻¹¹
10⁻¹²
10⁻¹³
10⁻¹⁴
10⁻¹⁵
0
2
4
6
8
10
12

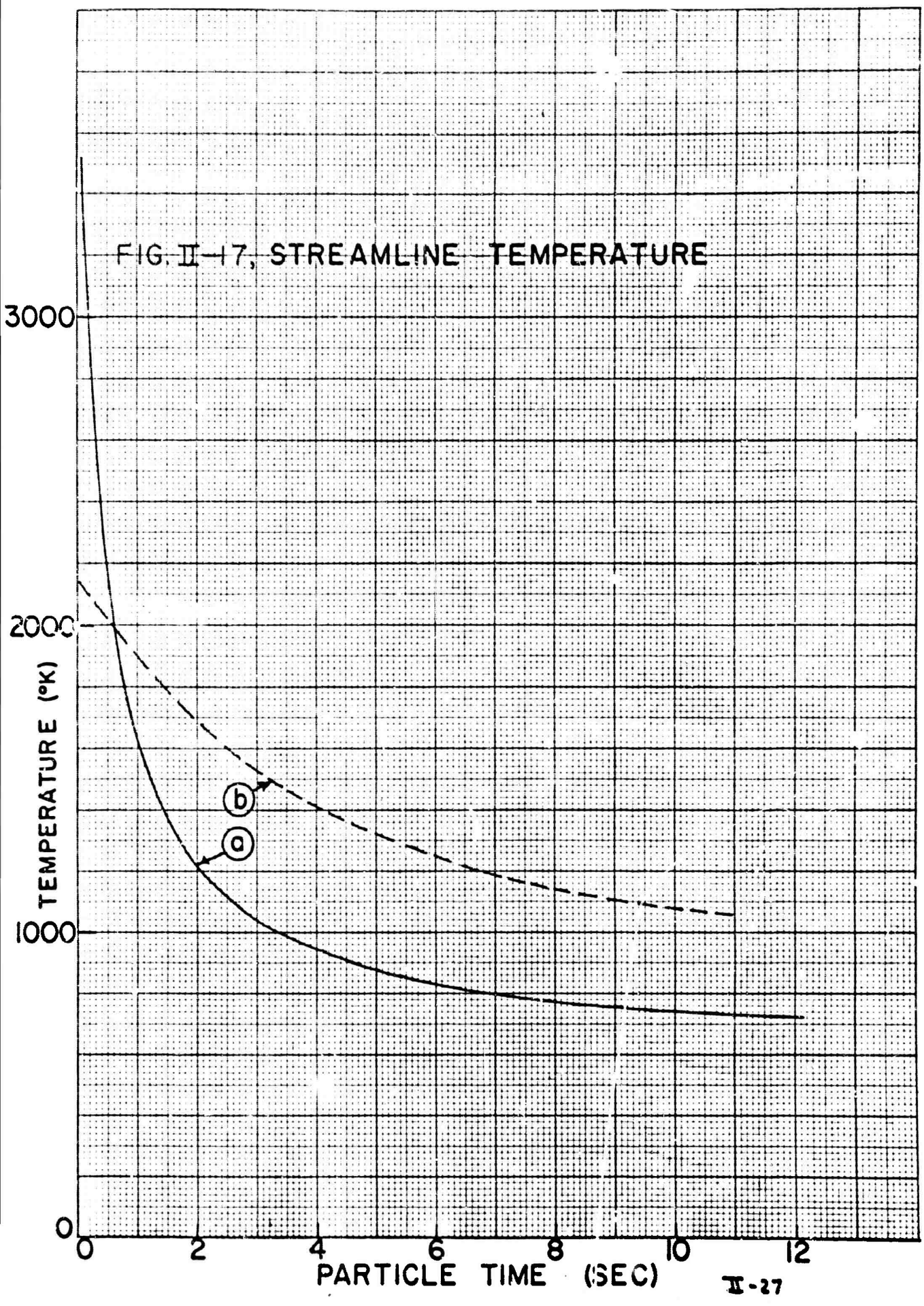

FIG. II-17, STREAMLINE TEMPERATURE

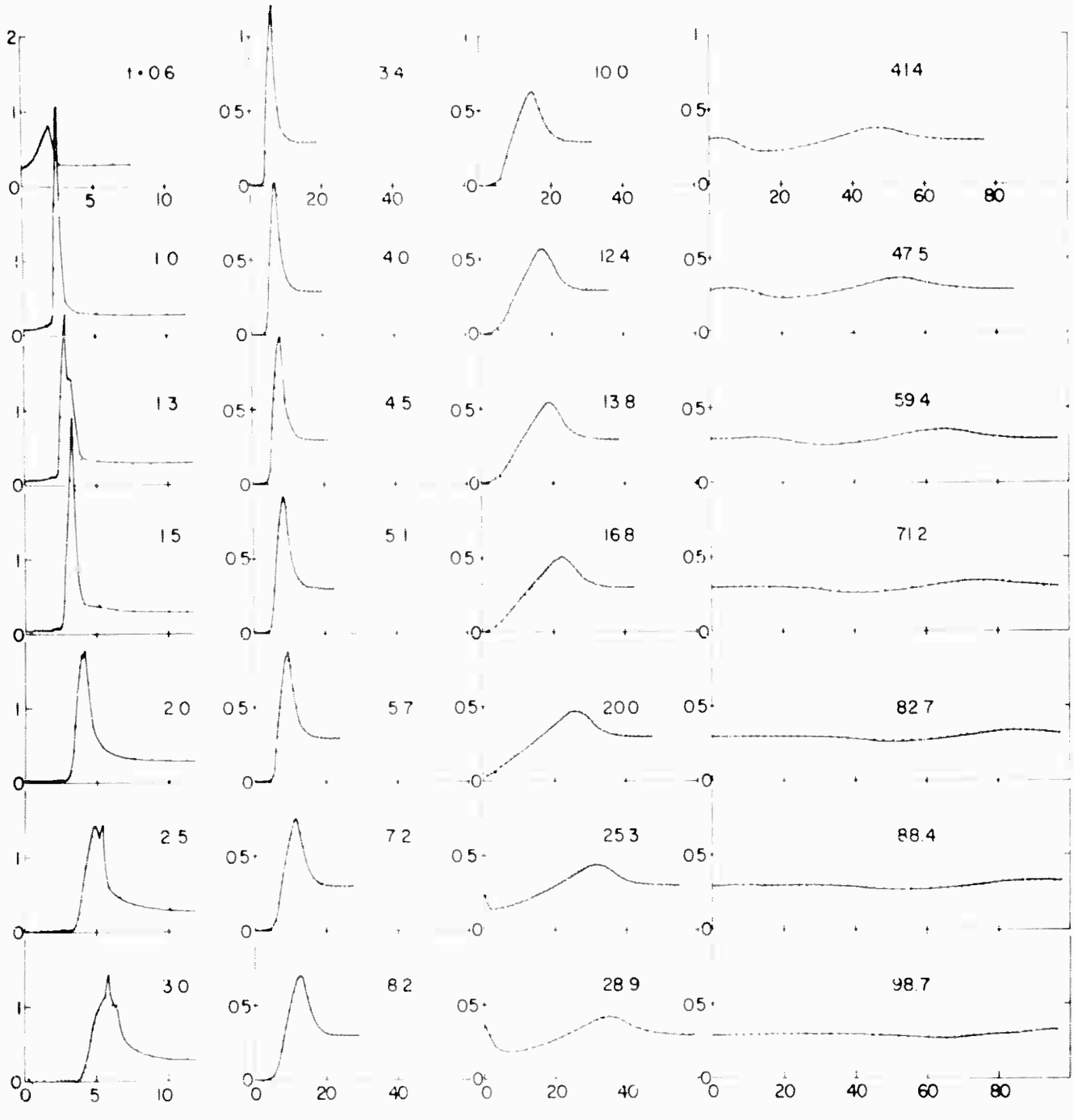

Fig. II-18. Pressure distribution at various times (t in seconds) in the small disturbance approximation at 290 km altitude. Ordinate is 1000 times the pressure in dynes/cm^2 and the abscissa is the radius in kilometers.

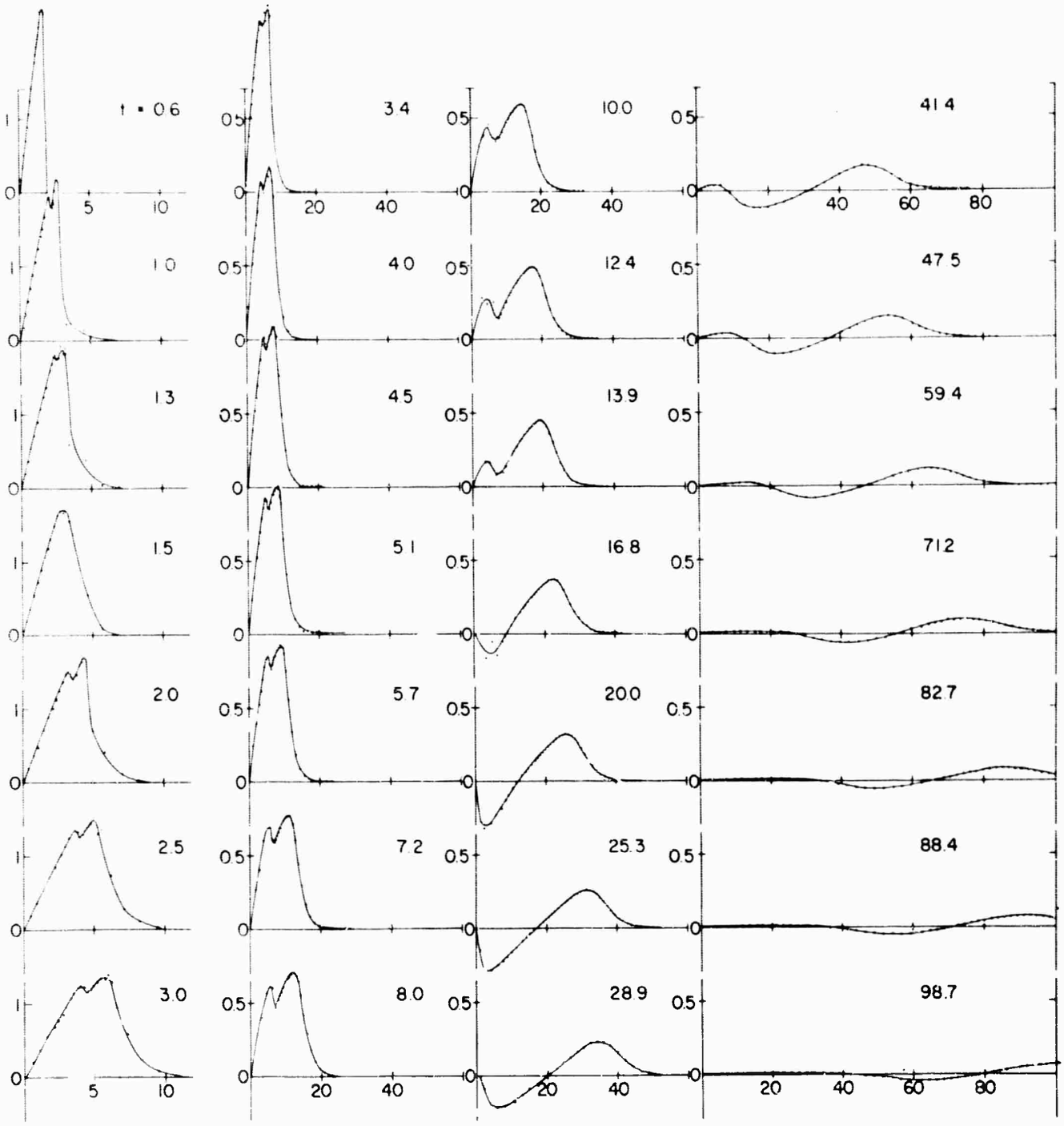

Fig. II-19. Radial velocity distribution at various times (in seconds) in the small disturbance approximation at 290 km. Ordinate is the velocity (km/sec) and the abscissa is the radius in kilometers.

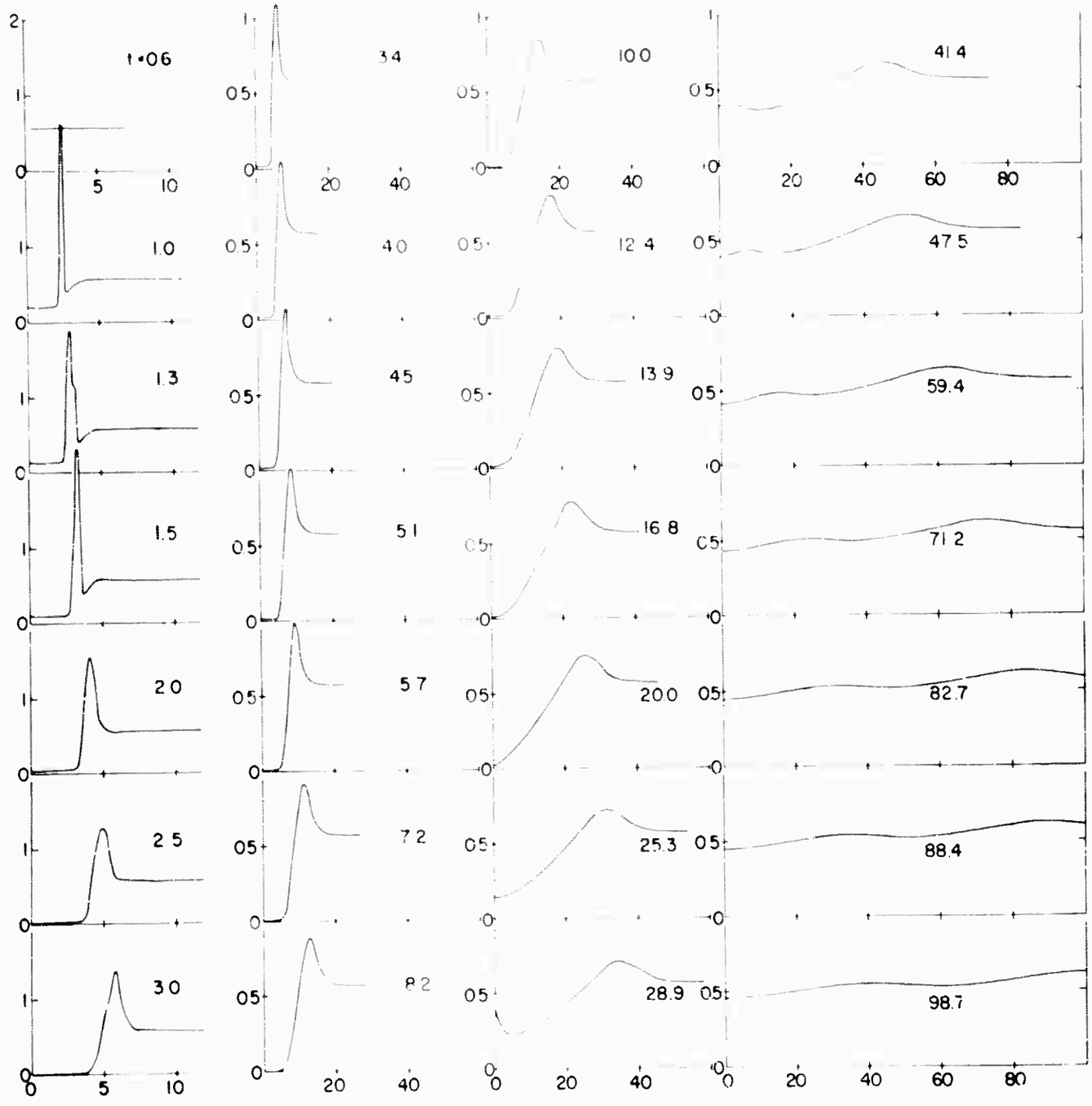

Fig. II-20. Air partial density distribution at various times (in seconds) in the small disturbance approximation at 290 km. Ordinate is 10^{15} times the density in gm/cm^3 and the abscissa is the radius in kilometers.

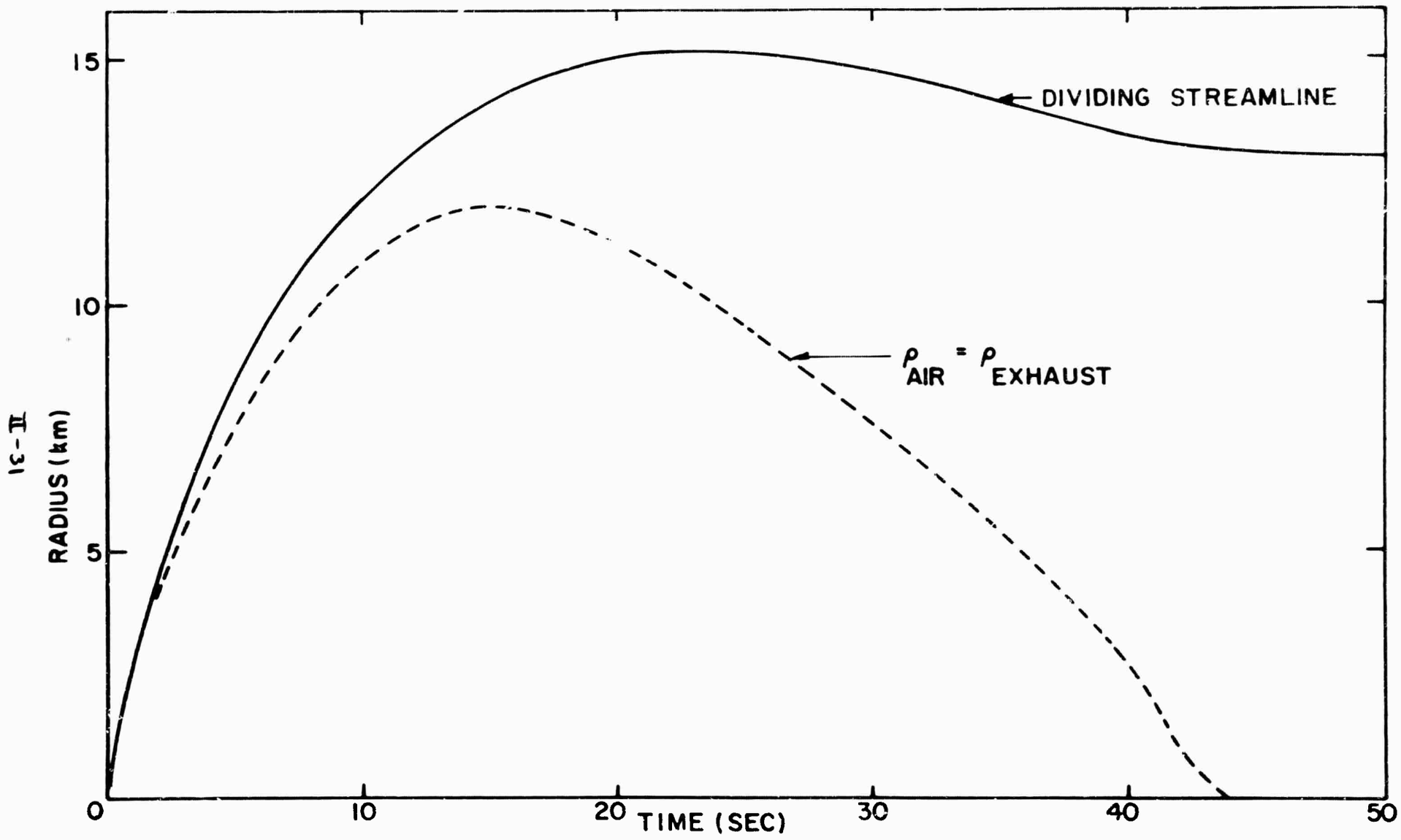

FIG. II-21, FLOWFIELD AT 290 km IN THE SMALL DISTURBANCE APPROXIMATION

FIG. II - 22, COMPARISON OF COLLISIONLESS APPROXIMATION WITH NUMERICAL CALCULATION

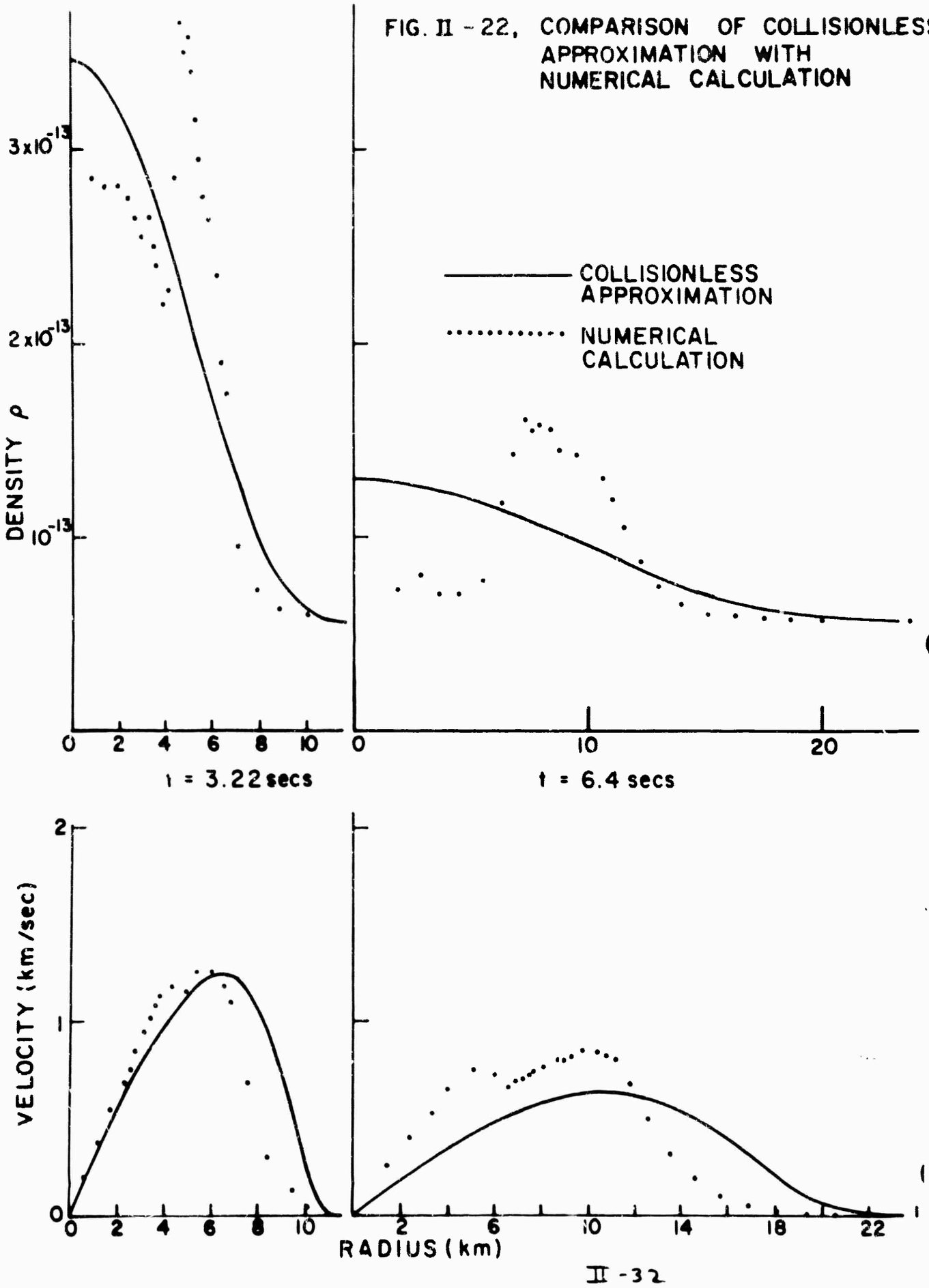

III. The Effect of the Geomagnetic Field

III-1. General Description

The ultimate purpose of the present study is to determine the electron density distribution in the vicinity of a powered-rocket in the ionosphere. Since, throughout much of the altitude range of interest, the Larmor radius of both ions and electrons may be considerably smaller than a mean free path, the geomagnetic field may considerably influence their motion. Lighthill[1] has considered the disturbance that would be induced by the passage of a satellite through the ionosphere and concluded that the perturbation produced would be primarily a one-dimensional motion of the ions parallel to the magnetic field. Although we are concerned with a somewhat wider range of altitudes, the neutral wind created by the passage of a rocket provides a similar but much stronger perturbation to the ion fluid.

It is known that the motion of a plasma in a magnetic field can be quite sensitive to the boundary conditions imposed. The effects are primarily due to the long range of the electromagnetic body forces. In our initial studies we have limited ourselves to two simplified approaches. The first is to consider sufficiently simple geometries for both the neutral flow field and the electromagnetic field that it is possible to obtain "exact" numerical solutions to the non-linear equations of motion. The second is to consider approximations of equations of motion that will allow consideration of more general symmetries and allow at least a semi-quantitative evaluation of the importance of properties of the neutral flow and the plasma (such as non-uniform distributions) that it is difficult to include in the detailed solutions.

For a detailed solution, we have chosen to consider first the case of a cylindrically symmetric neutral motion in an axial magnetic field. The basic a priori assumption that is made is that the level of ionization is sufficiently low that the motion of the neutral species is completely unaffected by the presence of the ionized species. In this case the neutral motion may be calculated without regard to the presence of the ionic species. The ion motion may then be determined by considering the ion fluid as a fully ionized plasma which moves under the influence of a strong body force (the net momentum transfer from the prespecified neutral wind to the ionized fluid) in addition to the electromagnetic field and its own pressure gradients. In addition, appreciable heat transfer to the ion fluid may take place as a result of the viscous stresses generated between the ions and the neutrals.

The condition for the neutral fluid to be independent of the ion motion can be estimated as follows. Suppose that the magnetic field is sufficiently strong that $u_r \ll V$.* Then the force exerted on the ions by the neutrals per unit mass of the neutrals is given by

$$\frac{\rho_i}{\rho} \nu_i V$$

Thus the neutral velocity will be appreciably reduced by this drag in a time of the order

$$t \approx \rho/\rho_i \nu_i$$

Thus, for frequencies less than $\frac{\rho_i}{\rho} \nu_i$, the neutral and ionized species move together as a single fluid. This frequency does not vary very strongly with altitude and at 180 km altitude is of the order of 10^{-3} sec^{-1}. Thus, for the much shorter time of present interest, we may ignore the influence of the ions

*Here u_r and V are the radial components of the ion and neutral velocity, respectively. The ion mass density is ρ_i, the neutral density is ρ and the ion-neutral collision frequency is ν_i.

on the neutrals.

If there were no magnetic field present, the ions would be pretty much swept along with the neutrals. When the magnetic field is considered, we must allow for the possibility that the ion motion across the field lines may be strongly hindered. A rough picture of the phenomena involved may be obtained by considering the expansion of a cylindrically symmetric neutral volume of gas into the ionosphere when the magnetic field is aligned parallel to the axis of symmetry. If the outward velocity of the neutrals is V and the ion velocity is u_r, then the force per unit volume exerted by the neutrals on the ions due to the ion slip will be of the order

$$\rho_i \nu_{in} (V - u_r)$$

where ν_{in} is a quantity of the order of the ion-neutral collision frequency (and may also depend on V). This force will cause an azimuthal drift of the ions and electrons. For a weakly ionized gas, this force, even when exerted over a depth of several kilometers, is small compared to the magnetic pressure $B^2/8\pi$. For example, if $n_i = 10^6$ cm^{-3}, $\nu_{in} = 10$ sec^{-1}, $V-u_r = 2 \times 10^5$ cm/sec over a 5 km distance, then the force per unit area is of the order of 3×10^{-5} dynes/cm^2 for an ion mass of 16. Thus a slight gradient in the magnetic field (.0002 gauss/km) is sufficient to balance this viscous stress.

Let us first consider the case when the ion mass and electron mass are equal, as are their interactions with the neutral fluid. Here, because of the symmetry, we may conclude that no charge separation will tend to occur. Thus both the axial and the radial electric field vanish identically. The azimuthal drift velocity will be of the order

$$v_{\theta_D} = \frac{c m_i \nu_{in} (V-u_r)}{e B}$$

Again, due to collisions with neutrals, there will be an azimuthal drag force of the order

$$m_i \nu_{in} v_{\theta_D} \quad .$$

Thus, the outward drift velocity will be

$$u_r = (\nu_{in}/\omega_{c_i})^2 (V - u_r)$$

or

$$u_r = \frac{\nu_{in}^2}{\nu_{in}^2 + \omega_{c_i}^2} V \qquad (1)$$

where $\omega_{c_i} = eB/m_i c$.

Thus strong hindrance of the motion across the field lines is expected when $\nu_{in} < \omega_{c_i}$ (~ 240 sec^{-1} for B = 0.4 gauss and an ion mass of 16).

When the ion and electron masses are unequal, radial fields due to charge separation may occur. These may considerably influence the motion. A very slight difference between the ion and the electron density can create large electric fields. Thus we expect that $n_i \simeq n_e$ to a good approximation. This condition implies that the ions and electrons will move radially with the same velocities.* This strong coupling of the two motions results in highly distorted Larmor orbits. If the ions were acted on by a velocity-independent radial force and the collision frequency were small, the two orbits would be azimuthally drifting ellipses having a ratio of semi-minor to semi-major axis of $\sqrt{\frac{m_e}{m_i}}$. The electron orbit would be elongated in the azimuthal direction whereas the ion orbit is elongated in the radial

*This conclusion depends specifically on the assumption that neither the neutral motion V nor the plasma properties vary in the direction of the magnetic field. As is shown in Section V-3 this requirement can be approximated in practice only if the flow field dimensions are extraordinarily large.

In this case it can be shown that the outward drift velocity has the form

$$u_r = \frac{\nu_{in}\,\nu_{en}}{\nu_{in}\,\nu_{en} + \omega_H^2}\,V \qquad (2)$$

where ω_H is the "hybrid" Larmor frequency ($\omega_H^2 = \omega_{c_i}\,\omega_{c_e}$) and ν_{en} is a quantity of the order of the electron-neutral collision frequency. Thus when the negative ion (electron) mass is small, the coupling to the magnetic field is stronger. Taking $\nu_{en} \approx \sqrt{\frac{m_i}{m_e}}\,\nu_{in}$, we find that appreciable ion slip will occur when $\nu_{in} < (m_i/m_e)^{1/4}\,\omega_{c_i}$ ($\simeq 3100$ sec^{-1} for $m_i = 16$). In Table III-1 we give the ion-neutral collision frequency in the ambient ion sphere at various altitudes assuming $\nu_{in} \simeq 6 \times 10^{-10}\,n_a$ where n_a is the neutral number density. Also in Table III-1 we indicate the collision frequency that might be expected behind a moderate strength shock (taken to be ≈ 10 times that in the ambient). It will be shown later that, because of the finite extent of the neutral flow in the direction of the magnetic field, the appropriate coupling parameter is ν_{in}/ω_{c_i}. Reference to Table III-1 then shows that appreciable slip effects will occur at altitudes above 120 km in the less dense parts of the flow field and at altitudes above 150 km even in the denser parts of the flow field.

Table III-1

Altitude km	n_a (cm^{-3})	ν_{in} (sec^{-1}) ambient	ν_{in} (sec^{-1}) shock	ω_{c_i} (sec^{-1})	$(\frac{m_i}{m_e})^{1/4}\,\omega_{c_i}$
100	8×10^{12}	4800	48000	240	3100
120	3×10^{11}	180	1800		
150	4×10^{10}	24	240		
200	8×10^{9}	4.8	48		
250	3×10^{9}	1.8	18		
300	1×10^{9}	0.6	6		

The discussion given in the preceding section indicates that, at high altitudes, the geomagnetic field strongly hinders the transverse motion of the ions in the less dense portions of the flow field. The neutral flow, which is essentially independent of the presence of the magnetic field, acts as a driving wind which stresses and heats the ion fluid. When the suppression of the transverse motion of the ions is strong, the ions move one-dimensionally along the magnetic field lines under the influence of this three-dimensional wind. Except in the region of the neutral flow where there are strong density gradients (shock fronts), the characteristic times for the motion are long compared to the time between ion-neutral collisions. In this approximation it is expected that the ion and electron temperature and pressure distributions will be reasonably isotropic and Maxwellian (see Section III-2) although the individual values for the ion and electron temperatures may differ considerably both from the neutral gas temperature and from each other.

Also when the motion of the ions across the magnetic field is strongly suppressed, the lateral transport of heat and momentum is markedly reduced. In this situation the problem of evaluating the three-dimensional electron density distributions may be reduced to a number of independent one-dimensional flow problems once the underlying neutral flow field has been evaluated. Here the magnetic field acts simply to confine the ionized fluid to essentially rigid, frictionless channels. The ionized gas then executes a one-dimensional motion under the influence of the momentum and heat input from the predetermined neutral wind. In this motion the electromagnetic fields play no role (except for ambipolar diffusion effects). At high altitudes we expect that this model of the motion will apply to

much of the flow field. Close to the vehicle, however, will always be a region where the gas density is sufficiently high to ensure that the ions from the ambient ionosphere are swept along with the neutral exhaust gases regardless of the magnetic field. For typical vehicles it is expected that this region may be of the order of a kilometer in diameter.

This model of the perturbations induced in the ionosphere by the passage of the vehicle was first proposed by Lighthill[1] to describe the perturbation to the F-region electron density distribution created by the passage of a satellite. The only difference lies in the magnitude of the effect and the nature of the source. Lighthill was primarily concerned with the far field disturbance induced by a relatively small body travelling in the upper regions of the F layer. In our case, the source of the disturbance, the neutral wind, is distributed over a large volume and is expanding at a speed somewhat greater than the local sound speed. Thus the acoustic type of motion induced in the ionized fluid will occupy roughly the same volume as the neutral flow field although the velocities and density distribution of the ions may be markedly different from those of the neutrals.

Since the ion motion is essentially one-dimensional, there is little geometrical "attenuation" of the disturbances induced in the ion fluid as compared to the $1/r$ or $1/r^2$ attenuation of the neutral flow. Thus, if there were negligible viscous dissipation of the motion, the disturbance generated in the ion fluid could travel long distances while retaining significant amplitude. However, this effect is not expected in the present case since the ion velocity is strongly coupled to the component of the neutral flow velocity parallel to the magnetic field. A disturbance in the ion fluid which propagates into a region where the neutral flow velocity is small would be damped within a few ion-neutral mean free paths.

Some non-acoustic types of disturbances may propagate beyond the confines of the neutral disturbance. The high thermal conductivity of the electron gas will cause the heat generated by the friction between the neutral wind and the electron gas to be spread throughout a volume which may be much larger than that of the neutral flow field. The effect is similar to the broad thermal layer in the electron gas which occurs in front of a shock travelling through a fully or partially ionized gas. (Jaffrin (2) ; Probstein and Jaffrin (3)). In the present case it is expected that these conduction lengths will be considerably larger than the dimension of the neutral flow field for most altitudes of interest. This, together with the fact that the mechanism of thermal energy transfer from the neutrals to the electrons is rather inefficient because of the small electron-neutral mass ratio, implies that the electron temperature will not be significantly altered by the friction of the neutral wind. Because of this high conductivity, compression or expansion of the ionized fluid is also not expected to alter the electron temperature appreciably. Thus it appears that the electron gas may be considered isothermal with a temperature equal to that of the ambient ionosphere.

Although the high thermal conductivity of the electron gas parallel to the magnetic field does not appear to give rise to any effects outside the region of the neutral flow, significant effects may arise as a result of the correspondingly high parallel electrical conductivity. Since the accelerations imparted to the positive ions due to their interaction with the neutral wind are generally different from those given to the electrons, charge separation will tend to occur within the confines of the neutral flow field. Because of the high longitudinal conductivity, these charges will spread rapidly along the field lines until they are eventually

neutralized by the small cross field leakage current. It is expected that this spreading constitutes an Alfvén motion guided along the field lines in a manner related to the magnetohydrodynamic whistler mode. However, the characteristic frequencies of this disturbance are considerably smaller than the collision frequency. Thus the motion will be more diffusive than wave-like.

Since the velocities associated with the neutral flow are very much less than the Alfvén speed (the Mach number based on the Alfvén speed is of the order of 0.01), the amplitude of the disturbance will be small. The nature of these far field disturbances is discussed further in Section V-6. A preliminary estimate of the disturbance expected in the steady state for an axially symmetric neutral flow in an aligned field indicates that the perturbation to the electron density beyond the confines of the neutral flow may be of the order

$$\frac{\Delta n_e}{n_e} \simeq + f \; \nu_i^2/(\nu_i^2 + \omega_e^2)$$

where f is the reduction factor defined in Section V-3. This probably is too small to be noticeable. In a transverse magnetic field, larger effects are expected. Also the time-dependence of the Alfvén motion and/or inhomogeneities in the density of the ambient ionosphere may give more pronounced effects, especially when the collision frequency is small. Further analysis will be required to evaluate the level of the field motion.

In this connection it is interesting to note that Drell, Foley and Ruderman have recently discussed a similar problem.(4) They were concerned with the interaction between a large satellite and the ionosphere and invoke an Alfvén type of motion radiated by the satellite to account for its observed drag. Except for the fact that collisions are less

important in their case because of the much higher altitude and that the source (ECHO 1) is small and of fixed size, the phenomena are quite closely related: in both cases the source acts as a battery which drives currents along the conducting field lines. These authors expect a perturbation in the electron density as large as 15% to be propagated along the field lines up to several hundred kilometers from the satellite. The present analysis has not been carried sufficiently far to give any real indication whether or not any perturbation approaching this magnitude may be induced by the wind created by a large rocket.

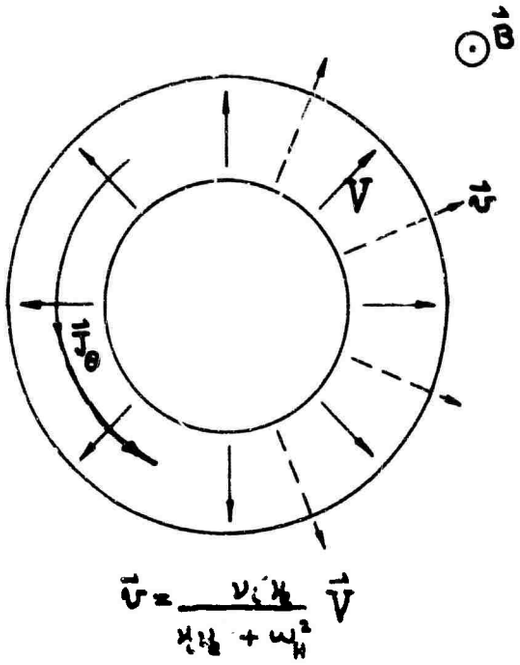

Fig. III-1a. Cylindrically symmetric plasma in an axial field.

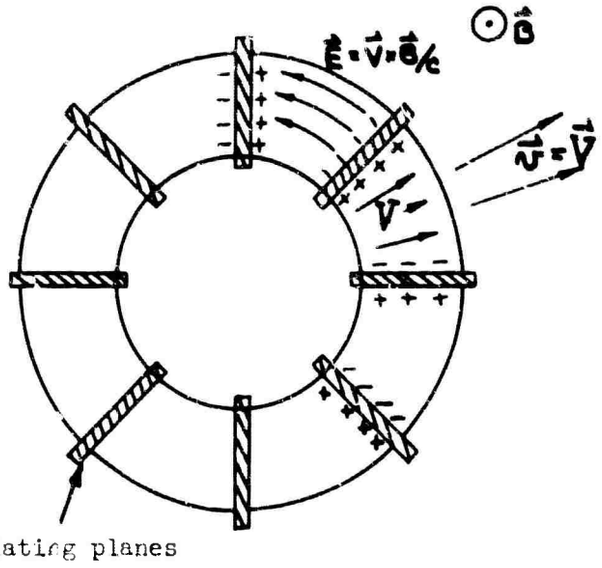

Fig. III-1b. Insulating planes preventing the flow of azimuthal currents.

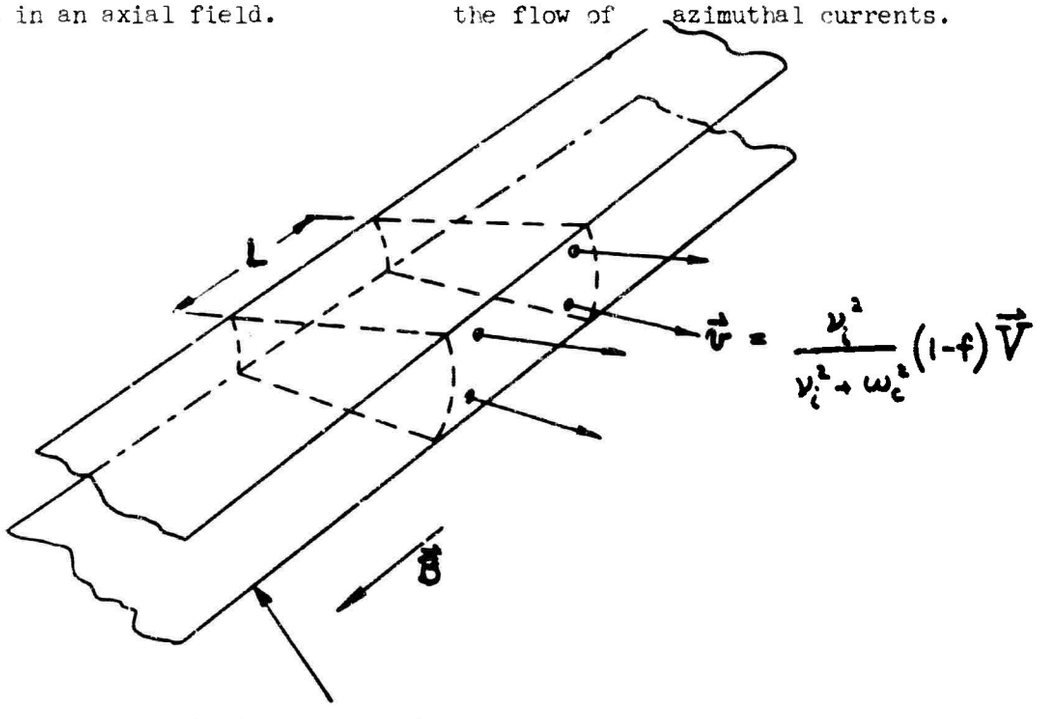

Fig. III-1c. Finite length axially symmetric plasma in an axial field.

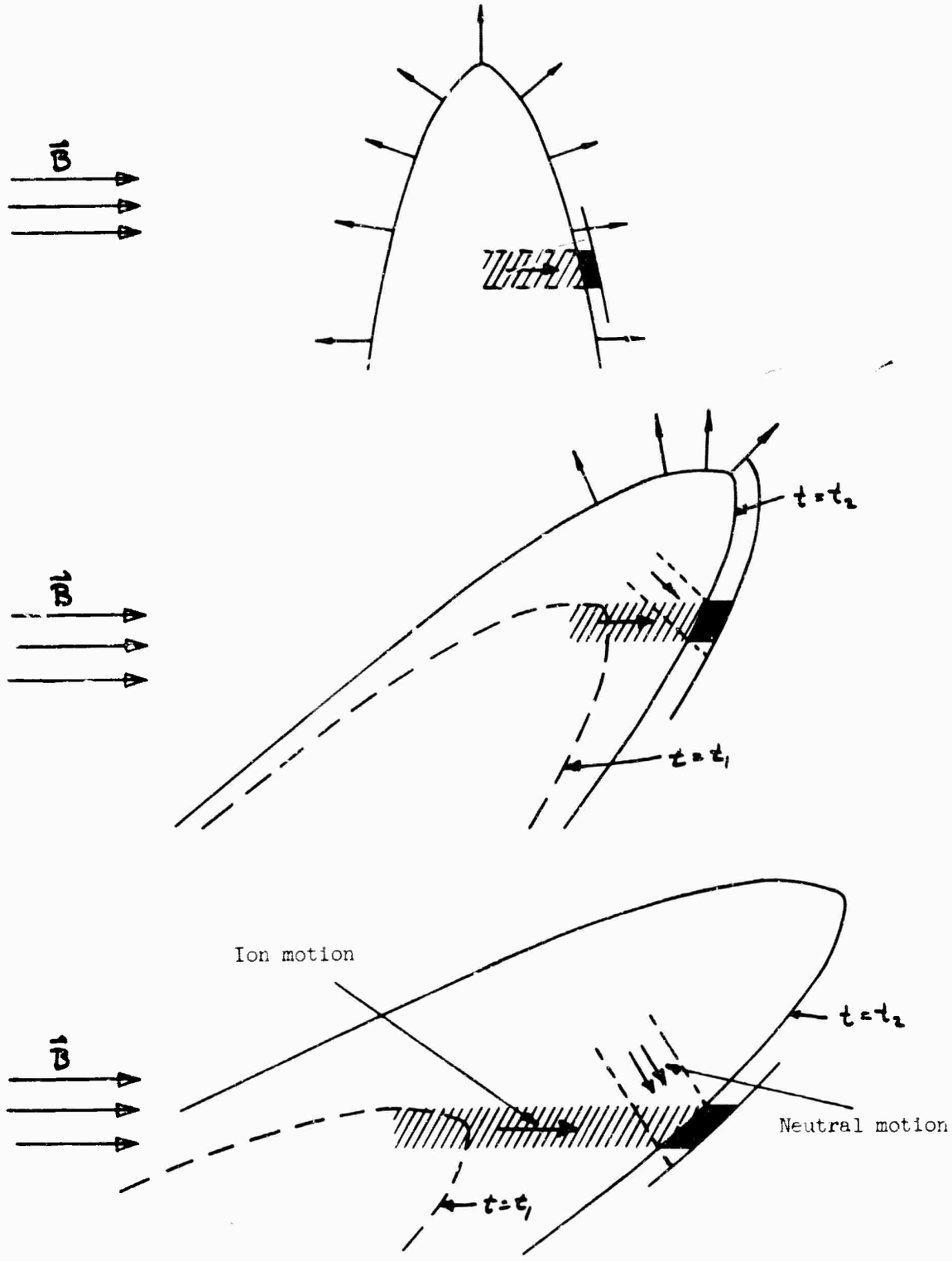

Fig. III-2. Relative motion of ions and neutrals at various inclinations of trajectory to magnetic field.

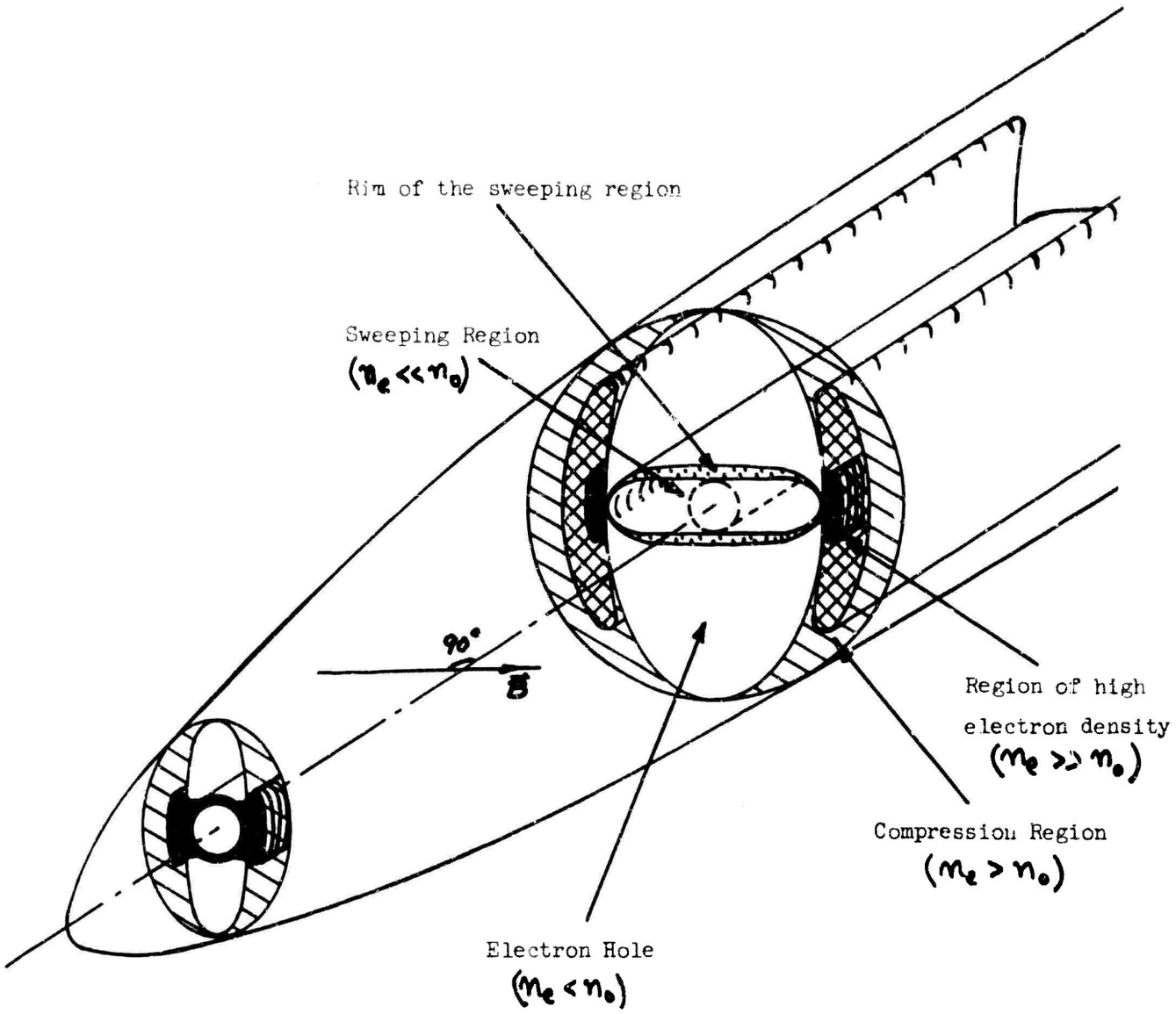

Fig.III-3. Schematic representation of the ion distribution according to the simple model (transverse magnetic field).

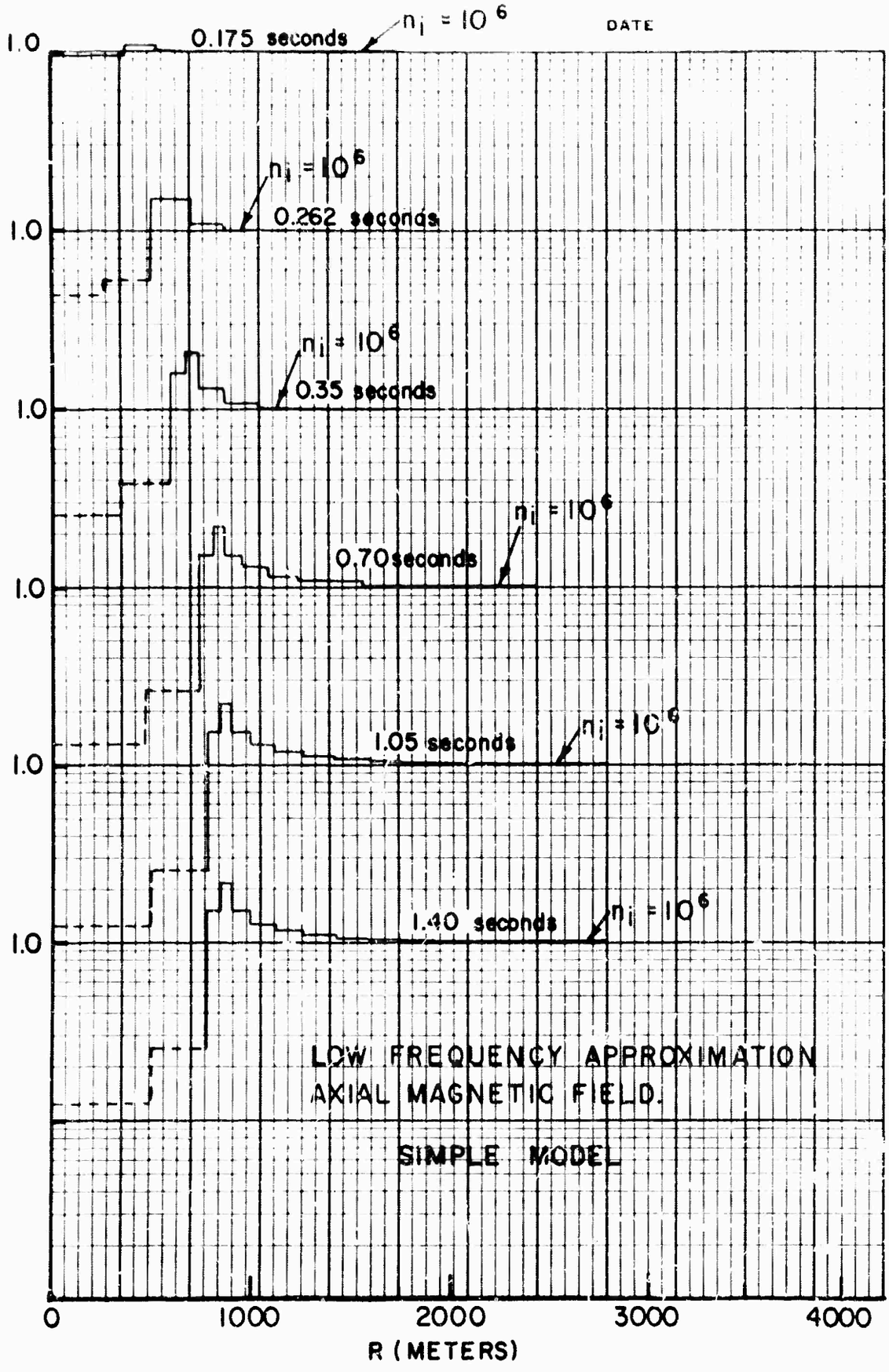

FIG. III-4, ION DENSITY RATIOS

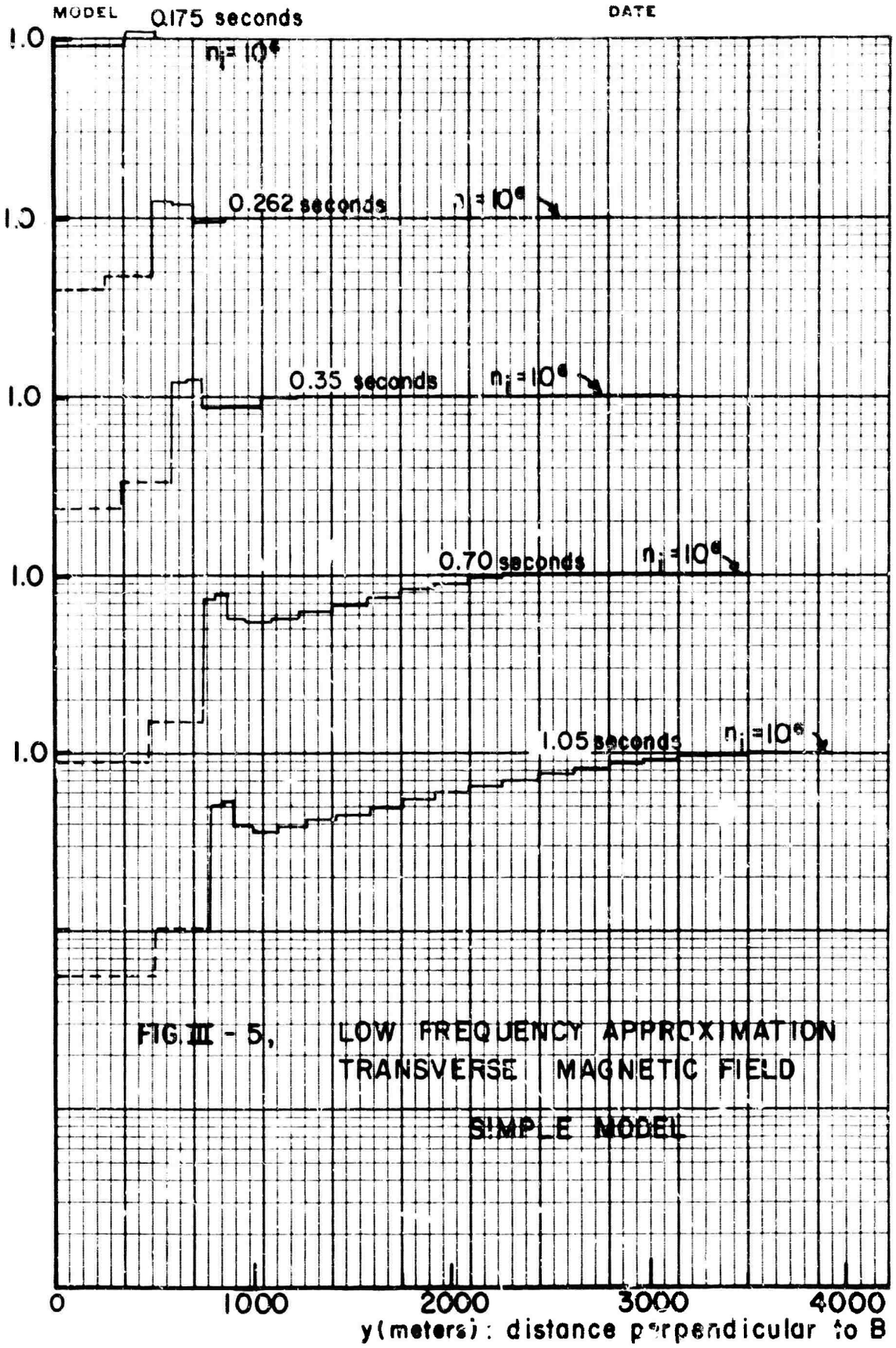

FIG III - 5, LOW FREQUENCY APPROXIMATION
TRANSVERSE MAGNETIC FIELD
SIMPLE MODEL

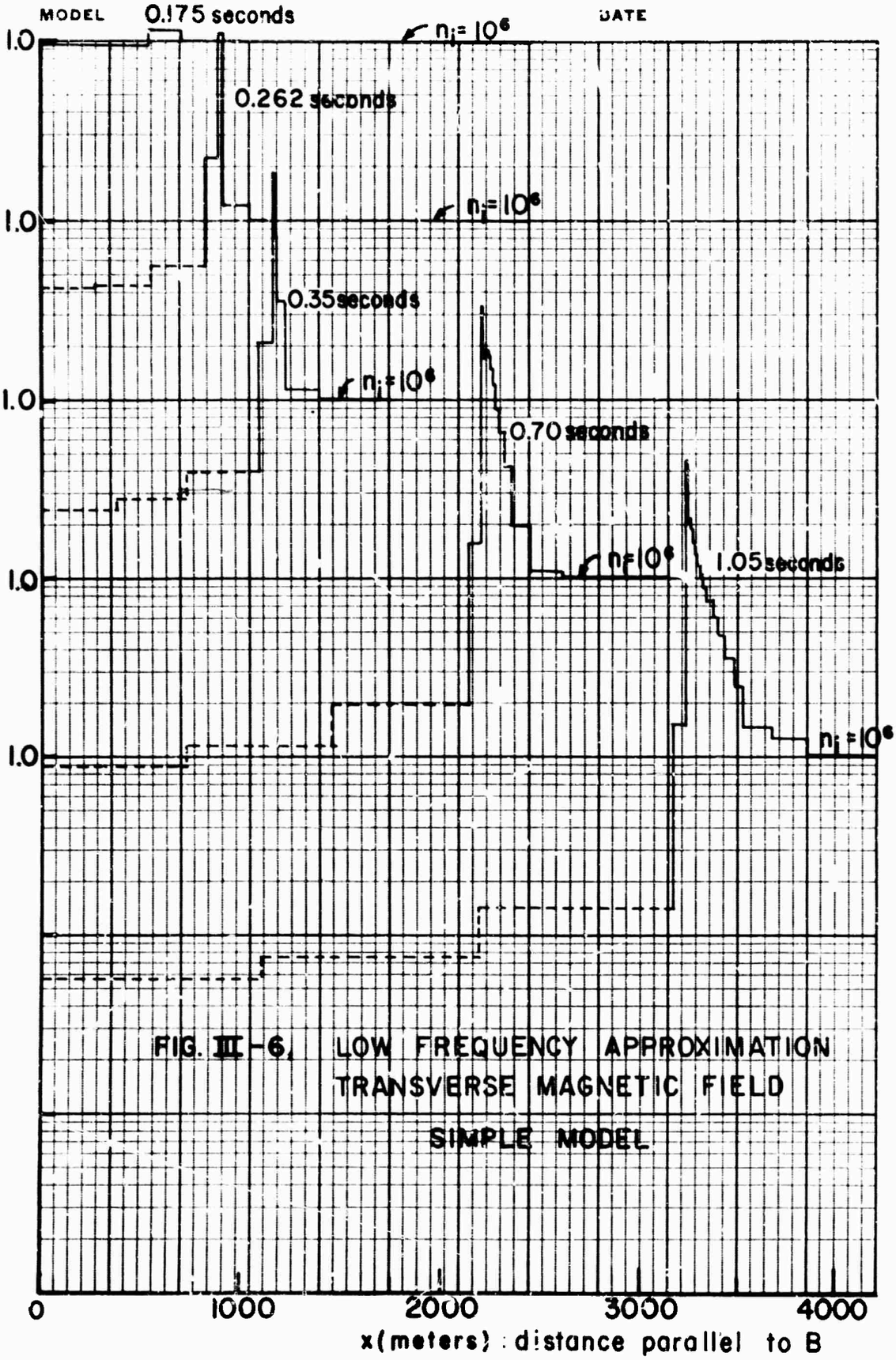

FIG. III-6. LOW FREQUENCY APPROXIMATION
TRANSVERSE MAGNETIC FIELD
SIMPLE MODEL

IV. Detailed Description of the Neutral Flow

IV-1. Background

During recent years an extensive literature dealing with the structure of high altitude rocket plumes has developed.[1-3] Experimental measurements, "exact" numerical methods and approximate analytical methods have been used. For example, schlieren and shadowgraph techniques have been used to study underexpanded jets expanding into still atmospheres by Ivatvala,[4,5] Wilcox et al.,[6] D'Attorre and Harshbarger.[7] Because of experimental difficulties laboratory data are generally limited to exit to ambient pressure ratios less 1000 and in most cases less than 100. These are much less than the values for a missile at ionospheric altitudes. The laboratory data for jets in highly supersonic streams is meager. Rosenberg[8] has used photographic techniques to define the outline of the plume at high altitude during a number of missile launches. From his data he has determined an approximate size and shape of the plume boundary (as defined by its luminosity). Hill and Gabert[9] have obtained approximate correlation of Rosenberg's data using blast wave theory.

No attempt at a complete review of the existent techniques will be made here in view of the several studies presently available. Adamson[10] has reviewed much of the unclassified literature on the inviscid aerodynamic structure of the rocket exhaust plume. Rosner[11] gives a more recent detailed survey of the state of the art for predicting plume structure at various altitudes with and without viscous effects. In general, reliable procedures are available for certain portions of the plume but not for others. The expansion into vacuum when the nozzle flow is reasonably uniform has been treated by a number of people using the method of characteristics for the

flow close to the nozzle and an asymptotic analysis for the source-like flow at great distances. In the presence of a low but finite pressure free stream, a complex shock structure develops. Upstream of the point where the jet shock returns to the axis the flow has a simple structure and has been treated by both exact and approximate methods. The reflection of the jet shock from the axis of symmetry typically results in the formation of a shock triple point and a Mach disc. The flow downstream of this point contains both supersonic and subsonic regions. Little detailed analysis has been successfully applied to this region for highly underexpanded jets.

The analytic techniques may be divided into three categories: linearized methods, approximate methods and "exact" or detailed numerical methods for obtaining solution of the equations without approximation. The linearized theories are concerned with small degrees of under and over-expansion and are not of primary interest to the present problem. The approximate methods attempt to obtain information about the plume structure, such as boundary and shock locations or the far downstream average properties without requiring a detailed calculation of the entire flow field. The boundary location procedures are reviewed in detail by Adamson.[9] In general the approximations involve a method for specifying a jet pressure and a stream pressure at the boundary and demanding equality of these pressures. Newtonian or Prandtl Meyer expansion approximations have been used to specify these pressures. These procedures appear to be capable of predicting, within a reasonable approximation, the boundary location not too far from the nozzle, but the approximations typically worsen downstream. Hill and Habert[9] have been able to obtain reasonable correlation of the high altitude

plume shape using blast wave theory. Thomson[12] has used an asymptotic analysis to correlate the properties of the far downstream pressure equilibrated jet to the nose shape. Alden, Hill and Habert[13] treat the shock layer as thin and obtain a universal plume shape at high altitudes for hypersonic free streams. Albini[14] uses an inviscid two shock layer formulation for the very high altitude jet which includes centrifugal relief. He also assumes thin shock layers and a hypersonic free stream. It is expected that these approximate techniques will yield useful information about the gross plume structure but how accurately they represent the detailed profiles is questionable.

The basic difficulty with many of the approximate techniques that have been developed is that the validity of the various approximations is difficult to ascertain a priori. In many cases a detailed assessment of the accuracy of the approximations has also not been made a posteriori, often because the results sometimes appear to agree well with certain features of observed plume shapes or more detailed numerical calculations of the plume shape. The difficulty, of course, is that the agreement is often limited to one quantity, such as shape. A classic example is that of the blast wave similarity approximation of a cylindrical or spherical explosion. Here the location of the shock front is well described by the approximate theory long after the similarity approximations break When the details of the internal structure are compared, however, disparities often appear. For the present problem the detailed structure is of primary interest. For this purpose it appears that an "exact" numerical solution is required in order to obtain reliable information.

Several numerical programs, using the method-of-characteristics, have been developed.[15-17] Some of these are isentropic programs and are most useful

for nozzle or vacuum expansion calculations or for nearly balanced nozzles where the shocks are weak. Others treat the air and jet shock as non-isentropic discontinuities assuming the air shock is attached to the nozzle lip. When the free stream is hypersonic and the air shock detaches, creating a subsonic region, the jet flow alone may be evaluated by using the Newtonian approximation to specify the boundary pressure. When the Newtonian approximation is valid the jet flow may be computed first, yielding a blunt body contour around which the air flow may be evaluated subsequently.[18] In the present problem the shock may be detached so that the Newtonian approximation is useful at the forward part of the plume, but the Mach numbers are not high enough that this is a good approximation for the downstream portion of the plume. At present there does not appear to exist a complete "exact" numerical procedure for treating this problem.

There are very few treatments of a highly underexpanded jet including diffusion effects. Vasiliu has formulated the problem in the boundary layer approximation (very thin mixing layer).[19] However, the procedure is an implicit one and is awkward to apply. Some calculations have been carried out for a turbulent thin boundary layer along the plume boundary. In any case, the strong lateral gradients that occur at high altitude make the boundary layer approximation suspect.

The approach used in the present study is a combination of procedures that have been developed for axisymmetric jet flows and for hypersonic flows over solid bodies. In the following paragraphs we discuss some of the characteristics of the available procedures as they pertain to the present problem.

Within the limits of continuum theory the Navier-Stokes equations are usually assumed to provide a reasonable description of moderately rarefied flow fields. Questions exist concerning the validity of these equations

for the structure of very strong shocks but at present no suitable alternative has been presented. Many different useful methods have been developed for obtaining exact or approximate solutions to these equations for various boundary conditions. One powerful tool has been the use of the similarity assumption. The similarity technique assumes that a separation of variables is possible in the differential equation and the boundary conditions. With this assumption the partial differential equation is reduced to two sets of ordinary differential equations which may be integrated by standard techniques. In general similarity may be obtained only for certain types of boundary conditions. The similarity technique has proved a powerful tool for treating the hypersonic flow over slender bodies. Here, when the small disturbance approximations are valid, ($\delta \ll 1$ and $M_\infty \delta^2 \ll 1$ where δ is a characteristic body slope and M_∞ the free stream Mach number) solutions to an equivalent unsteady one dimensional flow may be sought.[20] Similar solutions[21-23] are obtained for flows over bodies where radius r_b varies as power of the axial distance:

$$r_b = cx^n .$$

Here $n = 1$ is the wedge or cone, and $\frac{2}{3+\nu} < n < 1$ yields convex bodies. Here $\nu = 0$ for planar bodies and $\nu = 1$ for axisymmetric bodies. The special case $n = \frac{2}{3+\nu}$ yields the so-called blast wave solutions corresponding to the one dimensional unsteady problem of an intense energy release along the axis of symmetry at $t = 0$. For axially symmetric bodies the blast wave solution corresponds to a parabolic body ($n = 1/2$). Blast wave theory has been used[9] to correlate empirical data for the plume shape at high altitude. The ease of application of the theory justifies its application for obtaining order of magnitude results. In order to use blast wave theory for the flow

over a paraboloic body the effect of the blunt nose, where the slender body assumption fails, must be considered. It has been shown[24,25] that nose blunting of otherwise slender bodies can have a disproportionately large effect on the flow field about the body. Here the strong and highly curved shock at the nose of the body produces a strong gradient in the entropy near the body surface. Blast wave theory may possibly be used for the flow far from the body if an approximate account of the entropy layer is included (see Sychev[26] and Yakuva[27]). When the similarity assumption may not be invoked the partial differential equations must be treated directly. Normally this means a numerical procedure is required.

Numerical Methods for Inviscid Flow

Supersonic Flow

One of the most useful methods for obtaining numerical solutions of the partial differential equations for supersonic flow has proven to be the method of characteristics. Properly used this method yields an "exact" solution. In the high Mach number regions of the plume flow, however, difficulties arise in the application of this method in a numerical procedure.

Since the characteristic lines make an angle

$$\sigma = \sin^{-1}\left(\frac{1}{M}\right)$$

the characteristic grid is elongated in the streamwise direction when the Mach number is large. As a result, errors will be magnified in the stream direction and the inaccuracies in locating the interaction of characteristics will be large. To overcome these inaccuracies, small grids (i.e., small in the direction transverse to the streamlines) would be necessary.

In the plume problem, this shortcoming of the method of characteristics becomes serious many nozzle exit diameters from the nozzle exit. Fortunately, the regions in which the characteristic angles are small are regions in which other methods (e.g., finite-difference techniques) become quite useful.

Under the heading of finite-difference techniques we include all numerical methods for direct numerical integration of the partial differential equation other than the method of characteristics. Basically two types may be distinguished: those that use a prescribed set of mesh points and those that include the determination of the location of the mesh points in the calculation. The distinguishing property of supersonic flows is that the differential equations are of the hyperbolic type. Consequently, finite difference marching techniques may be directly applied.

Subsonic Flow:

Nose Region Solutions for the External Shock Layer

The methods discussed so far are inapplicable in the nose region of the stream shock layer where the flow is subsonic. Here the elliptic nature of the equations prevents the direct application of finite difference marching techniques. For the present problem the subsonic region is expected to be small and to exert a relatively minor influence on the overall flow field. In order to obtain the initial values for the calculation in the supersonic region, however, an estimate of the subsonic flow in the nose region is required.

The evaluation of the hypersonic flow over a blunt body has been studied extensively during recent years and several methods for inviscid flow are available, including the Newtonian solution,[28,29] the thin-layer approximation,[30,31] the integral relations method,[32,33] and the various numerical methods of Swigart,[34] Van Dyke,[35] Garabedian and Lieberstein,[36] etc.

Since the free stream is hypersonic, the Newtonian approximation may be used to specify the pressure on the jet boundary in the subsonic nose region. This provides an appropriate boundary condition for the solution of the jet flow in the inviscid approximation. Given this boundary one of the various approximation procedures may then be used to estimate the subsonic flow.

IV-2. The Inviscid Flow Field Evaluation

IV-2a. Finite Difference Procedure Used for the Supersonic Flow

The momentum equation for inviscid steady flow is

$$(\vec{u} \cdot \text{grad})\, u = -\frac{1}{\rho} \text{grad}\, p \,. \tag{1}$$

The energy equation is

$$\vec{u} \cdot \text{grad}\, (h + \frac{1}{2} \vec{u}^2) = 0 \,, \tag{2}$$

and the continuity equation is

$$\text{div}\, \rho\vec{u} = 0 \,. \tag{3}$$

The equation of state is $p = \rho RT$.

The momentum equation may be rewritten in the form

$$u^2 \frac{\partial \vec{n}}{\partial s} + u \frac{\partial u}{\partial s} \vec{n} = -\frac{\text{grad}\, p}{\rho} \tag{4}$$

where $u = un$, n is a unit vector parallel to the streamline and s is the distance along the streamline. For two-dimensional flow we may write

$$u \frac{\partial u}{\partial s} + \frac{1}{\rho} \frac{\partial p}{\partial s} = 0 \tag{5}$$

and

$$u^2 \frac{\partial \varphi}{\partial s} + \frac{1}{\rho} \frac{\partial p}{\partial y} = 0 \,. \tag{6}$$

Here φ is the angular inclination of the streamline and y is the distance along the surface normal to the streamline. Equation (6) may be rewritten as

$$-T \frac{\partial S}{\partial s} + \frac{\partial}{\partial s} (h + \frac{1}{2} u^2) = 0. \tag{7}$$

where the entropy S is given by $S = R\, [\ell n\, (p/\rho^{\gamma})]/(\gamma-1)$.

Thus the flow is isentropic along streamlines.

Here $h = \frac{\gamma}{\gamma - 1} RT$. Equations 2, 3, 7, may be integrated along streamlines to give

$$\begin{aligned} h + \frac{1}{2} u^2 &= \text{constant} \\ p/\rho^{\gamma} &= \text{constant} \\ \rho u A &= \text{constant} \\ p &= \rho RT \end{aligned} \tag{8}$$

Here A is the area of an individual streamtube. The remaining equation is the centrifugal equation:

$$\frac{\partial \varphi}{\partial s} = - \frac{1}{\gamma M^2} \frac{\partial}{\partial y} (\ell n\ p) \tag{9}$$

where we have set $\frac{\rho u^2}{p} = \gamma M^2$.

The finite difference approximation is carried out as follows. The flow is divided into a finite number of streamtubes. Initial data is fed in along an orthogonal surface. The initial data consists of the local streamtube properties and the coordinates of the dividing streamlines, on the input surface. The calculation proceeds by predicting the flow properties on a new orthogonal surface using the flow data on the previous surface plus the boundary condition at each edge of the surface. The curvature $\kappa(K,L)$ of the streamline K at the point where it intersects the surface L is evaluated from the lateral pressure gradient determined from the pressures in the adjacent streamtubes (K, K + 1) and (K - 1, K) on the surface L (see Figure IV-1). This curvature is used to extend the streamline K to the surface L + 1. This procedure is repeated for each streamline in the flow. From the thus determined streamtube areas on the surface L + 1 the fluid dynamic properties for each tube are then evaluated from the three conservation equations.

It is known that the straightforward application of the marching procedure described above is unconditionally unstable. However, it may be rendered stable by the following procedure. Having determined the fluid properties on the surface L = l, the curvature κ' (K, L + 1) of the streamline K at the surface L + 1 is evaluated from the pressure gradients on this surface. Then the surface L + 1 is recalculated using for the mean curvature of the streamline K between the surface L and L + 1 the expression

$$\kappa = (1-\alpha)\,\kappa(K,L) + \alpha\,\kappa'(K,L+1).$$

Perturbation theory (acoustic approximation) shows that this procedure is stable when $\alpha > 1/2$, is unstable when $\alpha < 1/2$ and is neutrally stable when $\alpha = 1/2$. In addition to this restriction the step length between the surfaces L and L + 1 must be chosen to be less than the value of the separation between the streamlines K and K ± 1 multiplied by a number of the order of $\sqrt{M^2 - 1}$. Calculations with various test flows show that when $\alpha > 1/2$, perturbations (sound waves) are damped. In practical calculations it is usually convenient and sometimes necessary to choose α slightly greater than 1/2 in order to smooth out perturbations.

As presently programmed, the procedure marches through an axisymmetric or planar flow generating the orthogonal surfaces. On each surface it calculates the flow between two boundaries. These boundaries may be of various types: a shock, a solid, or a free (pressure given as a function of boundary inclination) boundary. The shock boundary condition uses the Rankine-Hugoniot relations to connect the interior flow to the external flow. The external flow may be non-uniform and may be given in analytic or tabular form. The input tabular data is required to be in the same form as the data the program calculates.

In the evaluation of the high altitude flow field, we first calculate the undisturbed flow into a vacuum. This calculation is carried sufficiently far from the nozzle that an analytic extrapolation to infinity may be carried out. It is convenient to represent this flow in an analytic form to be used as the flow into which the jet-intercepting shock propagates. A procedure for doing this is outlined in Section IV-2b.

IV-2b. Representation of the Undisturbed Jet Flow

The flow into a vacuum is relatively easily calculated and there are a number of formulations available. Here viscous effects (except for nozzle and combustion chamber boundary layers) are expected to be small. In Figure IV-2 we show the streamlines calculated with the finite difference streamtube program for the 50:1 sustainer engine expanding into vacuum. In this particular calculation, the flow was prevented from expanding more than 85° by an artificial wall. At the present time the program is not set up to calculate a flow which turns through more than 90°. Although this type of flow can be allowed for with relatively minor changes, it is not anticipated that this will be necessary. For this nozzle the mass flow which, in a vacuum expansion, turns through more than even 60° is a small fraction of the total flow (less than 1%). Thus, in this case, we do not expect this large angle flow to have much effect on the downstream flow. Also, in practice, this portion of the flow will be largely nozzle boundary layer flow and is not well defined at present (Fig. IV-4). (The flow that turns more than 60° is confined to an annulus less than 1 mm thick at the nozzle lip.)

For the finite difference calculation, it is convenient to express the undisturbed flow in an analytic form. Since the flow distribution is singular at the nozzle lip, the zero pressure streamline and the point at infinity, it is convenient to choose an analytic form that gives the correct limiting form of the flow at these singular points. A useful form is the following Taylor series representation of the density:

$$\left(\frac{\rho}{\rho_e}\right)^{\frac{\gamma-1}{2}} = \eta^{(\gamma-1)} \sum a_{mn}\, \eta^m \cos\left(\pi(n+\tfrac{1}{2})\,\frac{\theta}{\theta_\infty}\right) \qquad (1)$$

where

ρ_e is the exit plane density at the nozzle edge,

$\eta = r_e / \sqrt{r^2 + (x-x_o)^2}$

$\theta = \tan^{-1} r/x$

θ_∞ = the turning angle for the zero pressure streamline, and

x is measured from the intercept of the zero pressure line with the axis. This form gives the correct dependence of ρ far from the nozzle ($\rho \sim r^{-2}$) and the correct dependence on θ close to the zero pressure line ($\rho \sim (\theta_\infty - \theta)^{2/\gamma-1}$). The coefficients a_{mn} may be evaluated as follows:

Let

$$G_n(\eta) = \sum_m^{M_{max}} a_{mn}\, \eta^m. \qquad (2)$$

Then

$$G_n(\eta) = \frac{2}{\theta_\infty\, \eta^{1(\gamma-1)}} \int_o^{\theta_\infty} \left(\frac{\rho}{\rho_e}\right)^{\frac{\gamma-1}{2}} \cos\left(\pi(n+\tfrac{1}{2})\,\frac{\theta}{\theta_\infty}\right) d\theta. \qquad (3)$$

The quantities $G_n(\eta)$ may be evaluated numerically at various values of η from the vacuum flow field calculation. The values of the a_{mn} may then be found by standard least squares fit procedures. Standard computer routines are available for this latter fit.

A procedure similar to this has been used previously and was found to be a good fit to the flow throughout most of the field with a 28 term series.

In addition to the density we also need the flow inclination angle φ. Here an appropriate representation is:

$$\varphi = \theta \left[1 + \eta \sum_{m=0}^{M'_{max}} A'_{mn} \eta^m \cos \frac{\pi}{2}\left(n - \frac{1}{2}\right)\frac{\theta}{\theta_\infty} \right] \qquad (4)$$

The same procedure as that outlined above may be used here. In Figs. IV-3 and 4, we show the comparison between the numerical calculation of the density profile and streamline locations and the analytic representation obtained with a 6x6 polynomial-Fourier representation.

The outer parts of the vacuum flow field are appreciably affected by the peripheral mass flows associated with the rocket and by the turbulent boundary layer within the nozzle. In Fig. IV-5 we show the effect of the boundary layer on the vacuum flow for the 50:1 engine. (The boundary layer was calculated using a Von Karman-Pohlhausen method.) In Fig. IV-6 we show the effect of the sonic exit exhausterator which surrounds the 25:1 engine. About 3% of the total mass flow is released through this exhausterator.

In the far field, the flow from any nozzle becomes source-like ($\rho \sim R^{-2}$). In Fig. IV-7, we show the mass flow angular distribution for a number of different nozzles. In the far field limit the analytic representation is a Fourier series representation of $R^2\rho^{\left|\frac{\gamma-1}{2}\right|}$. In the present calculation we have typically used a 5 or 6 term sum. For approximate purposes, it often suffices to use a one-term representation:

$$\frac{dm}{d\Omega} = a\left|\cos \frac{\pi}{2}\frac{\theta}{\theta_\infty}\right|^{\frac{2}{\gamma-1}} \qquad (5)$$

In Fig. IV-8 we compare the detailed mass flow distributions for various nozzles with this simple form. In Table IV-1 we list the corresponding values of the parameter a. Reference to this figure indicates this form gives a reasonable representation of the density distribution obtained (within a factor of 2). The advantage of using this form is that it may be evaluated for any nozzle without requiring a detailed numerical evaluation of the vacuum flow. Mirels and Mullens have suggested a similar approximation: $\sqrt{1 - (\theta/\theta_\infty)^2}$ instead of $\cos\left(\frac{\pi}{2}\frac{\theta}{\theta_\infty}\right)$. Either formula gives a reasonable rough representation of the numerical calculations.

In Figure II-10 we show the far field distributions for three nozzles: the 50:1 nonuniform exit nozzle and two 25:1 nozzles, #1 and #2.* Nozzle #2 represents the far field flow for the S-4 engine whose exit plane pressure profile is shown in Fig. IV-9. This distribution, denoted Nozzle #1, was intended to represent this flow but, due to a mistake in the analytic fit procedure, the far field flow distribution actually was incorrectly computed at large angles to the axis. To a certain extent the errors are of a nature similar to a boundary layer effect. Unfortunately, this flow distribution was used to evaluate the flow fields at 100 and 135 km. The effects on the external flow fields are expected to be relatively small and confined to the bow region of the plume. Thus we do not know exactly what shape nozzle the flow labeled #1 corresponds to. However, differences in the flow are probably less than the absolute accuracy of the overall calculation.

*The two nozzles shown in Fig. II-10 have a sufficiently non-uniform exit plane profile that a precise calculation would predict a significant Mach disc shock structure near the nozzle exit. In the present calculation this difficulty was circumvented by choosing the mesh size large enough that no shock structure was apparent. The resulting errors are expected to be confined principally to the flow near the axis.

IV-2c. APPROXIMATE TREATMENT OF THE NOSE INVISCID SHOCK LAYER

The inviscid flow around a blunt body moving at hypersonic speeds has been treated extensively. Hayes and Probstein[37] give an excellent review of most of the techniques used. For the present problem the subsonic region is not expected to exert a major influence on the downstream flow. For high area ratio nozzles, the air shock may remain attached (i.e., no subsonic region) to rather high altitudes. Thus, at least for the initial evaluations, it is not expected that a sophisticated treatment of this region is necessary. Of the several procedures available those that assume a simple relation for the pressure distribution more or less a priori and use the conservation laws to roughly define the subsonic region are particularly suitable to be used with the marching technique used here for the supersonic flow. Here the evaluation of the subsonic calculation may essentially be reduced to a boundary condition at air-exhaust dividing streamline. One procedure that will be considered is outlined in the following paragraphs.

Here the thin layer approximation is used to estimate the pressure gradients normal to the boundary streamline. In this approximation and away from the stagnation point the pressure at a height y above (i.e., normal to) the boundary is

$$p(y) = p_B + K \int_0^y \rho u^2 dy \qquad (1)$$

where K is the boundary curvature. Assuming that the streamlines are approximately parallel to the surface, the mass flux per unit area is given by

$$\rho u = \frac{2Gp}{u} \left(\frac{p_t}{p}\right)^{1/G} \sqrt{1 - \left(\frac{p}{p_t}\right)^{1/G}} \,. \qquad (2)$$

Here G is h/RT and p_t is the total pressure for a given streamline. This

total pressure may be expressed in terms of the shock inclination at the point where the streamline enters the bow shock. Mass conservation requires that

$$dy = \rho_\infty u_\infty R\, dR/r\rho u \tag{3}$$

where R is the radial displacement of the streamline at the point where it enters the shock. Thus we may write

$$y = y(R) = \frac{\rho_\infty u_\infty u_m}{2G} \int_0^R \frac{1}{p}\left(\frac{p}{p_t}\right)^{1/G}\left(1-\left(\frac{p}{p_t}\right)^{1/G}\right)^{-1/2} \frac{R'd\,R'}{r} \tag{4}$$

and

$$p(y) = K\,\rho_\infty u_\infty u_m \int \sqrt{1-\left(\frac{p}{p_t}\right)^{1/G}}\,\frac{R'}{r}\,dR' + p_B. \tag{5}$$

Also the local radial displacement of the streamline is

$$r = r_B + y\cos\theta \tag{6}$$

where $\tan\theta = dr_B/dz$.

At each station the shock location is determined by solving

$$R_S = r_B + y(R_S)\cos\theta \tag{7}$$

where $y(R_S)$ is given by Equation 4.

In order to evaluate the pressure p, the boundary pressure p_B must be evaluated in the Newtonian approximation. A somewhat improved value may be obtained by requiring that the pressure behind the shock computed from Equation (5) agree with the value obtained from the Rankine-Hugoniot relations; however, this has not been incorporated in the present calculation.

This procedure is not valid near the symmetry axis. However, the effect on the downstream flow involved in using it into the axis is expected to be small. To start the calculation, we need a value for the shock stand-off

distance that is compatible with the above procedure. If the Newtonian form for the boundary pressure close to the axis is assumed, and the jet flow evaluated using this boundary pressure, then an average radius of curvature R_o for the nose may be defined. The boundary curvature should be averaged over radii of the order of the expected stand-off distance δ. Assuming that $p/p_t = 1$ and that $\delta/R_o \ll 1$, Equation 4, in the limit of $R/R_o \ll 1$, may be reduced to the form

$$\delta = y(0) = \frac{\rho_\infty u_\infty u_m}{p_t(0)G} \frac{\sqrt{G}}{2} R_o. \tag{8}$$

For hypersonic flow

$$\delta \simeq \frac{1}{2}\left(\frac{\gamma-1}{\gamma+1}\right)\sqrt{\frac{\gamma}{\gamma-1}}\, R_o. \tag{9}$$

These relations give a stand-off distance that is compatible with the procedure described by Equations 4 to 7.

In practice, however, a simpler procedure is more convenient: the stand-off distance is first assumed zero and the entropy gain through the shock calculated from the slope of the line joining the axis starting point and the first shock point given by Equation 1 (unless this inclination exceeds 90^o). If this latter condition occurs, the entropy gain is set equal to that for a normal shock.

In using this procedure, it was found that the shock front tended to be unstable. The method was altered to a mixed marching-relaxation procedure in which the flow is calculated a number of times. The streamline total pressure p_t and the streamline curvature $K(r,z)$ (assumed now to vary linearly across the shock layer) for the $(N+1)$th iteration are evaluated from the Nth iteration. For the first iteration, the shock slope

is assumed to be the same as the boundary slope and the streamline curvature to be the same as the local boundary curvature. This procedure appears to converge within 3 or 4 iterations when used with typical boundaries. It may be convergent only in an asymptotic sense in that it is not clear that small irregularities in the boundary contour do not result in an increasingly fluctuating shock profile. However, in the present calculations, the amplification factor is sufficiently small that it does not cause any difficulty. (See Figure IV-10).

IV-2d. The Mach Disc Region

It is well known that the reflection of the jet shock from the symmetry axis is of the irregular type with triple shock point and Mach disc formation.[38] The detailed solution for this transonic flow requires the solution of a set of mixed elliptic-hyperbolic equations. Various approximate criteria have been suggested to determine the Mach disc location in a simple fashion.[39,40] Of these, that suggested by Bowyer, D'Attorre and Yoshihara[40] seems to give the best agreement with experiment. Here the inclinations of the Mach disc and the reflected shock are calculated at each point along the jet shock using the condition that the pressure and flow direction downstream of the triple point are the same for streamlines passing on either side of the triple point. The actual triple point is supposed to occur at the station where the Mach disc is locally normal to the incoming flow. In other words, the flow passing just inside the triple point is assumed to suffer only a slight deflection (see Figure IV-11).

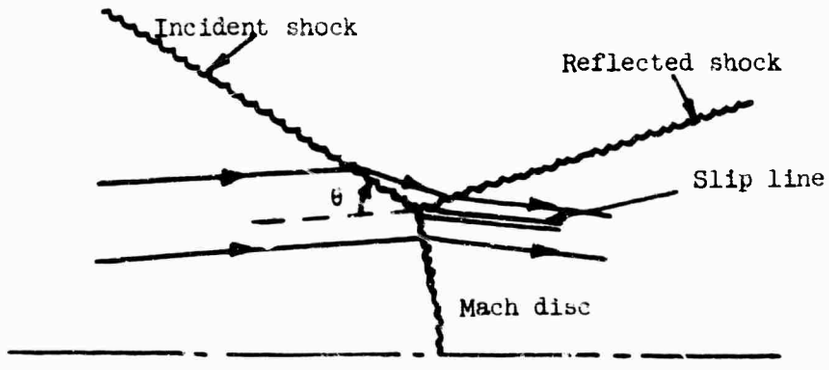

Fig. IV-11. Mach Disc Geometry

When, as in the high altitude jet, the Mach number in front of the shock is high (~ 100), this criterion for the triple point formation may be expressed rather simply. In this hypersonic limit, it may be shown that the Mach disc would form when the wave angle of the jet shock reaches a critical value (θ^*) which depends only on the specific heat ratio:

$$\left[\frac{\gamma+1}{2(\gamma-1)}\left(1 - \epsilon(\theta^*)\right) - 1\right] \sin 2\theta^* = (\gamma+1 - 2\sin^2\theta^*)\sqrt{\frac{\gamma+1}{\gamma-1} Z(\theta^*) - 1}$$

where

$$Z(\theta^*) = \left(1 - \frac{4\gamma}{(\gamma+1)^2}\sin^2\theta^*\right) \Big/ \left(1 + \frac{\gamma-1}{\gamma+1}\sin^2\theta^*\right)$$

and

$$\epsilon(\theta^*) = \left(\frac{\gamma-1}{\gamma+1}\right)^2 \sin^2\theta^*.$$

For $\gamma = 1.3$, θ^* takes the value 19.2°. For $(\gamma+1)/(\gamma-1) \gg 1$, θ^* may be approximated by the much simpler expression

$$\theta^* \approx \sqrt{\frac{\gamma-1}{\gamma+1}}$$

For $\gamma = 1.3$, this approximate relation yields a value of θ^* close to the exact one (20.7°).

The Mach numbers in the neighborhood of the Mach disc indicate the nature of the flow in this region. Behind the incident shock, the Mach number is 7.3, behind the reflected shock, 4.64, and behind the Mach disc, 0.32. The pressure behind the Mach disc is about 2[illegible]% above the ambient value.

We expect that this criterion (the Mach disc locally normal to the flow) will somewhat overestimate its size. Since the subsonic flow must contract in order to lower its pressure, the streamline passing just below the triple point should be deflected slightly inwards. If the slip line were required to have a downward inclination of only 0.5°, the Mach disc radius would be reduced by about 40%. Although D'Attorre and Harshbarger have compared the locally normal criterion to a variety of experimental data and conclude that the triple point occurs close to this condition, the sensitivity of the size of the disc to the particular criterion chosen would make a more detailed study of the flow in this region desirable. In any case, the disc diameter appears to be sufficiently small in the present cases treated that its presence can probably be ignored for most practical purposes. Reference to Figures II-1 and II-2 shows that, at 180 km and $M_{\infty} = 4.3$, the disc diameter is less than one-tenth the maximum jet diameter. For these highly underexpanded jets, the scaling laws show that the diameter of the Mach disc (for a given nozzle) depends only on the values of the specific heat ratios and the value of the free stream Mach number (M_{∞}). Since 4.3 tends to be a lower limit to the Mach number during sustainer flight, the Mach disc will be even less important at other altitudes (see Figures II-4 and 6).

These conclusions are subject to the qualification that the vacuum flow near the axis is properly represented. For highly non-uniform nozzles the near axis flow may be improperly evaluated in the present calculation due to the smearing out of the Mach disc structure near the nozzle exit plane. A more realistic evaluation of this part of the flow would be required to evaluate in detail the influence of the nozzle non-uniformities on the downstream Mach disc structure.

IV-3. Viscous Effects

Since the altitude range of interest for the present study is 100 to 300 km, the viscous and non-continuum effects may have a significant influence on certain regions of the flow field. The free stream mean-free-path, for instance, is about the length of a typical vehicle (20m) at 135 km altitude. Thus the vehicle itself is in free-molecular flow over most of the altitude range. The Reynolds number and Knudsen number based upon free stream conditions and the plume nose radius vary over quite large ranges.

The photographic measurements of Rosenberg and his coworkers[42] indicate that the outline of the visible plume is roughly parabolic in shape and, at an altitude of about 180 km, the radius of curvature of the nose region for an Atlas or Titan vehicle is about 1 km. For a vehicle velocity of 4 km/sec at this altitude the Reynolds number based on the free stream velocity and density, the plume nose radius and the viscosity at the stagnation temperature ($\sim 9000^{\circ}K$ for no shock induced dissociation) is of the order of 30. (Here we have assumed a square root variation of viscosity with temperature).

Cheng has treated the evaluation of the flow field in the nose region of a hypersonic solid blunt body at low Reynolds number.[2] He has developed a thin two layer model for this calculation in which the evaluation of the shock layer is carried out independently of the evaluation of the "shock transition" region and the two profiles matched at their common boundary. At very high Reynolds numbers the "shock transition" region may be identified as the shock itself and the shock layer as the inviscid flow

behind it. At low Reynolds number (merged flow) the separation is a mathematical artifice.

In Fig. I-3 we have reproduced Cheng's Figure 5.3 in which he compares the thin two layer evaluation of the flow with that obtained by Levinsky and Yoshihara along the symmetry axis. Except for the wall boundary conditions, the flow conditions are similar to those expected at about 180 km altitude for nose regions of the plume of an Atlas or Titan vehicle. Reference to Fig.I-2 and to Fig. I-3 shows that viscous effects will be quite important in the nose region of the plume. Although, as Cheng points out, the good agreement between the two calculations is not an indication of the absolute accuracy of Cheng's method, it does give us confidence in extending the thin two layer procedure to the evaluation of the flow field induced by the rocket.

The importance of viscous effects far from the nose region is more difficult to evaluate. In the following paragraphs we go into some detail to get an estimate of the magnitude of the effect since this pretty well determines the approach required for the numerical calculations.

One measure of the importance of the viscous effects is the ratio δ_B/δ, where δ_B is a boundary layer thickness and δ is the thickness of the air shock layer assuming inviscid flow. If $\rho(\bar{r})$ and $u(\bar{r})$ are mean values for the density and velocity across the layer at the point where the boundary is displaced radius r from the axis, then

$$\frac{\delta}{r} \sim \frac{1}{2} \frac{\rho_\infty u_\infty}{\bar{\rho}\,\bar{u}}$$

In order to estimate the value of δ/r we note that, in the supersonic portion of the flow, $\bar{u}$ varies between $\sqrt{\frac{\gamma-1}{\gamma+1}}\, u_m$ and u_m where u_m is the

limiting velocity ($\simeq u_\infty$ for hypersonic flow). For $\gamma = 1.4$, $0.41 < \bar{u}/u_\infty < 1$.

The mean density may be estimated as follows. The density at any point in the inviscid air layer may be written in the form

$$\rho = \rho_s (p/p_s)^{1/\gamma} \tag{1}$$

where p is the local pressure and the subscript s refers to conditions on the given streamline just behind the air shock. When the air shock is strong (i.e., when $M_\infty^2 \sin^2\theta_B >> 1$ where $\tan\theta_B (= dr/dz)$ is the boundary slope)

$$p_s \sim \rho_\infty u_\infty^2 \sin^2\theta_B$$

and

$$\rho_s \simeq \frac{\gamma+1}{\gamma-1} \rho_\infty \tag{2}$$

Rosenberg's field observations indicate that the plume boundary is roughly parabolic:

$$r_B(z) \sim \sqrt{2R_n z} \tag{3}$$

where R_n is the nose radius. Thus, at the station z, the shock layer pressure is of the order

$$p \sim \rho_\infty u_\infty^2 / (1 + r^2/R_n^2). \tag{4}$$

As a mean value of the initial pressure p_s we choose the value

$$p_s \sim \rho_\infty u_\infty^2 / \left(1 + \frac{1}{2} (r/R_N)^2\right). \tag{5}$$

This is the value of p_s for the median streamline (on a mass flow basis). Thus, in the supersonic region (roughly $r > R_n$),

$$\frac{1}{2} \leq \bar{p}/p_s \leq \frac{3}{4} \tag{6}$$

or $3.65 \leq \bar{\rho}/\rho_\infty \leq 4.9$ for $\gamma = 1.4$.

Near the sonic line, therefore, $\overline{\rho u} \sim 2.0\ \rho_\infty u_\infty$ whereas far downstream $\overline{\rho u} \sim 3.6\ \rho_\infty u_\infty$. These values apply only to the region where the shock is strong. When $M_\infty \sin \theta_B \simeq 1$, the shock will begin to diverge from the exhaust plume and the shock layer width will begin to grow linearly with distance downstream. Also here the parabolic form of the boundary shape will become a poor approximation. Assuming a parabolic shape so long as $dr_B/dz > 1/M_\infty$, we estimate the value of the boundary radius at the point where the shock begins to diverge from the exhaust plume as

$$r' \sim M_\infty R_n .$$

Thus we expect the preceding approximations to be useful for boundary radii lying between R_n and $M_\infty R_n$.

Choosing an average value of $2.8\ \rho_\infty u_\infty$ for $\overline{\rho u}$ we obtain as a rough estimate of the air shock layer thickness the value

$$\delta \sim 0.2r$$

for $1 \leq r/R_n \leq M_\infty$. In the downstream supersonic portion of the shock layer we may roughly expect the boundary layer thickness to grow according to

$$\delta_B \sim \sqrt{z} ,$$

i.e., for a parabolic plume $\delta_B \sim r$. Thus the ratio of boundary layer thickness to shock layer thickness (δ_B/δ) appears to be roughly independent of radius for $R_n \leq r \leq M_\infty R_n$. For $r > M_\infty R_n$, however, we may expect the ratio of the boundary layer width to the shock-boundary separation distance to decrease roughly according to

$$\delta_B/\delta \sim z^{-1/2} .$$

Another measure of the importance of viscous effects is the ratio of the shock transition zone thickness to the shock layer width. For a normal

shock a measure of the shock thickness is

$$\Delta_S = \frac{v_2 - v_1}{(dv/dy)_{max}} \quad . \tag{7}$$

For Pr = Le = 1, $h + \frac{1}{2} v^2$ is constant through the shock and dv/dy is maximum at the sonic point. In this case the shock thickness may be expressed in the form

$$\Delta_S = \frac{\mu^*}{\rho_1 v_1} \frac{2\gamma}{\gamma+1} \left(\frac{M_1^*+1}{M_1^*-1} \right) . \tag{8}$$

Here μ^* is the viscosity at the sonic point and $M_1^* = v_1/a^*$ where a^* is the sound speed when M = 1. For an oblique shock having a wave angle θ, (assuming $\mu \sim \sqrt{T}$) the shock width may be expressed in the form

$$\Delta_S \sim C \frac{\sqrt{1 + \frac{\gamma-1}{2} M_\infty^2 \sin^2 \theta}}{M_\infty \sin \theta} \left(\frac{M_1^*+1}{M_1^*-1} \right) . \tag{9}$$

Here

$$M_1^* = \frac{M_\infty \sin \theta}{\sqrt{1 + \frac{\gamma-1}{\gamma+1} (M_\infty^2 \sin^2 \theta - 1)}}$$

and C is a constant dependent on the free stream conditions $\left(C = \frac{2\gamma}{\gamma+1} \left(\frac{\mu_1}{p_1 a_1} \right) \right)$.**

In a Mach 8 free stream with $\gamma = 1.40$, the shock transition widths and the shock layer widths are compared in the following table for a parabolic shock ($\tan \theta = dr/dz \sim R_n/R$):

**For air with $\gamma = 1.4$, $C = 5.8 \times 10^{-9}/\rho$ cm where ρ is in gms/cm^3 (at 180 km, $C \sim 10^4$ cm).

R/R_n	$M_\infty \sin\theta$	M_1^*	At 180 km with R_n = 1 km		
			δ km	ΔS km	$(\frac{\Delta S}{\delta})$
0	8.0	2.71	.16	.10	0.62[†]
1.0	5.69	2.27	.2	.12	0.62
2.0	3.58	2.07	.4	.15	0.38
4.0	1.94	1.60	.8	.29	0.37

Thus it appears that the ratio of shock transition width to shock layer width varies relatively slowly in the strong shock region ($1 \leq R/R_n < M_\infty$).

In the outer region ($R/R_n > M_\infty$), where the shock is weak, the shock width Δ_S increases proportional to $\frac{1}{M_1^*-1}$. In other words, when the shock is weak, $\Delta_S \sim \frac{1}{\Delta p}$ where Δp is the pressure jump across the shock. Far from the exhaust gas structure, the wave is expected to develop an N-wave form. The strength of the trailing shock of the N-wave depends on the extent to which the boundary pressure drops below ambient. The amplitude of the wave, neglecting the viscous effects, decreases according to

$$\Delta p \sim R^{-3/4}$$

whereas the characteristic width of the wave form increases as $R^{1/4}$ (Whitham, 1952; Bethe, 1948). Thus the shock thickness varies as $R^{3/4}$ and the ratio of shock thickness to N-wave width increases as $\sqrt{R}$. At sufficiently large radii, therefore, the N-wave structure will be engulfed by the shock transition region. At larger radii the wave appears as a smooth acoustic pulse traveling at the local sound speed. If the viscous

[†]For the nose region, we estimate δ as 0.16 R_n (see Section IV-2c).

attenuation were negligible, the wave shape would be maintained and the amplitude would decay as $R^{-1/2}$. However, because of the viscosity, the wave is both distorted and attenuated. Since the attenuation depends strongly on wavenumber, the change of the wave shape is best examined by considering its Fourier components.

For weak sound waves the viscous equation of motion may be written in the form

$$\frac{\partial^2 \delta}{\partial t^2} = c^2 \frac{\partial^2 \delta}{\partial x^2} + \frac{4\mu}{3\rho} \frac{\partial^2}{\partial x^2} \left(\frac{\partial \delta}{\partial t} \right) \tag{10}$$

where δ is the local displacement. For $\delta = \delta_o e^{i\omega t - ikx}$ we have the dispersion relation:

$$c^2 k^2 = \omega^2 / \left(1 + i \frac{4\mu\omega}{3\rho c^2} \right) . \tag{11}$$

Assuming the viscous term is small, we may write

$$k \simeq k_o - i \frac{4\mu}{3\rho c} k_o^2 \tag{12}$$

where $k_o = \omega/c$. Thus the absorption coefficient is

$$L_a^{-1} = 4\mu k_o^2 / 3\rho c = 4\mu (2\pi)^2 / 3\rho c \lambda_o^2 \tag{13}$$

where λ_o is the wavelength of the disturbance. An examination of the geometry of N-wave formation indicates that an N-wave wavelength (λ_o) of the order of $M_\infty R_N$ may be expected. The numerical calculations of the flow at 180 km for $M_\infty = 4.3$ indicate that an estimate of about 4 times $M_\infty R_N$ is more realistic. At 180 km this corresponds to about 20 km for a typical Atlas or Titan vehicle, implying an N-wave damping distance of about 100 km. Since considerations of the scaling of the plume shape with altitude[9] (see also Section II-2) indicate that the term $\rho_\infty R_N^2 M_\infty^2$ is expected to vary

little with altitude, the N-wave damping distance is also roughly independent of altitude. Note that these considerations really only apply to a vertical trajectory where atmospheric stratification effects are not too important. At these altitudes the atmospheric scale height is about 50 km. For non-vertical trajectories the mode of decay of the N-wave is more complicated. The motion in the horizontal plane will be roughly similar to that in a non-stratified atmosphere but propagation in the vertical direction will be distorted by the atmospheric stratification. In any case, at very high altitudes where the plume dimensions become appreciable compared to the N-wave damping length, N-wave formation is not expected. At the lower altitudes with which we are primarily concerned, a disturbance will propagate away from the plume but the high frequency components will be largely absorbed within a few tens of kilometers from the plume axis. Only the low frequency components will persist to large radii.

IV-3a. THE SUPERSONIC MERGED LAYER CALCULATION

In the two layer flow model the flow field is divided into two regions: the shock layer and the shock transition zone. Following Cheng,[2] we denote the interface separating these regions as the "shock interface." In general the shock layer is the region between the air shock transition zone and the jet shock transition zone. We first consider the equations of motion in the shock layer.

The basic assumption (equivalent to the thin layer assumption) is that heat, momentum or species diffusion parallel to the streamlines may be neglected compared with the lateral transport (i.e., $\frac{\partial}{\partial y} \gg \frac{\partial}{\partial s}$). With this assumption the Navier-Stokes equations may be reduced to the form:

$$\text{div } \rho\vec{u} = 0 \tag{1}$$

$$u \frac{\partial u}{\partial s} + \frac{1}{\rho} \frac{\partial p}{\partial s} = \frac{1}{\rho} \frac{\partial}{\partial y}\left(\mu \frac{\partial u}{\partial y}\right) \tag{2}$$

$$u \frac{\partial H}{\partial s} = \frac{1}{\rho} \frac{\partial}{\partial y}\left(\mu \frac{\partial}{\partial y}\left[H + \left(\frac{1}{Pr} - 1\right) h\right]\right) + \frac{\mu}{\rho} \frac{u^2}{3} \left(\frac{\partial \varphi}{\partial y}\right)^2 \tag{3}$$

$$u^2 \frac{\partial \varphi}{\partial s} = - \frac{1}{\rho} \frac{\partial p}{\partial y} + \frac{4}{3\rho} \frac{\partial}{\partial y}\left(\mu u \frac{\partial \varphi}{\partial y}\right) \tag{4}$$

Equation 2-2 may be written in the form

$$T \frac{\partial S}{\partial s} = \frac{\partial H}{\partial s} - \frac{1}{\rho} \frac{\partial}{\partial y}\left(\mu \frac{\partial u}{\partial y}\right) \tag{5}$$

When the viscous effects are significant only the continuity equation may be directly integrated along streamlines:

$$\rho u A = \text{constant.} \tag{6}$$

Equations 3, 4, 5, and 6 plus the equation of state form a convenient set for the finite difference procedure. Here the marching procedure is to be carried out in a manner similar to the inviscid case except that Eqs. 3 and 5 are used to evaluate the change of the stagnation enthalpy and the entropy along streamlines.

For the present problem we will assume, at least initially, that the diffusion may be described in terms of a single binary diffusion coefficient. With this assumption the continuity equation for each species is

$$v \frac{\partial c_i}{\partial s} = \frac{1}{\rho} \frac{\partial}{\partial y}\left(\frac{\mu}{Pr} \frac{\partial c_i}{\partial y}\right) + \frac{\omega_i}{\rho} \tag{7}$$

where c_i is the mass fraction of the ith species and ω_i the mass rate of formation of the ith species per unit volume per second due to chemical reaction. In the present study chemical reactions are expected to have a negligible influence on the flow field, so that setting $\omega_i = 0$ is expected to be a reasonable approximation. With these approximations Equation 7 is decoupled from the other flow equations and thus may be used to determine the species distribution, but is not required to determine the total density and temperature distribution. This is strictly true only when the local mean molecular weight does not vary through the mixing layer. However, since the purpose of monitoring the species diffusion is primarily to determine the mean specific heat and the air partial density, this approximation is considered to be a reasonable first approach.

IV-3b. THE MODIFIED RANKINE-HUGONIOT RELATIONS

The shock transition zone equations (given in the following section) when evaluated at the shock interface, yield a modified set of Rankine-Hugoniot equations which are to be used as the boundary conditions for the calculation of the shock layer. When the external flow is a uniform stream having a density ρ_∞, a pressure p_∞, velocity U_∞ and stagnation enthalpy H_∞, these modified equations have the form:

$$\rho_\infty U_\infty \sin\psi\left[u_2 \cos(\psi - \varphi_2) - U_\infty \cos\psi\right] = -\left[\mu \frac{\partial}{\partial y}\left(u \cos(\psi - \varphi)\right)\right]_2 \tag{1}$$

$$p_2 - p_\infty + \rho_\infty U_\infty \sin\psi\left[u_2 \sin(\psi - \varphi_2) - U_\infty \sin\psi\right] \tag{2}$$

$$= \frac{4}{3}\left[\mu \frac{\partial}{\partial y}(u \sin(\psi - \varphi))\right]_2 \tag{3}$$

$$\rho_\infty U_\infty \sin\psi\left[H_2 - H_\infty\right] = -\left[\mu \frac{\partial}{\partial y}\left(H + \left(\frac{1}{P_r} - 1\right)u + \frac{u^2}{6}\sin^2(\psi - \varphi)\right)\right]_2 \tag{4}$$

and

$$\rho_\infty U_\infty \sin\psi = \rho_2 u_2 \sin(\psi - \varphi_2). \tag{5}$$

Here $\tan\psi$ is the slope of the shock interface and the subscript 2 refers to conditions in the shock layer evaluated at the shock interface. For a non-uniform stream such as the internal jet flow, appropriately modified equations are required. In the transport terms of these equations some factors of the order of $\cos(\psi - \varphi_2)$ have been set equal to unity (here $\psi - \varphi_2$ is the angle between the shock and the local streamline direction). Thus these equations are useful for shock angles such that the angle $(\psi - \varphi)_2$ is small. This latter condition is not too restrictive in the downstream

flow when the free stream is hypersonic since, for example, for $\gamma = 1.4$ and $M_\infty = 6.0$, $\nu - \omega_2$ is less than 19° when the Mach number behind the shock is greater than 1.3.

When μ is set equal to zero in Equations 1 to 5, they reduce to the normal Hugoniot relations.

IV-3c. THE SHOCK TRANSITION ZONE CALCULATION

The basic approximation made in the two layer model is that diffusion fluxes are significant only in one direction, which is essentially specified to be one of the coordinate directions. In the supersonic shock layer this direction is assumed to be the orthogonal to the streamlines. In the shock transition region the appropriate direction is normal to the shock interface. In order that a reasonable approximation be obtained these two directions should differ by only a small angle at the matching boundary, the shock interface. In the nose region the shock layer coordinates are chosen as the normals to the body surface and the associated orthogonal surfaces. The small angle condition requires that the shock and the body surface be approximately concentric. This will normally be satisfied in hypersonic flow. In the downstream supersonic flow we require that, at the shock interface, the streamline normal makes only a small angle with the interface normal. This condition is usually approximated in hypersonic flow. Far downstream, where the shock is weak, the angle between these two normals approaches $(M_\infty)^{-1}$. In the intermediate region where $M_\infty^2 \sin^2\psi \gg 1$ but ψ is not too large (ψ is the wave angle of the shock) this difference angle is of the order of $\frac{\gamma-1}{2}$. Thus the two-layer approximation is expected to be useful for hypersonic flow for small values of $(\gamma-1)/2$.

For the shock transition region, Cheng chooses a coordinate system in which $y = 0$ corresponds to the shock interface. Here gradients parallel to the shock interface are to be neglected. With these approximations we may write (Cheng's Equation (5.7))

$$\frac{\partial}{\partial y}(\rho v) = 0 \qquad (1)$$

$$\rho v \frac{\partial u}{\partial y} = \frac{\partial}{\partial y}\left(\mu \frac{\partial u}{\partial y}\right) \tag{2}$$

$$\frac{\partial p}{\partial y} + \rho v \frac{\partial v}{\partial y} = \frac{4}{3}\frac{\partial}{\partial y}\left(\mu \frac{\partial v}{\partial y}\right) \tag{3}$$

$$\rho v \frac{\partial H}{\partial y} = \frac{\partial}{\partial y}\left(\mu \frac{\partial}{\partial y}\left[H + \left(\frac{1}{P_r} - 1\right) h + \frac{v^2}{6}\right]\right) \tag{4}$$

Here v is the velocity normal to the shock interface and y the distance along the normal.

The free stream boundary conditions are: $p_1 = p_\infty$, $\rho_1 = \rho_\infty$, $h_1 = h_\infty$ $u_1 = U_\infty \cos \psi$ and $v_1 = U_\infty \sin \psi$ where $\tan \psi$ the local slope of the shock interface.

Integrating these equations across the shock transition zone we get for arbitrary strength shocks the relations

$$\rho v = \rho_1 v_1 \tag{5}$$

$$p + \rho_1 v_1 v = \frac{4}{3}\mu \frac{\partial v}{\partial y} + p_1 + \rho_1 v_1^2 \tag{6}$$

$$\rho_1 v_1 u = \mu \frac{\partial u}{\partial y} + \rho_1 v_1 u_1 \tag{7}$$

$$\rho_1 v_1 H = \mu \frac{\partial}{\partial y}\left(H + \left(\frac{1}{P_r} - 1\right)h + \frac{v^2}{6}\right) + \rho_1 v_1 H_1 \tag{8}$$

This set of ordinary differential equations may be directly integrated to give the shock transition zone structure. Here the method would be to start at the shock interface with the values of the flow parameters that were obtained from the shock layer calculation and integrate outwards along the normal to the shock interface.

When the Prandtl number has the particular value 3/4 these equations may be reduced to a single quadrature. Since expected values are of this order (0.70-0.72), we have utilized this approximation to evaluate the shock profiles.

IV-3d. THE NOSE MERGED LAYER

This is the problem that Cheng treats for the nose region of a blunt body. The shock transition zone equations are those given in Section IV-3c and are the same as for the downstream portion of the flow. There are two essential differences in the shock layer calculation between the nose region and the downstream region. First, in the nose region it is assumed that the diffusive fluxes occur in the direction parallel to the local normal drawn out from the body surface instead of being normal to the local streamline direction. Second, since the flow equations are elliptic in the subsonic region, the momentum equations are altered to convert the equations to a set of parabolic equations. The resulting set of equations (given by Hayes and Probstein [34]) is

$$\frac{\partial}{\partial x}(\rho\, u\, r) + \frac{\partial}{\partial y}(\rho\, v\, r) = 0 \tag{1}$$

$$\frac{\partial p}{\partial x} - \rho\, K_c\, u\, v + \rho\left(u\,\frac{\partial u}{\partial x} + v\,\frac{\partial u}{\partial y}\right) = \frac{\partial}{\partial y}\left(\mu\,\frac{\partial u}{\partial y}\right) \tag{2}$$

$$\frac{\partial p}{\partial y} + \rho\, K_c\, u^2 + \rho\left(u\,\frac{\partial v}{\partial x} + v\,\frac{\partial v}{\partial y}\right) = \frac{4}{3}\frac{\partial}{\partial y}\left(\mu\,\frac{\partial v}{\partial y}\right) \tag{3}$$

$$\rho\left(u\,\frac{\partial H}{\partial x} + v\,\frac{\partial H}{\partial y}\right) = \frac{\partial}{\partial y}\left(\mu\,\frac{\partial}{\partial y}\left(\frac{h}{P_r} + \frac{u^2}{2} + \frac{2}{3}\,v^2\right)\right) \tag{4}$$

Here u is the x component of velocity, v the y component, y the distance along the outward normal and x the distance along a surface parallel to the body surface. $K_c = K_c(x)$ is the curvature of the body surface (of the dividing streamline in the jet case). In the case of the jet we would take one of the streamlines which originate at the nozzle lip as the dividing

streamline. For the flow inside this streamline we use the supersonic formalism of Sec. IV-2a and the above formalism for the flow outside this region. An appropriate matching condition is required at the dividing streamline: equal pressure, equal and parallel velocity and equal transverse fluxes. From this boundary condition would come the equation that specified $K_c(x)$.

Since the symmetry axis contains a singular point, the stagnation point, a method for starting the marching process is required. For the blunt body problem, Cheng expands the equations in a Taylor series about $x = 0$ and solves for the zeroth and first order terms. A similar procedure may be possible for the jet.

An alternate approach is to solve the inviscid jet flow assuming the dividing streamline pressure is that given by Newtonian theory. Then, using the thus determined nose radius for the exhaust plume, obtain the starting conditions for the marching process using Cheng's expansion procedure.

The change-over from the subsonic nose calculation to the supersonic downstream calculation does not have to be made right at the sonic point. It should be made downstream at a point where the angle between the shock and the adjacent internal streamline is small but not so far downstream that the streamline curvature varies significantly across the shock layer.

IV-3e. Small Disturbance Approximation

An approximation which has proved very useful in the treatment of the flow around hypersonic slender bodies is the so-called small disturbance approximation. Here it is assumed that the steady two-dimensional axisymmetric flow about the body is equivalent to a one-dimensional unsteady flow that would be seen by an observer at rest in the ambient atmosphere. The requirement for the validity of this approximation is that the perturbations in the axial component of the velocity be negligibly small. If a characteristic deflection angle for the flow is τ, then the perturbation in the axial component of the velocity is of the order of $u(1 - \cos \tau)$ or $\frac{u\tau^2}{2}$. In order that this velocity perturbation induce only a slight pressure variation, it should be small compared to the local sound speed. In other words, the small disturbance approximation will prove useful when

$$M\tau^2 \ll 1$$

where τ is a characteristic flow inclination. The free stream Mach numbers experienced by a typical missile traveling through the ionosphere range between 4 and 12. Thus we expect that the small disturbance approximation will prove useful when the flow inclinations are less than about 5 degrees. In air the shock wave from a vehicle traveling at a Mach number of 5 will give rise to a deflection of less than 5 degrees at distances downstream where the pressure jump across the shock is less than a factor of 2. Thus the small disturbance approximation will be strictly valid only for the far field part of the flow. For the near field the more complicated two-dimensional steady equations are required.

The one-dimensional flow equations may be written in the form:

$$\rho \frac{DH}{Dt} = \frac{\partial p}{\partial t} + \frac{1}{y^J} \frac{\partial}{\partial y} \left(y^J \frac{\mu}{Pr} \left[\frac{\partial H}{\partial y} + \frac{1}{2} \left(\frac{4}{3} Pr - 1 \right) \frac{\partial u^2}{\partial y} \right] \right) \tag{1}$$

$$\rho \frac{Du}{Dt} = - \frac{\partial r}{\partial y} + \frac{1}{y^J} \frac{\partial}{\partial y} \left(\frac{4}{3} y^J \mu \frac{\partial u}{\partial y} \right) \tag{2}$$

$$\frac{1}{\rho} \frac{D\rho}{Dt} = - \frac{1}{y^J} \frac{\partial (u y^J)}{\partial y} \tag{3}$$

where

$$H = h + \frac{1}{2} u^2 \tag{4}$$

and

$$p = \frac{\gamma - 1}{\gamma} \rho \left(H - \frac{u^2}{2} \right) . \tag{5}$$

Here J = 0 for planar, J = 1 for axially symmetric, and J = 2 for spherically symmetric flows. These equations may be recast in a form more convenient for numerical evaluation:

$$\frac{Dh}{Dt} = \frac{c_p}{c_p - R} \left\{ \frac{1}{\rho y^J} \frac{\partial f_q}{\partial y} - \left(\frac{h}{c_p} - \frac{f_p}{\rho y^J} \right) \frac{\partial u}{\partial y} \right\} \tag{6}$$

$$\frac{Du}{Dt} = - \frac{1}{\rho} \frac{\partial p}{\partial y} + \frac{1}{\rho y^J} \frac{\partial f_p}{\partial y} \tag{7}$$

$$\frac{D}{Dt} (\rho y^J \Delta y) = 0 \tag{8}$$

$$\frac{Dy}{Dt} = 0 \tag{9}$$

where

$$f_p = \frac{4}{3} y^J \mu \frac{\partial u}{\partial y}$$

$$f_q = \frac{\mu}{Pr} y^J \frac{\partial h}{\partial y}$$

$$\rho = \rho h / c_p$$

Here y is the mass point coordinate and Δy the spacing between two adjacent points. These equations have been programmed for the IBM 7090. Representative flow distributions calculated for a simulated sustainer engine at 290 km altitude are shown in Figures

The Air-Jet Mixing Layer - Boundary Layer Approximation

At sufficiently low altitudes the mixing layer at the jet-air interface will remain thin compared to the shock layer thickness if it remains laminar. In order to estimate the importance of the viscous dissipation at the jet-air interface a much simplified model has been used to evaluate the mixing layer profile at low altitudes. Although the mixing layer is unstable to become turbulent, it is expected that the time required for transition to take place will be long compared to the flow time (through the major part of the jet) at least at the higher altitudes.

In order to obtain an easily applied analysis two approximations have been made: first; that the mixing layer remains sufficiently thin that the variation of the inviscid flow field properties across the mixing layer is negligible; second, that the rate of change of the inviscid flow field with distance downstream is sufficiently slow that the mixing layer profile may be assumed to be self-preserving. In this approximation it can be shown that the air-jet mixing layer profile is equivalent to that between two parallel and uniform streams. It turns out, however, that even for the lower altitudes of our interest neither of these two approximations may be expected to be very good - particularly the former. In Figure IV-1 we show density, pressure, and temperature distribution in the neighborhood of the boundary calculated for the 25:1 engine at 135 km altitude assuming no viscous transfer. Also in Figure IV-1 we show the self-preserving mixing layer profile calculated assuming that the conditions at the jet-air boundary were maintained

across the mixing layer. Reference to this figure shows that, especially in the jet shock layer, the inviscid pressure and density both vary strongly across the mixing layer.

Because of the strong variation of the temperature and density across the jet shock layer the calculated self-preserving profile cannot be expected to be too meaningful. Techniques are available which will allow, in an approximate manner, for some variations in the free stream flow outside the mixing layer. However, since it appears that, at least above 135 km altitude, the jet shock layer may be completely merged, it appears that, at the very least, a viscous layer calculation will be required to evaluate the entire shock layer.

Thus, for the present, it does not appear too useful to try and refine this mixing layer calculation in the boundary layer approximation. The description of the analysis of the mixing layer keeping the self-preserving assumption will be reported subsequently. In brief the procedure is to treat the equivalent mixing layer between two uniform free streams. Here the equations admit a similarity solution in the classical compressible boundary layer approximation. The Von Karman-Pohlhausen method is used to obtain an approximation of the solution to these equations.[43] The procedure has been programmed for the IBM 7090 computer.

The basic conclusion of this analysis is that the jet shock layer will be strongly affected by the diffusive fluxes. In our present description of the electron distribution, the neutral density distribution within the jet region may exert a strong influence on the electron distribution. Thus it appears necessary to obtain a considerably more sophisticated description of the jet flow than that resulting from a simple self-preserving boundary layer approach.

IV-3g. Evaluation of the Initial Flow Distribution at Very High Altitudes in the Collisionless Approximation

The mixing layer calculations carried out at 135 km altitude indicate that the jet shock layer may be completely merged even at this relatively low altitude. Although at this altitude the shock widths are relatively thin compared to the shock layer thicknesses, this will not be the case at very high altitudes. At sufficiently high altitudes that the shock layer width is comparable to a mean free path, the flow will be poorly described by the continuum equations. This situation is approached in the bow region at altitudes above 200 km.

An alternate approach to a complete continuum calculation is to compute the early non-continuum part of the flow assuming zero interaction of the exhaust gases with the ambient atmosphere (cross sections for collisions between exhaust molecules and air molecules vanish), and then, at some more or less arbitrary time, start a one-fluid continuum calculation. This is a particularly useful procedure at high altitudes from a numerical point of view, since a large amount of computing time is normally required to compute the flow close to the vehicle when the continuum equations are used throughout.

We first of all consider this collisionless approximation of the initial flow in the small disturbance approximation. The small disturbance approximation gives a useful description of the flow field when the axial gradients of the various flow properties are small compared to the radial gradients and may be neglected. If, in addition, the variation of the axial component of the velocity is small across the entire flow field, a Galilean transformation

may be used to transform the steady state two dimensional flow to a one dimensional unsteady flow problem. We restrict the present discussion to this case.

Suppose the vehicle velocity relative to the atmosphere is V_m. We assume therefore that the axial component of the exhaust gas velocity relative to the vehicle is also V_m. At high altitudes V_m is therefore related to the enthalpy release in the combustion chamber by the expression

$$V_m = \sqrt{2 h_c} \tag{1}$$

where h_c is in units of ergs per gram. At very high altitudes the exhaust flow close to vehicle is source-like. Thus we may write (see Section IV-2b)

$$\rho = \frac{\dot{m} f(\varphi) \sin^2 \varphi}{V_m r^2} \tag{2}$$

where

$$\varphi = \tan^{-1} r/z \ , \tag{3}$$

and

$$2\pi \int_0^{\pi} f(\varphi) \sin \varphi \, d\varphi = 1 \ , \tag{4}$$

r is the radial displacement from the symmetry axis and z the axial distance ($z \approx V_m t$). The radial component, v, of the velocity is $V_m \sin \varphi$. If $\dot{m}$ is the total exhaust mass flow rate, then $\dot{m}/V_m$ is the mass deposited per unit length along the trajectory. The fraction of the exhaust flow that has a radial velocity between v and v + dv is given by, approximately,

$$\frac{1}{\dot{m}} \frac{d\dot{m}}{dv} = 2\pi \frac{f(\varphi)}{V_m} \tan \varphi \tag{5}$$

where $\sin \varphi = v/V_m$.

For the vacuum expansion the radial velocity as a function of radius and time is

$$v = r/t \tag{6}$$

The exhaust gas density as a function of radius and time is (for $R < V_m t$)

$$\rho = \frac{\dot{m}}{V_m^3} \frac{f(\varphi)}{t^2} \tag{7}$$

where $\varphi = \sin^{-1} \left(\frac{r}{V_m t}\right)$. A useful approximation for $f(\varphi)$ is $a \left(\cos \frac{\pi}{2} \varphi/\theta_\infty\right)^{\frac{2}{\gamma-1}}$ for $\varphi < \theta_\infty$ (see Section IV·2b) where θ_∞ is the limiting expansion angle. In this small disturbance approximation θ_∞ is assumed less than unity.

In order to initiate a continuum calculation, we require the mean fluid properties to be specified in terms of a one fluid model. The mean fluid velocity will be given by

$$v = \rho_e v_e / [\rho_a + \rho_e] \tag{8}$$

where ρ_a is the ambient density.

The fluid density is given by

$$\rho = \rho_e + \rho_a \tag{9}$$

and the enthalpy by

$$h = [\rho_a h_a + \tfrac{1}{2} \rho_e v_e^2 - \tfrac{1}{2} \rho\ v^2] \frac{1}{\rho} \quad . \tag{10}$$

In Fig. IV-13, we show the collisionless approximation to the flow field at an altitude of about 290 km.

This model gives an accurate description of the flow only when the

mean free path for exhaust-air collisions at all points in the flow field is larger than the flow field dimension. Although this condition is not even approached in the rocket flow field at any altitude of interest, nevertheless this approximation provides a useful representation of certain aspects of the flow while retaining a very simple analytic structure. In the remainder of this section we examine the validity of the collisionless approximation.

It should be emphasized at this point that, in these approximations, we are primarily concerned with the early part of the flow (i.e., the bow region of the plume). As will be apparent in the ensuing discussion, the specific criterion is that the exhaust gas density on the axis of symmetry be much larger than that of the ambient atmosphere. In order to get a better understanding of the approximations involved we will first consider another simplified but more accurate description of the early part of the flow. Here we assume that, in the region where collisions of ambient molecules with exhaust molecules occur, the exhaust gas density is much larger than the ambient gas density. As long as the effect of the ambient atmosphere is small, the exhaust gas density rises from zero at the edge of the vacuum plume with a high power $(\frac{2}{\gamma-1})$ of the distance from the edge (see Section IV-2b). Close to this edge the exhaust gas temperature is near zero and the velocity attains its limiting value, V_m. In a coordinate system moving with the exhaust gas the ambient atmosphere appears to impinge on the stationary exhaust molecules with a velocity V_m.

Let us consider first the sequence of events which occur during the expansion when the molecular weight of the atmospheric species is much larger

than that of the exhaust gases. This would apply to a rocket exhausting pure hydrogen, for example. In this case the atmospheric molecules penetrate deeply into the exhaust gases losing small amounts of momentum and energy at each collision. The fractional energy loss per collision is of the order ϵ, where ϵ is twice the mass ratio, and the average scattering angle is $\epsilon/2$. The kinetic energy is reduced by an order of magnitude after about $1.2/\epsilon$ collisions. The rms scattering angle at this point is of the order $\sqrt{\epsilon/2}$ radians. Thus, when the exhaust molecules are light, the atmospheric molecules penetrate the exhaust in essentially straight lines and come to rest with respect to the exhaust molecules after a few collisions. The kinetic energy is dissipated in heating the exhaust. Until such time that the fractional concentration of atmospheric molecules becomes significant, the increase in the exhaust gas temperature is slight. Because of the strong rate of increase of exhaust gas density with distance, the bombarding molecules will all be stopped at roughly the same depth. Thus, in this model, we expect a snowplow action in which ambient molecules are swept up into a thin layer located some distance from the plume edge. Initially, the density of ions in this layer increases at a constant rate. This process will continue until the deposited energy raises the temperature of the mixture sufficiently to cause an expansion of the gas into the oncoming flow. This constitutes the development of the shock layer. A non-continuum transient period now follows as the shock layer becomes fully developed. In the fully developed state we expect that the peak electron density will be limited to the value corresponding to a strong shock. Thus, according to this model the electron density may go through a maximum as the flow develops.

This maximum value may or may not exceed the value expected behind a strong shock.

The opposite situation obtains in the other limiting case when the molecular weight of the atmospheric molecules is much smaller than that of the exhaust gases. Here again there is little energy transfer per collision but the average scattering angle is large. The incoming molecules emerge from the exhaust gas structure after a few collisions with essentially the same energy with which they entered but are traveling in random directions. In this approximation the exhaust gas acts like a rigid, diffusely reflecting, adiabatic wall. The atmospheric shock layer will be established in front of it in a few collision times. In this limit, the electron density is expected to rise smoothly to its maximum value.

In cases of practical interest the molecular weights of the exhaust gas and of the ambient atmosphere are comparable. Thus we expect a state intermediate between the two models described above. Since the structure of the shock layer is considerably different in these two limiting models, it would appear that a fairly detailed description of this non-continuum regime is required to obtain a reasonably accurate description of the flow. Attempts in this direction have not, in general, met with much success. The approach usually invoked is to assume that the continuum Navier-Stokes equations apply throughout the flow. In this case, even though the distribution functions are not Maxwellian, a one-fluid model is used in which a unique temperature and stream velocity is assigned to each point in the flow.

The collisionless approximation (defined by Eqs. 8, 9, and 10). is equivalent, near the plume edge, to a one-fluid approximation of the heavy atmospheric molecule case. However, this simple prescription fails

in the neighborhood of the thin layer where most of the atmospheric molecules collect. Rough calculations of the density of atmospheric molecules in this layer indicate that the fractional concentration of air here is of the order

where ϵ is the fractional energy loss per collision ($\epsilon \approx 2\ m/M$), γ is the specific heat ratio, R the exhaust gas radius, λ_a the mean free path in the ambient atmosphere, n_a the number density in the ambient and n_c the number density on the axis of symmetry. This expression is useful when both $(\gamma+1)/(\gamma-1)$ and the density ratio n_c/n_a have large values. For our conditions we expect values of the density ratio between 10^4 and unity. For $\gamma = 1.4$, and $\epsilon \simeq 0.3$, for example, the fractional concentration in the deposition layer is then of the order 0.1 to 0.5 times $(R/\lambda_{amb})^{5/6}$. Thus we expect the collisionless approximation to be useful so long as the radius of the vacuum boundary is smaller than the mean free path in the ambient atmosphere. At later times in the expansion the heating of the exhaust gases by the entrained atmosphere will result in the development of an appreciable shock layer structure.

This procedure has been used to provide initial profiles for a small disturbance calculation of the flow field at very high altitude (290 km). In a small disturbance approximation, the flow is assumed identical to an

unsteady cylindrically symmetric viscous expansion. A solution of the one-dimensional unsteady Navier-Stokes equations has been obtained numerically using a finite difference procedure. The density, velocity and pressure distribution at various times are shown in Figs. II-18, 19, and 20. The calculation was initiated 0.6 seconds after the exhaust gas was expelled from the nozzle and used the collisionless representation as the initial state. At this time the radius of the exhaust plume was about 2 km. Since the mean free path at this altitude is about 1.5 km, the collisionless approximation is expected to be unreliable after this time. In Fig. II-21 we have plotted, versus time, the radius of the cylinder containing a mass equal to that of the exhaust products. Also shown in Fig. II-21 is the locus of the points of equal exhaust-air mass fraction. The dividing streamline, which bounds a mass equal to that of the exhaust gases, expands rapidly for 20 seconds at which time it attains its maximum value of about 15 km. After this, it contracts slightly, reaching a minimum of 13 km at 50 seconds. After 44 seconds, the exhaust gases are so diluted with air that nowhere does the fractional air concentration drop below 50%.

Although the collisionless representation is not expected to be valid when the plume radius is greater than the ambient mean free path, it apparently gives a rough approximation of some features of the flow field throughout the early part of the expansion even when the radius considerably exceeds the mean free path. In Fig. II-22 we have plotted the velocity and density profiles at 3.2 and 6.5 seconds. References to this figure show that the collisionless approximation gives quite a reasonable, although smoothed out, representation of the velocity profile even at these relatively late times. The density

distribution is less well represented, especially in the shock layer region. Nevertheless, since the gross features of the flow are reasonably well reproduced, the very simple analytic form of this approximation makes it quite useful for eliciting qualitative and semi-quantitative information about the interaction of the ionized species with the neutral wind during the early part of the expansion.

So far we have only considered a cylindrical expansion. It is expected that similar agreement (and lack of agreement) may be expected in the more general axially symmetric case. Even the general three dimensional problem of a rocket traveling in a stratified atmosphere is trivially formulated in this collisionless approximation.

IV-3h. Kinetic Effects

The calculations carried out at 180 km indicate that the high temperature region is confined to a small volume in the bow region of the plume. Although the stagnation temperature of the air stream is relatively high (~ 6500°K at 180 km altitude) the cooling of the air stream by the outward diffusion of the cold exhaust gases maintains the gases at relatively low temperatures. The high temperature, low density entropy layer that would exist adjacent to the jet boundary if the diffusive effects were negligible, does not occur at these altitudes (see Figure II-12).

In Figures II-16 and 17 we show the temperature and density histories along two characteristic streamlines. The streamline locations are shown in Figure II-1. Reference to these figures indicates that, even for fluid elements which enter the air shock layer relatively close to the stagnation point, the temperature exceeds 2000°K for less than a second. Since the collision frequency in the nose region is less than 100 sec^{-1} only reactions having fairly high rate coefficients and low activation energies can be important.

At this altitude the atmosphere is compared primarily of N_2 and O. Reference 44 gives the mole fractions of N_2, O and O_2 as 0.55, 0.39 and 0.06 respectively. Even the most likely ionization reaction between the air constituents

$$N_2 + O \rightarrow NO + N$$

followed by

$$N + O \rightarrow NO^+ + e$$

will produce a negligible increase in the electron density. The mixing of the exhaust constituents with the ambient atomic oxygen may produce significant reaction.

Molecular hydrogen present in the exhaust gases will react with atomic oxygen according to

$$H_2 + O \rightarrow OH + H$$

Kaskan and Browne recommend a reaction rate of $3.3 \times 10^{12} \; e^{-3600°K/T} \; cm^3/mole\text{-}sec$.[45] Thus, along streamline a (see Figure II-1) the fraction of the hydrogen that reacts with atomic oxygen is estimated to be one or two per cent.

Observations by Rosenberg indicate the CH radical is present in the exhaust products of Atlas and Titan I vehicles.[46] It may form part of one of the products discharged from the gas generators. Since these products will be concentrated at the periphery of the plume, we may characterize their environment as similar to that on streamline a. CH can give rise to ionization via the reaction

$$CH + O \rightarrow CHO^+ + e.$$

This reaction is considered to be a source of chemionization in hydrocarbon flames. Calcote gives a value of about 2×10^{12} $cm^3/mole\text{-}sec$ for the rate coefficient.[47]

This value implies that 10 to 20 per cent of the available CH radicals will yield free electrons. The concentration of CH in the exhaust gases in not known. In the Atlas engine about three per cent of the total mass flow is diverted through the gas generators. Since this portion of fuel flow is burnt at very rich conditions it is expected that a variety of hydrocarbons will be present. If more than one per cent of this mass flow results in the CH radical, the resulting contribution to the electron content of the flow field may be significant at this altitude. This source of ionization will be more important at lower altitudes and less at higher altitudes. However, it is difficult to determine its absolute importance without a more precise definition of the exhaust composition.

Glass quotes a value for the rate constant of acetelyne with atomic oxygen at low temperatures of 2×10^{-13} cm^3/sec.[48] For this value, we would expect about 1% of the available acetylene to react along streamline a. Since only a fraction of the flow will be hydrocarbons and only a fraction of those that do react with atomic oxygen will yield CH, this source of chemiionization may not be of major importance.

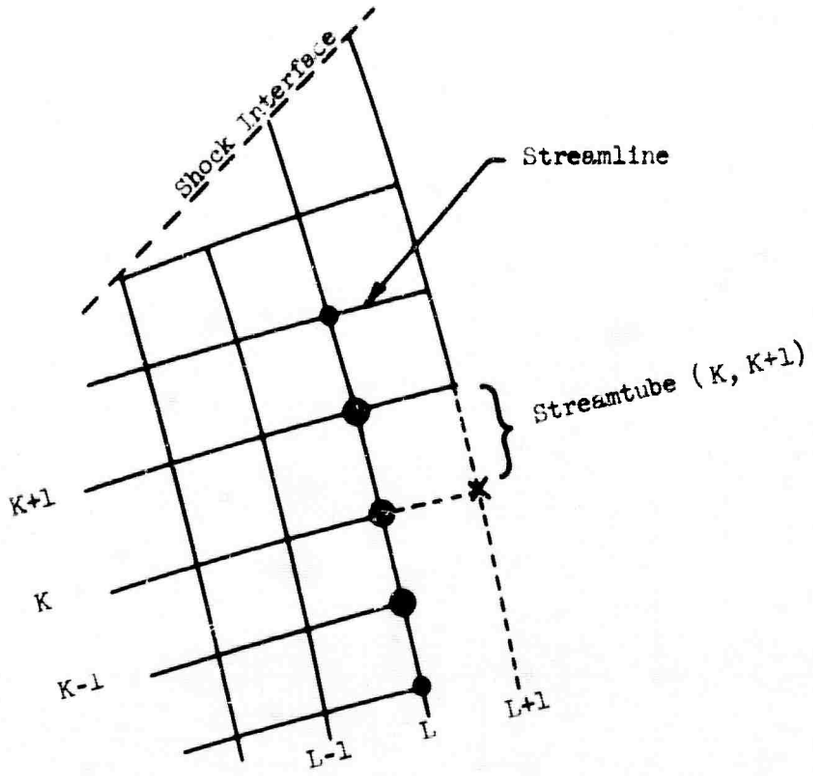

X POINT BEING CALCULATED

○ POINTS USED IN FIRST ITERATION

● POINTS USED IN BOTH ITERATIONS

Fig. IV-1. FINITE DIFFERENCE PROCEDURE

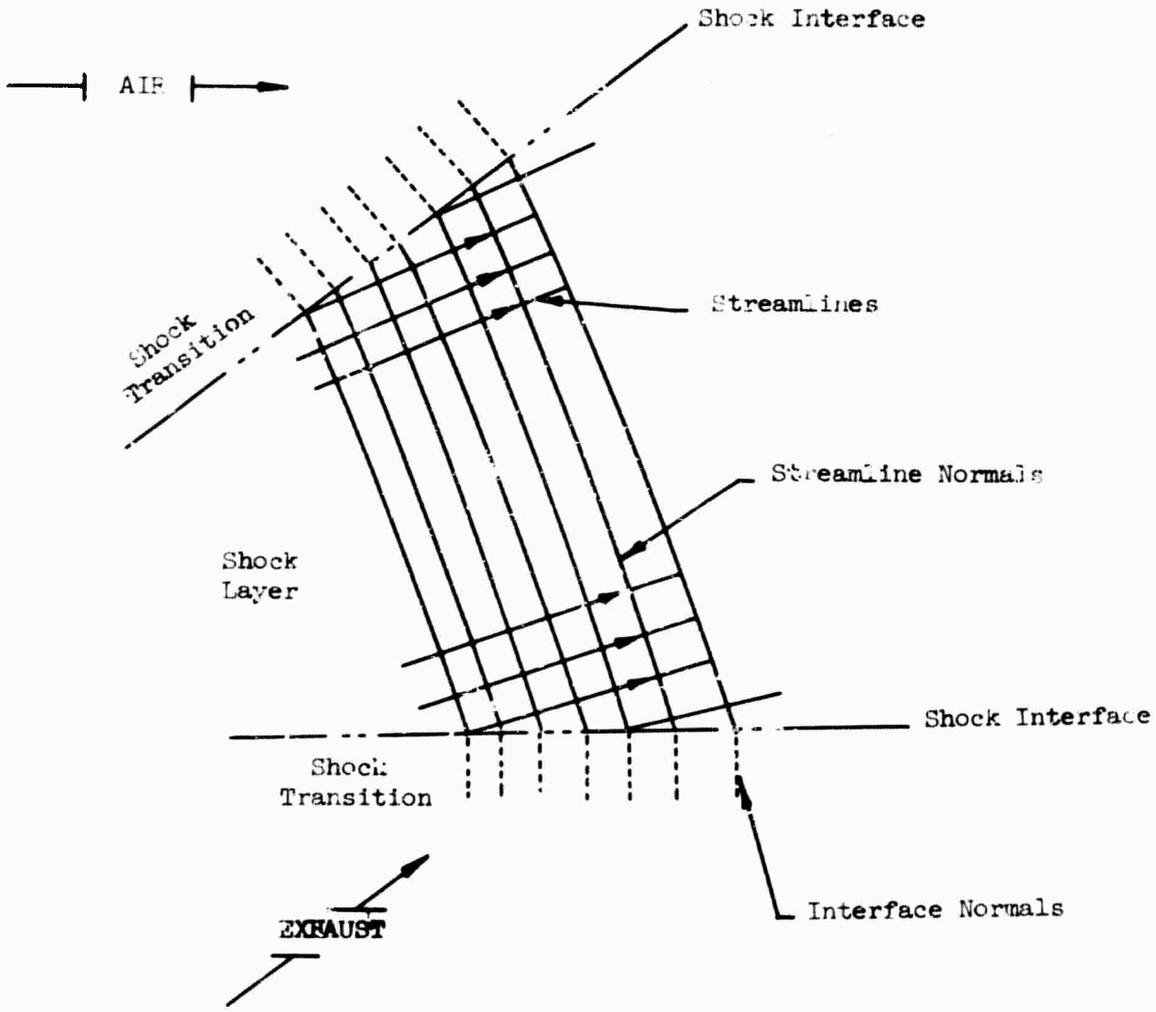

Fig. IV-1b. COORDINATE SYSTEM FOR THE MERGED LAYER

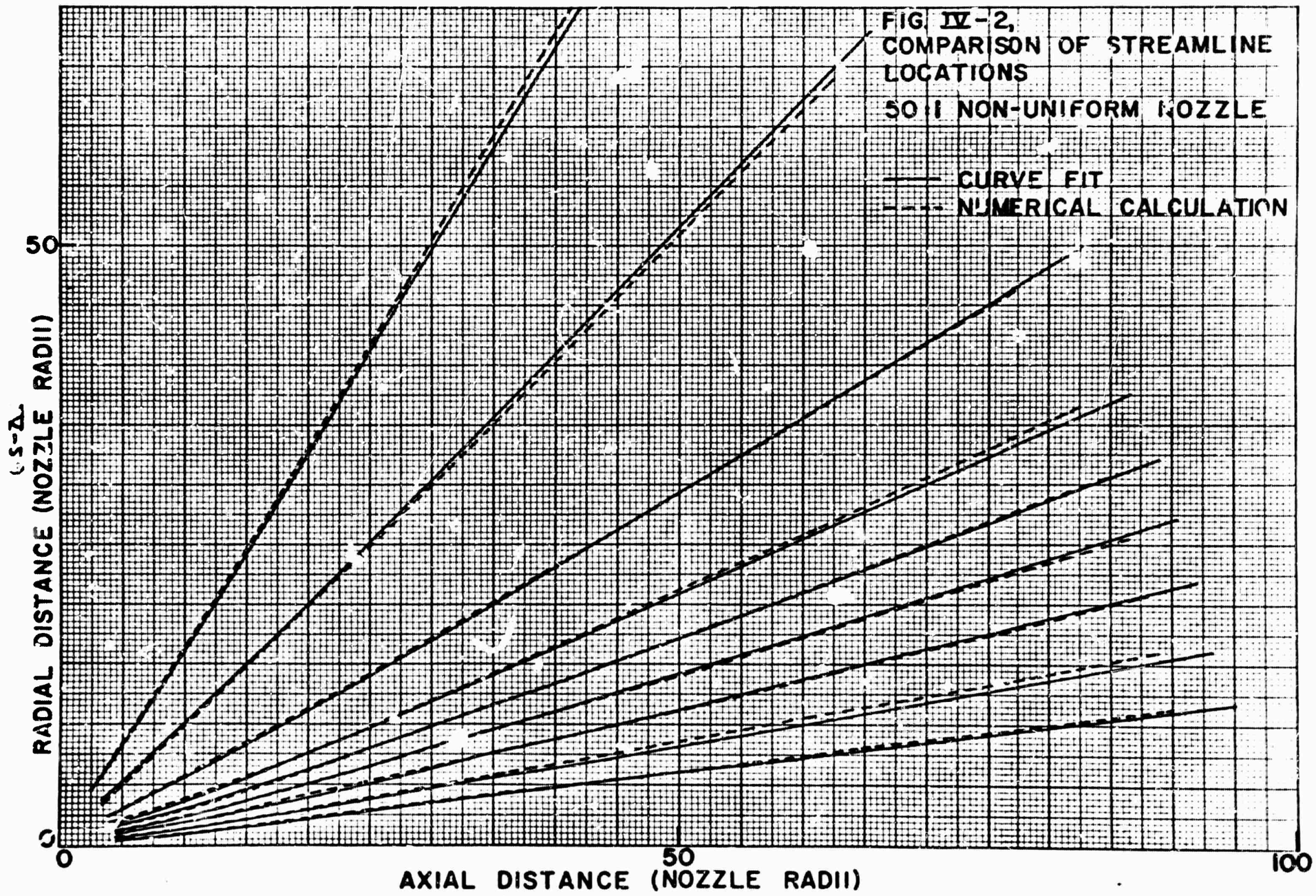
FIG. IV-2,
COMPARISON OF STREAMLINE LOCATIONS
50:1 NON-UNIFORM NOZZLE
—— CURVE FIT
---- NUMERICAL CALCULATION
RADIAL DISTANCE (NOZZLE RADII)
AXIAL DISTANCE (NOZZLE RADII)
0
50
100
0
50

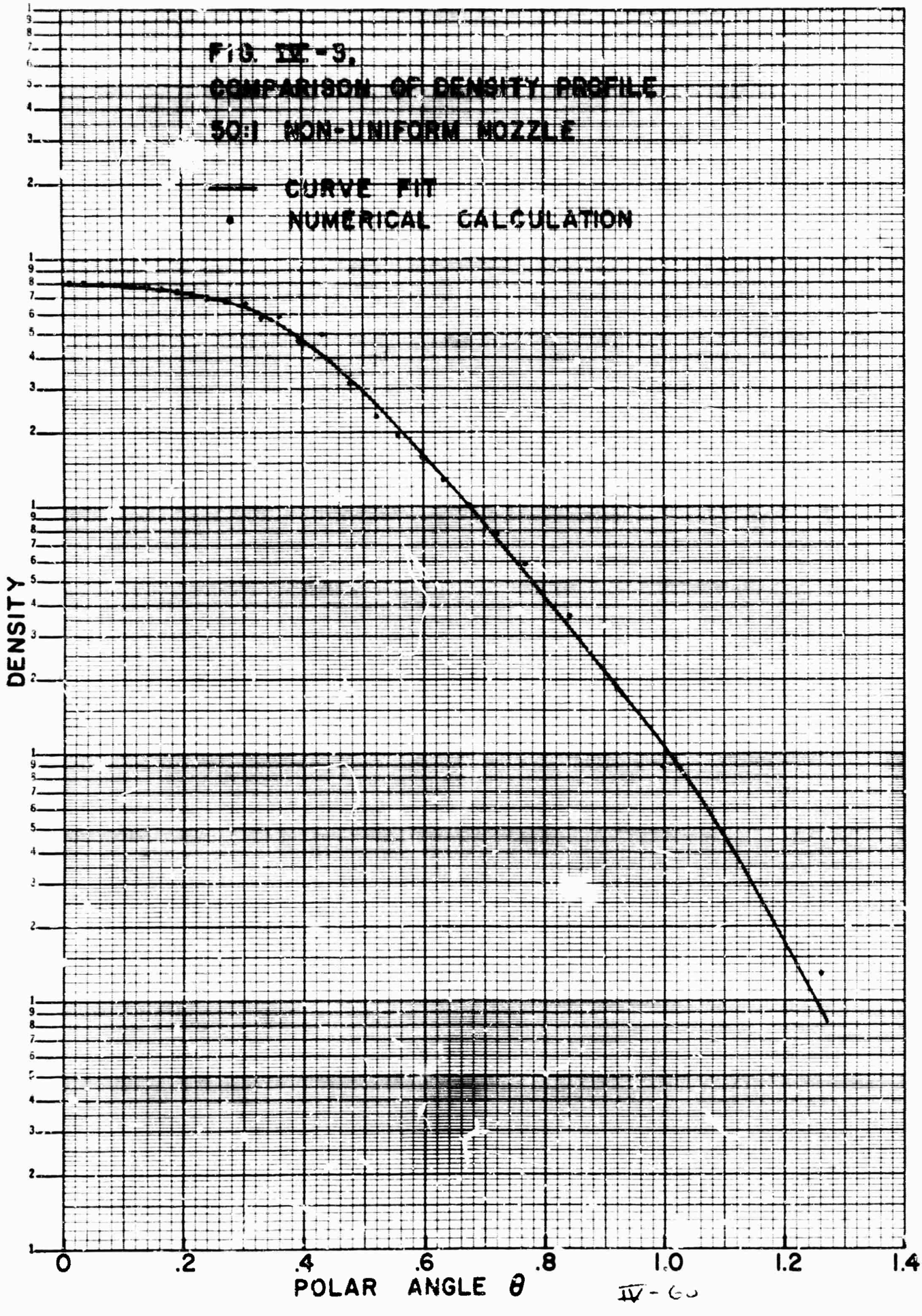
FIG. IV-3,
COMPARISON OF DENSITY PROFILE
50:1 NON-UNIFORM NOZZLE
CURVE FIT
NUMERICAL CALCULATION
DENSITY
POLAR ANGLE θ
0
.2
.4
.6
.8
1.0
1.2
1.4

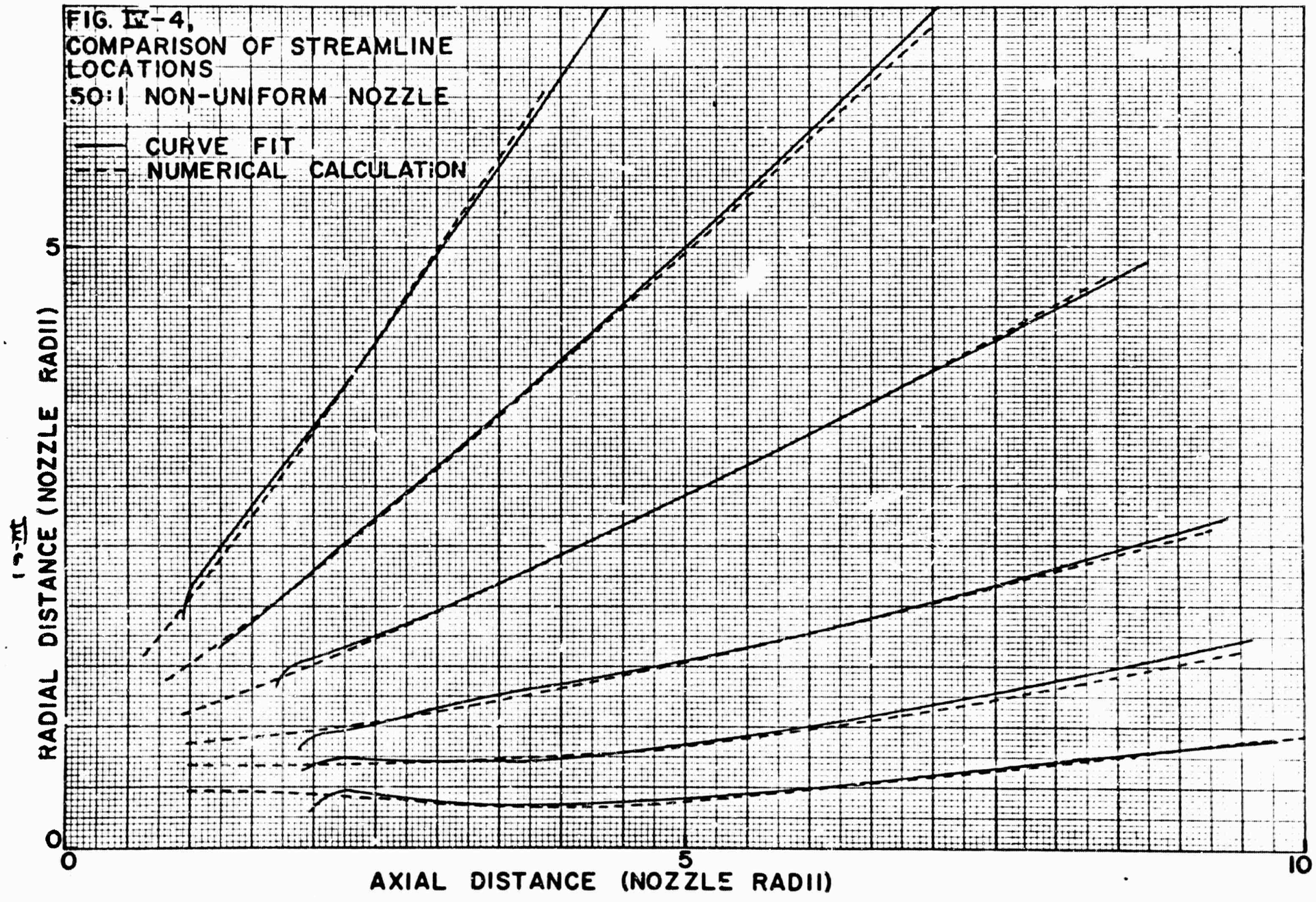
FIG. IV-4,
COMPARISON OF STREAMLINE LOCATIONS
50:1 NON-UNIFORM NOZZLE
CURVE FIT
NUMERICAL CALCULATION
RADIAL DISTANCE (NOZZLE RADII)
AXIAL DISTANCE (NOZZLE RADII)
0
5
10
IV-1

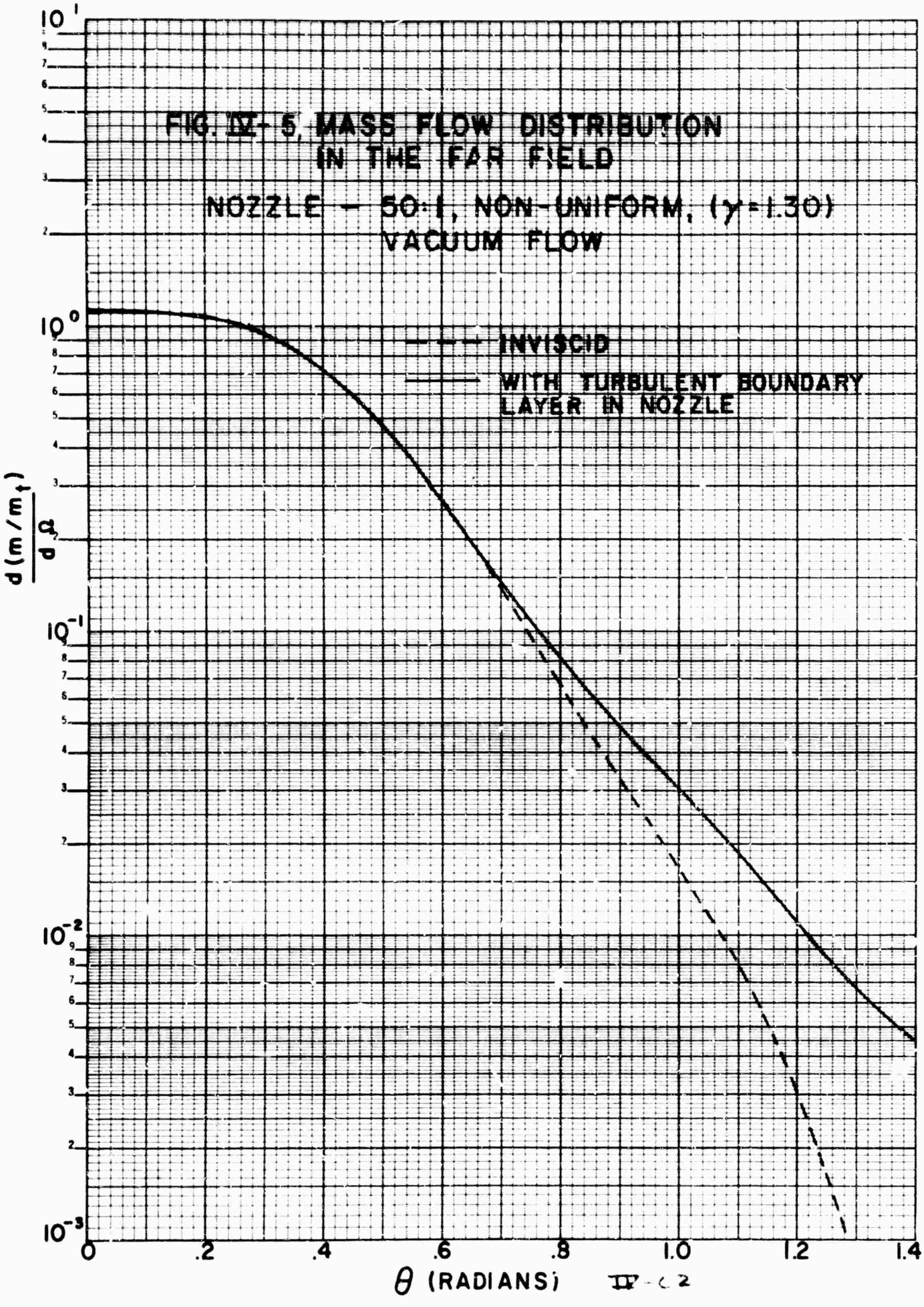
FIG. IV-5, MASS FLOW DISTRIBUTION IN THE FAR FIELD
NOZZLE - 50:1, NON-UNIFORM, (γ=1.30)
VACUUM FLOW
INVISCID
WITH TURBULENT BOUNDARY LAYER IN NOZZLE
d(m/m_t)/dΩ
θ (RADIANS)
10^1
10^0
10^-1
10^-2
10^-3
0
.2
.4
.6
.8
1.0
1.2
1.4

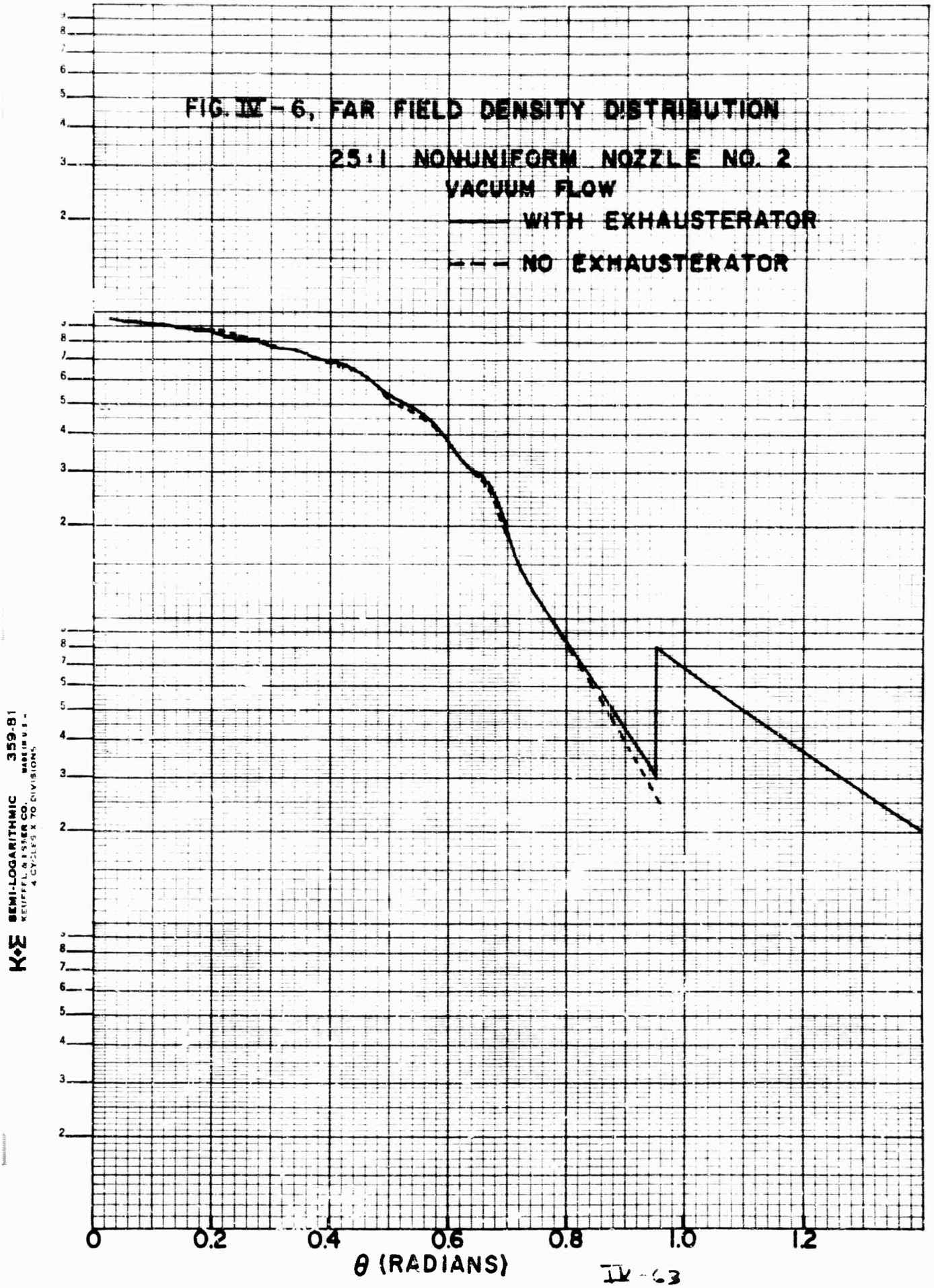

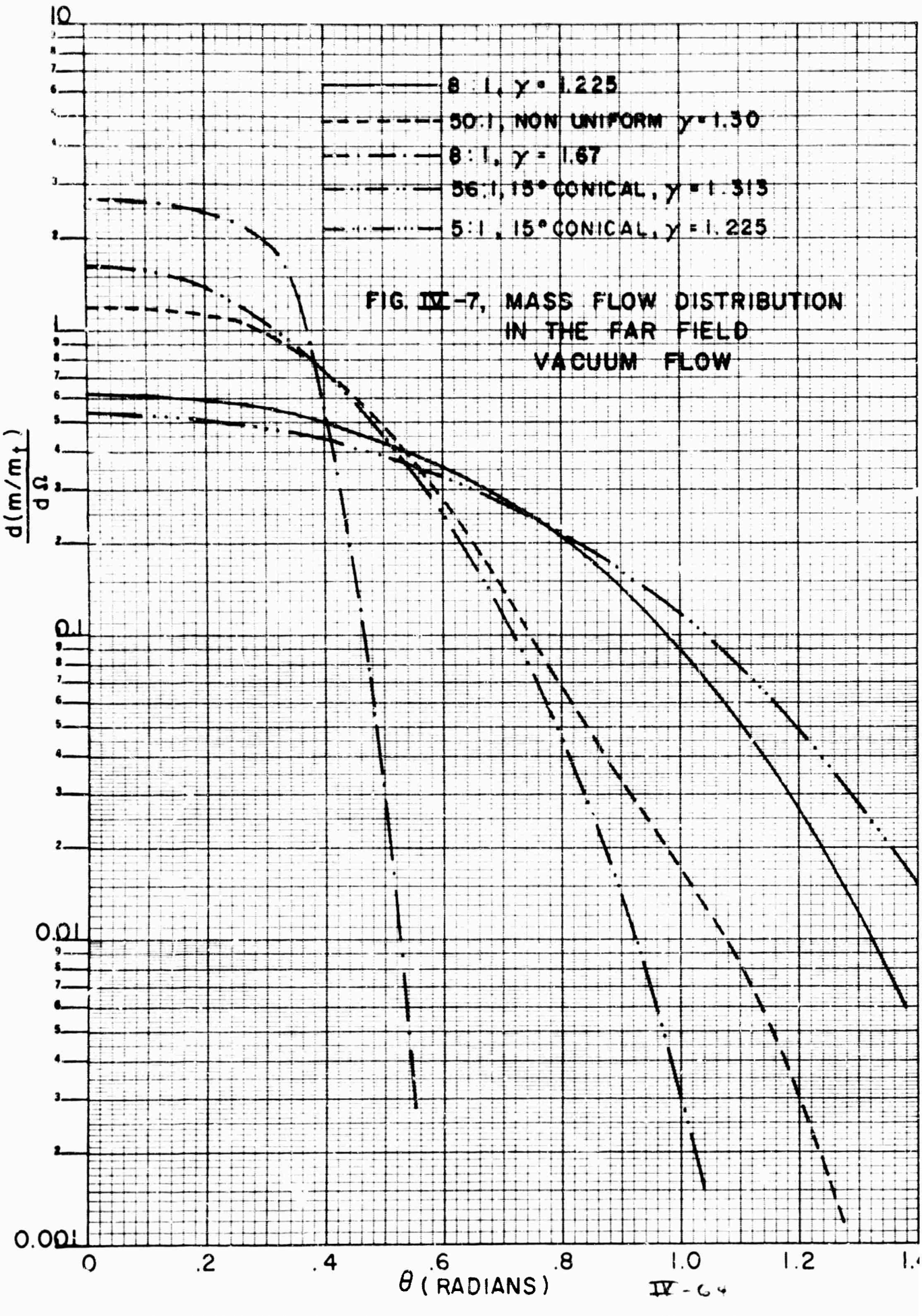
8 : 1, γ = 1.225
50 : 1, NON UNIFORM γ = 1.30
8 : 1, γ = 1.67
56 : 1, 15° CONICAL, γ = 1.313
5 : 1, 15° CONICAL, γ = 1.225
FIG. IV-7, MASS FLOW DISTRIBUTION IN THE FAR FIELD VACUUM FLOW
d(m/m_t)/dΩ
θ (RADIANS)
10
0.1
0.01
0.001
0
.2
.4
.6
.8
1.0
1.2

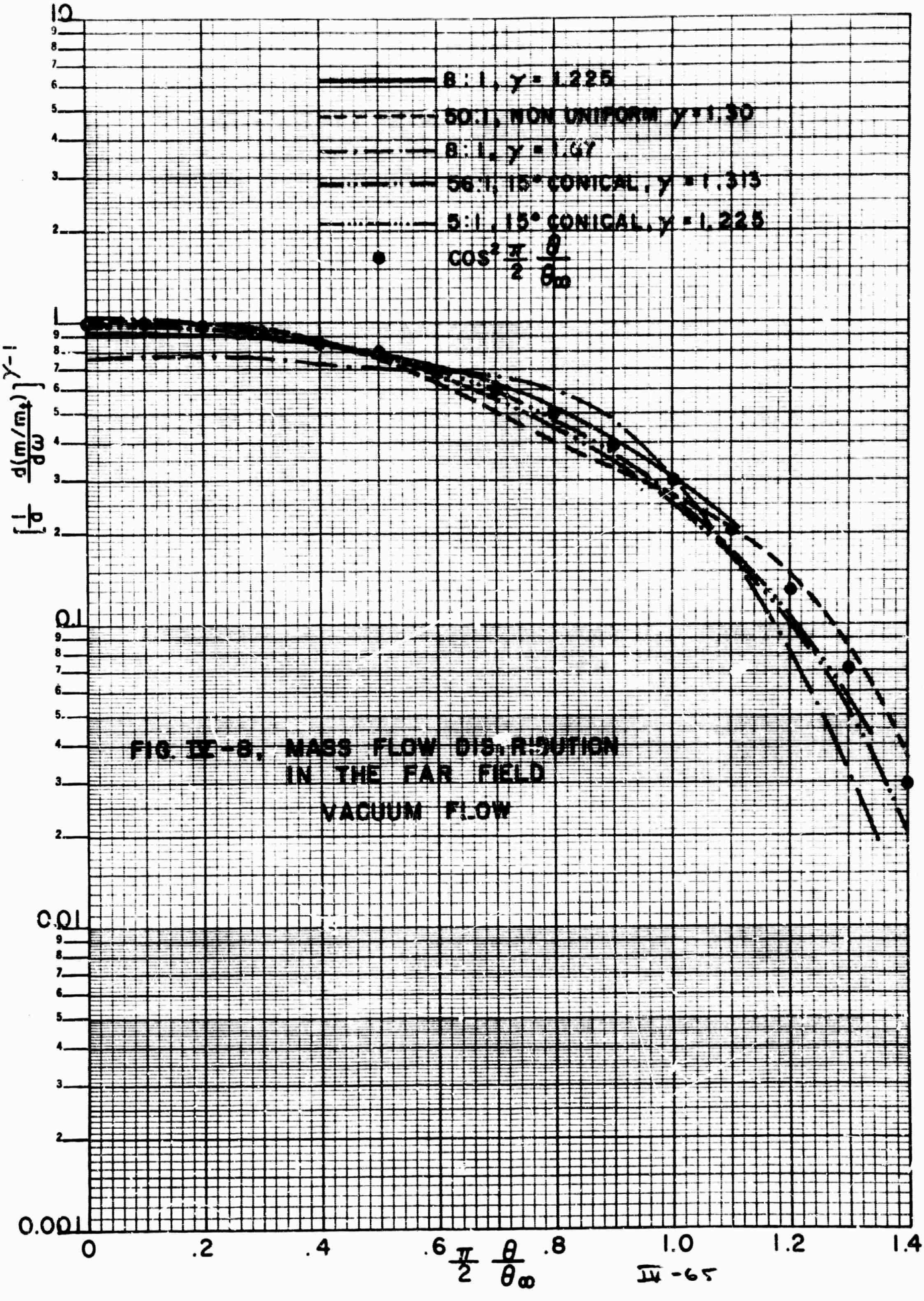

FIG. IV-8, MASS FLOW DISTRIBUTION IN THE FAR FIELD VACUUM FLOW

Fig. IV-9. EXIT PLANE PROPERTIES FOR THE 25:1 NOZZLE: COMPARISON OF CALCULATION TECHNIQUES

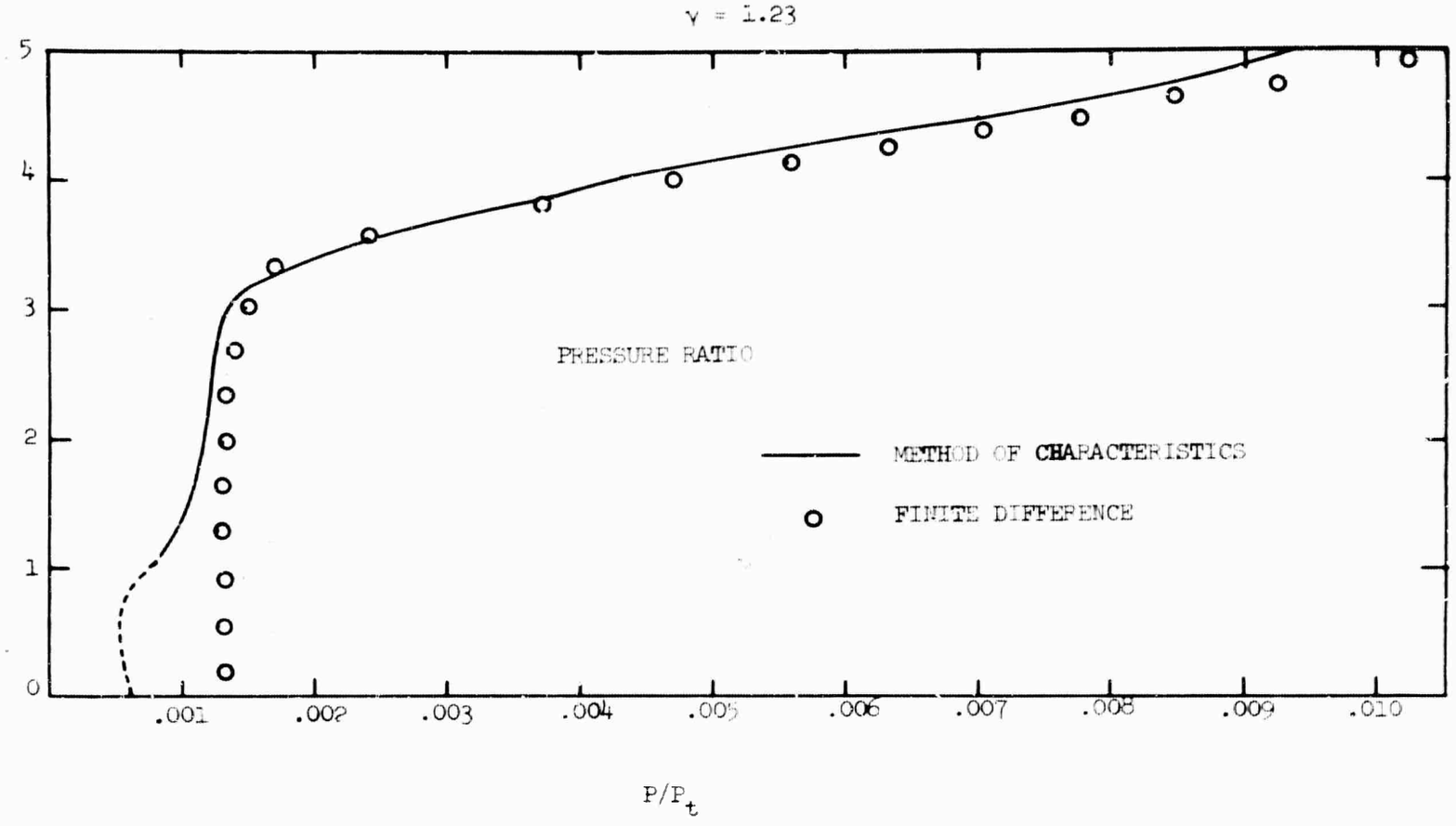

FIG. IV-10,
BOW SHOCK LOCATION
(180 KM ALTITUDE)

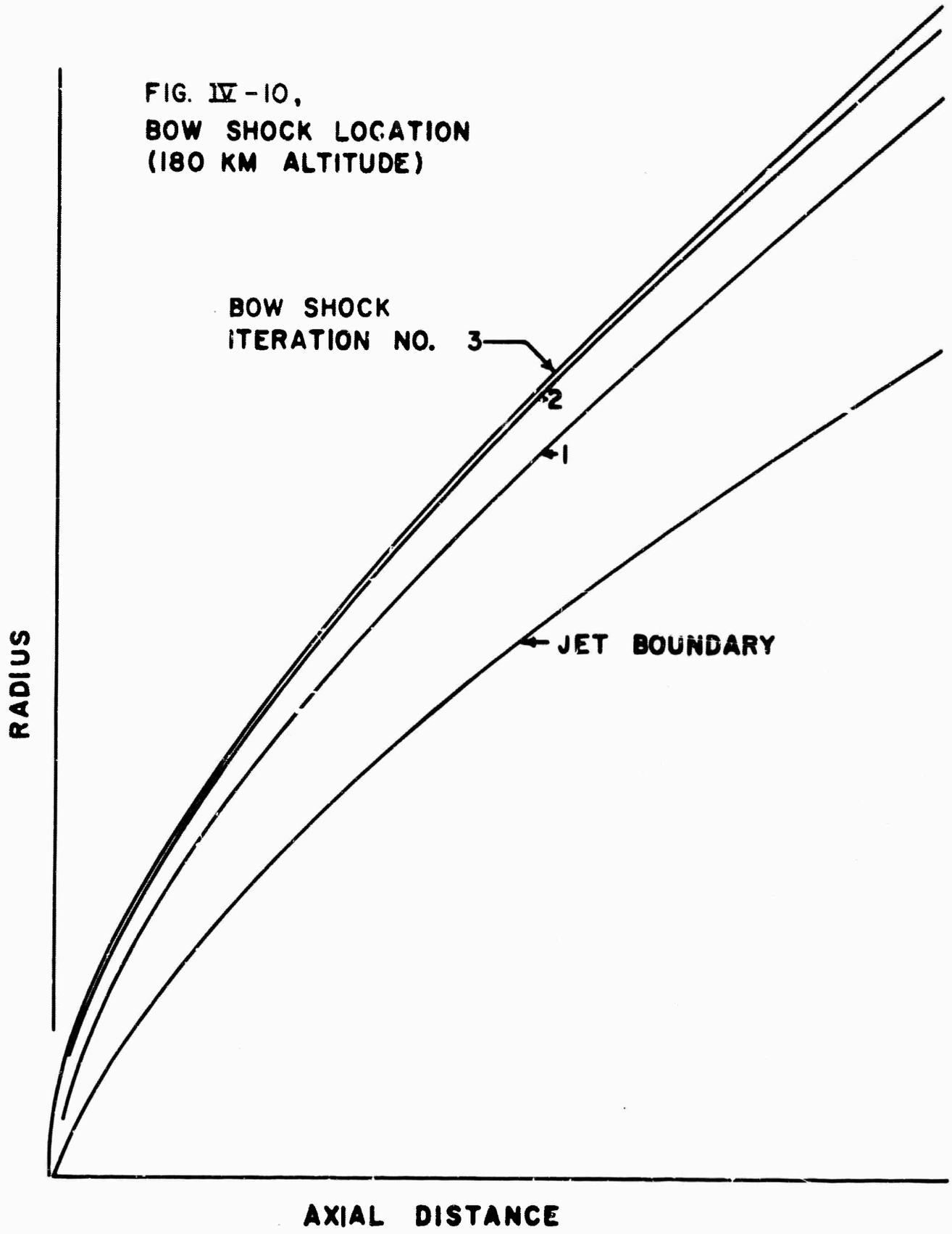

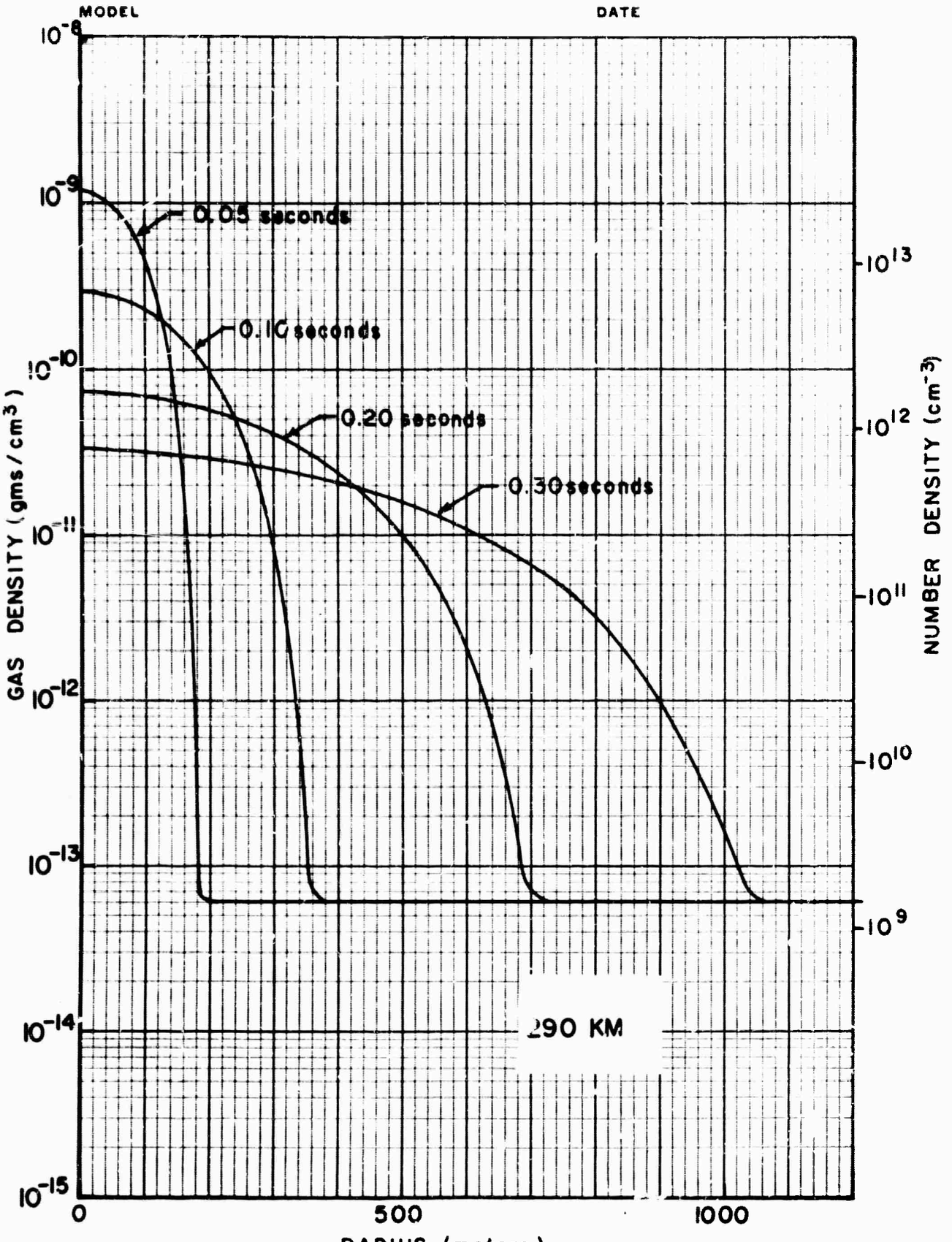

FIG. IV-14, COLLISIONLESS EXPANSION
NEUTRAL GAS DENSITY

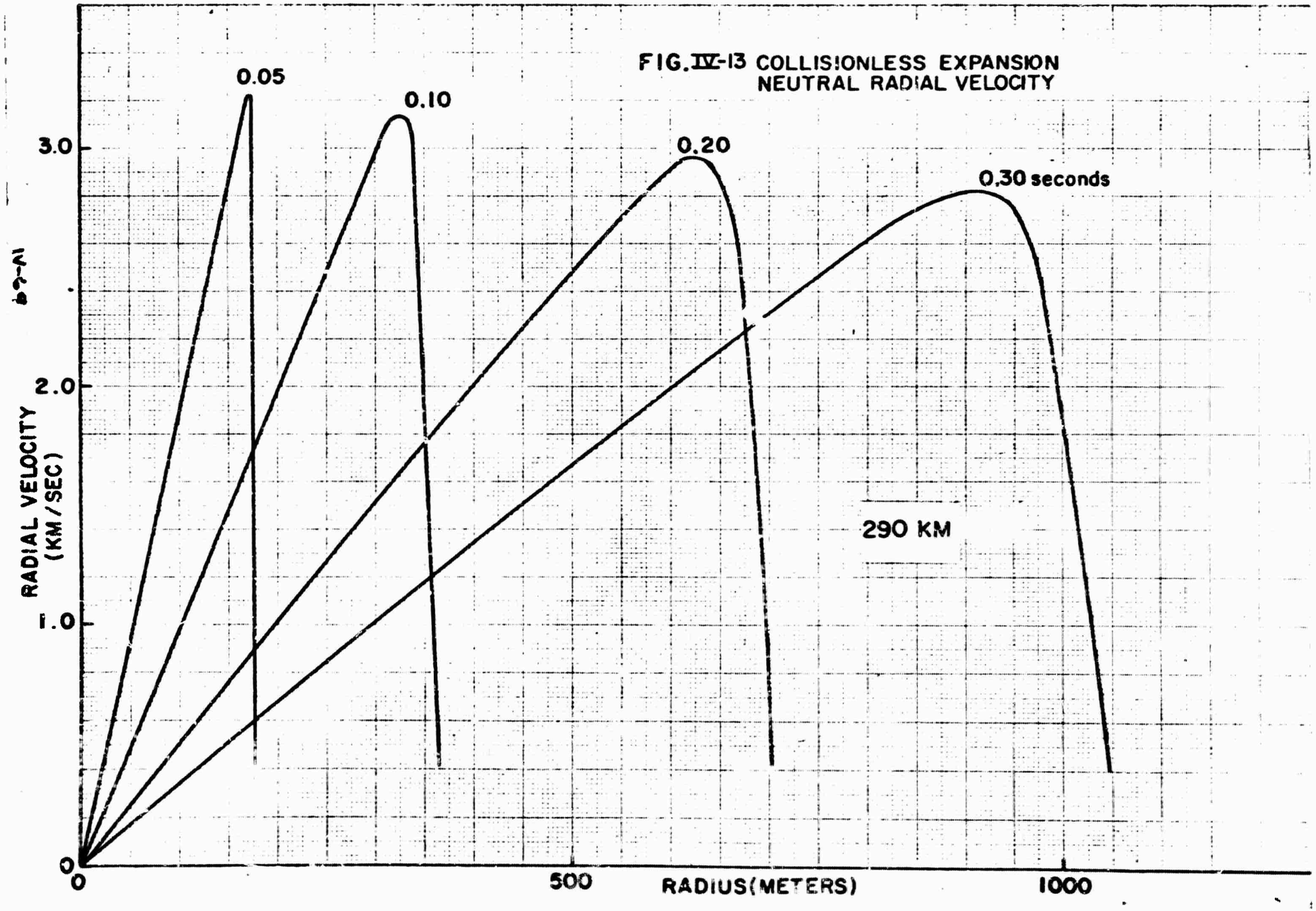
FIG. IV-13 COLLISIONLESS EXPANSION
NEUTRAL RADIAL VELOCITY
0.05
0.10
0.20
0.30 seconds
290 KM
RADIAL VELOCITY (KM/SEC)
3.0
2.0
1.0
0
0
500
1000
RADIUS(METERS)

V. THE EFFECT OF THE GEOMAGNETIC FIELD

V-1 Ion Distribution at Early Time - Simple Model

The discussion in Section III-2 indicates that the ion-neutral mean path may be appreciably smaller than the neutral-neutral value. In this section we develop a very simple model of the ion motion that is useful when these two mean free paths are widely different. We consider here only the early time motion of a cylindrically symmetric neutral flow in a longitudinal or transverse magnetic field.

In Section IV-3g the usefulness of the collisionless approximation of the neutral motion was discussed. There it was indicated that this approximation was a useful, although crude, representation of a one-fluid model of the neutral wind during the initial stages of the expansion. The time histories of the density and velocity distributions for a typical high altitude expansion are shown in Figs. IV-13 and 14.

Significant variations in the neutral flow can only occur over distances greater than a neutral-neutral mean free path. When the ion-neutral mean free path is much smaller than the neutral-neutral value, we may assume that the ion motion equilibrates with the local velocity of the neutral wind. To a first approximation, we expect that the ion velocity component parallel to the field lines thus will remain close to that of the neutral wind

$$v_{i_\parallel} \simeq V_\parallel \tag{1}$$

The perpendicular component will reach a quasi-steady diffusion value. As discussed in Section III-1 we would normally expect the velocity across the field lines to be of the order

$$v_{i_\perp} \simeq \frac{\nu^2}{\nu^2 + \omega_c^2} V_\perp \tag{2}$$

BLANK PAGE

for a finite length flow field.

Here we assume that the ion pressure gradients are not important and that polarization electric fields do not give rise to dominating effects (such as anomalous diffusion). Using the collisionless approximation for the flow field (Figs. IV-13 and 14) to specify $V_{\parallel}$, $V_{\perp}$ and ν as a function of position and time we have evaluated the ion density distributions corresponding to the ion velocity field given by Eqs. 1 and 2.* Here both a longitudinal and a transverse magnetic field have been considered. The density distributions at various times are shown in Figs. III-4, 5, and 6. Ion densities along a line parallel to $\vec{B}$ and along a line perpendicular to $\vec{B}$ are shown. In the calculation ν was set equal to 6×10^{-10} sec^{-1} and $\omega_c = 240$ sec^{-1} where n is the number density of the neutral wind.

The calculation was initiated at a time t = 0 assuming an initial uniform ion density distribution. A schematic representation of the resulting three dimensional ion density distribution is shown in Fig. III-3.

---

*In a previous progress report the calculation was carried out for a cylindrically symmetric neutral flow, in which case the radial electric field due to charge separation resulted in a much lower perpendicular diffusion velocity (corresponding to the value given in Eq. III-2 instead of 1). For the flow fields of practical interest, Eq. V-2 is considered more suitable.

V-2. Linearized Approximation for General Geometry

In the linearized approximation the equations of motion may be written in the form (see Section V-4)

$$\frac{\partial \vec{v}_i}{\partial t} = \frac{e}{m_i}\left(\vec{E} + \frac{\vec{v}_i \times \vec{B}}{c}\right) + \vec{a}_i - \nu_i \vec{v}_i \tag{1}$$

$$\frac{\partial \vec{v}_e}{\partial t} = -\frac{e}{m_e}\left(\vec{E} + \frac{\vec{v}_e \times \vec{B}}{c}\right) + \vec{a}_e - \nu_e \vec{v}_e \tag{2}$$

Here $\vec{a}_i$ and $\vec{a}_e$ are the accelerations of the charged particles induced by the neutral "wind." In terms of the momentum velocity $\vec{u}$, defined by

$$\vec{u} = (m_i \vec{v}_i + m_e \vec{v}_e)/(m_i + m_e) \tag{3}$$

and the current velocity $\vec{v}$, defined by

$$\vec{v} = \vec{v}_i - \vec{v}_e \tag{4}$$

these equations may be recast in the form

$$\dot{\vec{u}} = \vec{v} \times \vec{\omega}_c + \vec{a}_1 - \nu_1 \vec{u} + \beta^2 \nu_{12} \vec{v} \tag{5}$$

and

$$\beta^2 \dot{\vec{v}} = \vec{\mathcal{E}} + \left(\vec{u} - (1-\alpha)\vec{v}\right) \times \omega_c + \beta^2\left(\vec{a}_2 + \nu_{12}\vec{u} - \nu_2 \vec{v}\right). \tag{6}$$

The linearized form of Poisson's equation may be written in the form

$$\operatorname{div}\left(\dot{\vec{\mathcal{E}}} + \omega_p^2 \vec{v}\right) = 0. \tag{7}$$

Here we have used the notation

$$\begin{aligned} \vec{\mathcal{E}} &= e\vec{E}/(m_i + m_e) \\ \vec{\omega}_c &= e\vec{B}/(m_i + m_e)c \\ \omega_p^2 &= 4\pi n_e e^2/(m_i + m_e) \\ \beta^2 &= m_i m_e/(m_i + m_e)^2 \\ \alpha &= 2m_e/(m_i + m_e) \end{aligned} \tag{8}$$

$$
\begin{aligned}
\vec{a}_1 &= \vec{a}_i - \vec{a}_e \\
\vec{a}_2 &= (m_i \vec{a}_i + m_e \vec{a}_e)/(m_i + m_e) \\
\nu_1 &= (m_i \nu_i + m_e \nu_e)/(m_i + m_e) \\
\nu_2 &= (m_i \nu_e + m_e \nu_i)/(m_i + m_e) \\
\nu_{12} &= \nu_e - \nu_i \quad .
\end{aligned} \tag{8}
$$

In the general case the driving forces, represented by the accelerations $\vec{a}_1$ and $\vec{a}_2$, include the ion pressure gradients, and the ion-ion and ion-electron interactions in addition to the neutral-ion interactions.

At high altitudes where the ion-ion collision frequencies are comparable to the ion-neutral values and/or at late times when the neutral drag forces are small, these contributions to the acceleration terms can be significant and should be included. At the lower altitudes and/or at early times, the neutral interactions are expected to dominate (see Section III). For the present we will neglect these ion-ion contributions and assume that the terms $\vec{a}_1$ and $\vec{a}_2$ are known functions of position and time.

Even with these rather considerable simplifications, it is difficult to obtain detailed information concerning the reaction of the ion fluid to the neutral wind except in rather simple geometries. Thus we expect that a mathematical model suitable for computation of an actual flow field may be a drastic simplification of the general case. In order to gain an understanding of the importance of which features of the neutral flow and neutral-ion interaction which must be included in such a model we consider various limiting cases.

In Section the dispersion relations for the plasma are given and the various characteristic frequencies and propagation modes discussed. In Section the nature of the high and moderate frequency response of the plasma to the neutral wind is discussed in the linearized approximation for some simple geometries. In Section V-4 we consider the solution of the non-linear equations of motion, again for some simple geometries only.

In addition to the equations of motion, Eqs. 5, 6 and 7, we need the two Maxwell equations

$$\operatorname{curl} \vec{\mathcal{E}} = -\dot{\vec{\omega}}_c \tag{9}$$

and

$$\operatorname{curl} \vec{\omega}_c = \left(\dot{\vec{\mathcal{E}}} + \omega_p^2 \vec{v} \right)/c^2 . \tag{10}$$

The frequencies we are concerned with are well below the plasma frequency ω_p. In this case it is usually valid to neglect the displacement current term $\dot{\vec{\mathcal{E}}}$ in Eq.10. This is of considerable advantage since it materially reduces the complexity of both the analysis and the numerical evaluations. However, when polarization charges are important it is then necessary to introduce Poisson's equation (the divergence of Eq. 10) explicitly:

$$\operatorname{div} \left(\dot{\vec{\mathcal{E}}} + \omega_p^2 \vec{v} \right) = 0 .$$

Thus Eq. 10 becomes

$$\operatorname{curl} \vec{\omega}_c = \omega_p^2 \vec{v}/c^2 . \tag{11}$$

The approximation of the magnetic field resulting from Eq. 11 is one which is determined solely by a divergence-free current and thus cannot be used to deduce the charge distribution. For this we need the additional equation 7. Equations 5, 6, 7, 9 and 11 form a complete set from which solutions for the electromagnetic field $(\vec{\mathcal{E}}, \vec{\omega}_c)$, the electric current velocity $(\vec{v})$, and the mass velocity $(\vec{u})$ may be obtained in terms of the driving forces $\vec{a}_1$ and $\vec{a}_2$. In the general case $\vec{a}_1$ and $\vec{a}_2$ depend on the ion pressure gradients in addition to the neutral-ion interactions. When these are important we nee ntroduce the continuity equation for the ion fluid. This may be written in the (linearized) form

$$\dot{\rho} + \rho \operatorname{div} \vec{u} = 0 \tag{12}$$

where ρ is the mass density of the ionized species. Also required are energy equations for the ion and electron temperatures T_i and T_e.

For the low frequencies of our principal interest ($\omega \lesssim \nu_i, \nu_e$) it will usually be sufficiently accurate to assume that both the pressures and the temperatures are isotropic ($P_\perp = P_\parallel$, $T_\perp = T_\parallel$). On the other hand, because of the large ion-electron mass ratio, it is generally necessary to allow for differing values for the ion and electron temperatures.

For the present we will consider only the approximation in which the driving frequencies are sufficiently low and the neutral drag terms sufficiently strong that the pressure gradient terms are unimportant, i.e., that the driving terms $\vec{a}_1$ and $\vec{a}_2$ may be considered known a priori. This is formally equivalent to a cold plasma approximation ($T_i = T_e = 0$).

As discussed in Section III-2 two limiting models are of principal interest; the identical particle model (IPM) ($\nu_{12} = 0$, $\nu_1 = \nu_2$, $m_i = m_e$, $\vec{a}_2 = 0$, $\alpha = 1$) and the zero electron mass model (ZEM) ($m_e/m_i = 0$, $\alpha = 0$). For the identical particle model the governing equations become

$$\dot{\vec{u}} = \vec{v} \times \vec{\omega}_c + \vec{a}_1 - \nu_1 \vec{u} \tag{13}$$

$$\dot{\vec{v}} = \vec{\mathcal{E}} + \vec{u} \times \vec{\omega}_c - \frac{\nu_1 \vec{v}}{4} \tag{14}$$

$$\operatorname{curl} \vec{\omega}_c = (\dot{\vec{\mathcal{E}}} + \omega_p^2 \vec{v})/c^2 \tag{15}$$

$$\dot{\vec{\omega}}_c = - \operatorname{curl} \vec{\mathcal{E}} \tag{16}$$

The elementary single species magnetohydrodynamic equations result

from this model when it is assumed that the current and the electric field reach quasi-steady state values ($\dot{\vec{v}} \sim 0, \dot{\vec{\mathcal{E}}} \sim 0$). This state is approached when the driving frequencies are small compared to both the plasma frequency ω_p and the cyclotron frequency ω_c. In this approximation the electric field is given by

$$\vec{\mathcal{E}} = \frac{\nu}{4}\vec{v} - \vec{u}\times\vec{\omega}_c \tag{17}$$

and the equations of motion may be reduced to the form

$$\dot{\vec{u}} = \frac{c^2}{\omega_p^2}(\operatorname{curl}\vec{\omega}_c)\times\vec{\omega}_c + \vec{a}_1 - \nu_1\vec{u} \tag{18}$$

and

$$\dot{\vec{\omega}}_c = \operatorname{curl}(\vec{u}\times\vec{\omega}_c) + \frac{\nu_1 c^2}{4\omega_p^2}\nabla^2\vec{\omega}_c \,. \tag{19}$$

Historically, these equations (or the more general higher frequency ones using Eq.14) have proven quite useful for describing many aspects of the motion of a finitely conducting plasma in a magnetic field. The forms given in Eq.18 and 19 contain the description of damped Alfvén wave motion and diffusion of the magnetic field through the ionized fluid. The symmetry in the motion of the positive and negative ions in the identical particle model may be expected to allow the formulation and solution of problems for which it is difficult to reduce the non-identical particle equations to a tractable form. This applies also to the equivalent non-linear relations.

Of course, this model can only be expected to describe some of the aspects of the motion of a real plasma in which the positive and negative ion are different.

A second model which exhibits many of the features of the actual motion which are lost in the identical particle approximation is that obtained when the electron mass is allowed to approach zero. In this case (ZEM) the current equation (Eq. 14) reduces to the form

$$\vec{\mathcal{E}} = -(\vec{u} - \vec{v}) \times \vec{\omega}_c \quad . \tag{20}$$

The remaining equations are unchanged. In this model the conductivity parallel to the field lines is infinite (i.e., $\bar{\mathcal{E}}_{\parallel} = 0$). The plasma motion is, in general, more complicated in this model than in the identical particle model because of the lack of symmetry. The electrons, now having negligible inertia, respond instantly to the ion motion but their motion is typically very different from the positive ion motion. In the absence of electric fields the electrons move strictly along the magnetic field lines.

If it is known that polarization charges are not important then, for frequencies small compared to the plasma frequency, the displacement current in Eq. 15 may be neglected and the linearized equations recast in the form

$$\dot{\vec{u}} = \frac{c^2}{\omega_p^2} (\operatorname{curl} \vec{\omega}_c) \times \vec{\omega}_c + \vec{\alpha}_1 - \nu_1 \vec{u} \tag{21}$$

and

$$\dot{\vec{\omega}}_c = \operatorname{curl} (\vec{u} \times \vec{\omega}_c) - \frac{c^2}{\omega_p^2} (\vec{\omega}_c \cdot \nabla) \operatorname{curl} \vec{\omega}_c \quad . \tag{22}$$

Some aspects of the difference between these two models are readily seen in the corresponding dispersion relations. These are tabulated in Table V-1 for propagation parallel to the field lines and for propagation perpendicular to them. If the cyclotron frequency is much larger than both the collision frequency and the characteristic frequency of the driving forces, the

TABLE V-1. DISPERSION RELATIONS FOR $\omega \ll \omega_p$

Model	Propagation Direction	V^2/c_A^2	Polarization	
Identical Particle Model	perpendicular to $\vec{B}$	$\dfrac{1 + \left(\dfrac{\nu + i\omega}{\omega_c}\right)^2}{1 - i\dfrac{\nu}{\omega}}$	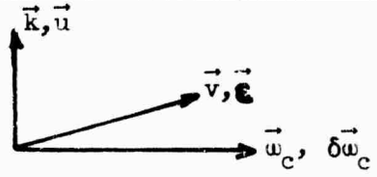	First mode (2 polarizations)
		$-\dfrac{\omega^2}{4\omega_c^2}\left(1 - i\dfrac{\nu}{\omega}\right)$	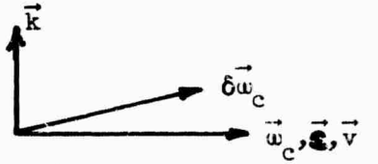	Second mode (evanescent)
Zero Electron Mass Model	perpendicular to $\vec{B}$	$1/(1 - i\,\nu/\omega)$		First mode
		0		Second mode
Identical Particle Model	parallel to $\vec{B}$	$\dfrac{1 - \dfrac{\omega_p^2}{\omega_c^2}\left(1 - i\dfrac{\nu}{\omega}\right)^2}{1 - i\dfrac{\nu}{\omega}}$	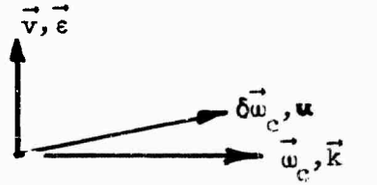	Two modes (circularly polarized)
Zero Electron Mass Model	parallel to $\vec{B}$	$\dfrac{1}{1 - i\dfrac{\nu}{\omega}} \pm \dfrac{\omega}{\omega_c}$	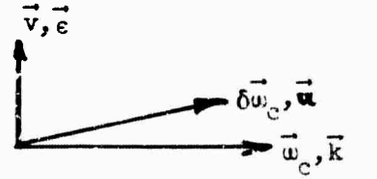	Two modes (circularly polarized)

dispersion relations for the two models are identical. In this case the magnetic forces are sufficiently strong that both the positive and the negative ions are constrained to motion along the field lines and the difference between the two models vanishes.

Differences between the two models may also be seen in the steady state approximation by examining the dependence of the mass velocity on the electric field. The mass velocity $\vec{u}$ may be expressed in terms of the electric field $\vec{\mathcal{E}}$ and the driving acceleration term $\vec{a}_1$. For the identical particle model Eqs. 18 and 19 may be combined to yield (when $\dot{\vec{u}} = 0$):

$$(\vec{u}_\perp)_{IPM} = \left(\frac{(2\vec{\mathcal{E}})}{\nu_1} \times \frac{(2\vec{\omega}_c)}{\nu_1} + \frac{\vec{a}_{1\perp}}{\nu_1} \right) \frac{\nu_1^2}{\nu_1^2 + (2\omega_c)^2} \quad (23)$$

The zero electron mass model yields the expression

$$(\vec{u}_\perp)_{ZEM} = \left(\frac{(\vec{\mathcal{E}} + \vec{a}_1)}{\nu_1} \times \frac{\vec{\omega}_c}{\nu_1} + \frac{\vec{a}_{1\perp} + \vec{\mathcal{E}}_\perp}{\nu_1} \right) \frac{\nu_1^2}{\nu_1^2 + \omega_c^2} \quad (24)$$

The factors of 2 appearing in Eq. 23 are due to the normalization of the electric and magnetic fields given in Eq. 8. $2\vec{\mathcal{E}}$ and $2\vec{\omega}_c$ correspond to the same electric and magnetic fields in the identical particle model as do $\vec{\mathcal{E}}$ and $\vec{\omega}_c$ in the zero electron mass model. In Eq. 24 two terms appear which do not occur in the identical particle model. These differences have obvious physical interpretations. First, when a radial driving force $\vec{a}_1$ is applied to an axially symmetric aligned field configuration, the two ions drift in opposite azimuthal directions with the same speed. Only when the

particles have the same mass does this motion give rise to a vanishing angular momentum of the plasma, corresponding to the first acceleration term in Eq. 24. Second, the application of a radial electric field gives rise to opposing radial diffusion velocities for the two ions. In this case, when the particles are identical, the net radial mass flux vanishes, as indicated by the absence of a term proportional to $\vec{\epsilon}_1$ in Eq. 23. In the zero electron mass model only the positive ions have a non-vanishing radial velocity.

V-3 Quasi-Steady Linearized Approximation

In this section we examine the nature of the solutions of the linearized equations of motion in a steady state approximation in which we assume the driving forces are time-dndependent. We are particularly interested in evaluating the effects of the polarization electric fields induced by various types of neutral winds and those due to the charge separation resulting from the mass difference of the positive and negative ions. We will first consider the identical particle model and then the non-identical one.

V-3a Identical Particle Model

When the ions are identical except for the sign of the charge the equations of motion become

$$\dot{\vec{u}} = \vec{v} \times \vec{\omega}_c + \vec{a}_1 - \nu_1 \vec{u} \tag{1}$$

$$\vec{v}/4 = \vec{E} + \vec{u} \times \vec{\omega}_c - \nu_1 \vec{v}/4 \tag{2}$$

$$\nabla \cdot \left(\dot{\vec{E}} + \omega_p^2 \vec{v} \right) = 0 . \tag{3}$$

We assume that the neutral-ion interaction is also independent of the sign of the charge ($\vec{a}_2 = 0$). In the steady state approximation these equations become

$$\vec{u} = (\vec{v} \times \vec{\omega}_c + \vec{a}_1)/\nu_1 \tag{4}$$

$$\vec{v} = \left(\nu_1 \vec{E} + \vec{a}_1 \times \vec{\omega}_c + (\vec{v} \cdot \vec{\omega}_c) \vec{\omega}_c \right) \Big/ \left(\omega_c^2 + \tfrac{1}{4} \nu^2 \right) \tag{5}$$

$$\operatorname{div} (\omega_p^2 \vec{v}) = 0 \tag{6}$$

and

$$\operatorname{curl} \vec{E} = - \qquad = 0 \tag{7}$$

$$- \frac{\dot{}}{\omega_c} \qquad .$$

Actually it is not consistent to set curl $\vec{\mathcal{E}} = 0$ for the general problem we want to consider, since the neutral flows of interest are those that tend to expand the plasma. The induced emf due to a finite $\partial\vec{B}/\partial t$ gives rise to a drift velocity $\vec{u}$ which in turn allows the field lines to move with the plasma. However, here we are primarily interested in the effects of the polarization fields. Since the equations are linear we may solve for these two motions separately - first those for which curl $\vec{\mathcal{E}} = 0$ and second those for which div $\vec{\mathcal{E}} = 0$ and then superpose the results. In this section we are concerned only with the former case. Thus we may derive the electric field from a potential φ:

$$\nabla\varphi = \vec{\mathcal{E}} \,. \tag{8}$$

Throughout the present analysis we assume that the magnetic field is constant and aligned in the z direction. The component of the current velocity $\vec{v}$ parallel to the magnetic field may be derived from Eq. 5 :

$$\vec{v}_{i_\parallel} = \vec{\mathcal{E}}_\parallel / (\tfrac{1}{4}\nu_1) \,.$$

Using Eqs. 5 and 8 , Eq. 6 may, after some manipulation, be reduced to the form

$$\nabla^2\varphi + \frac{\nabla\varkappa}{\varkappa}\cdot\nabla\varphi + \frac{4\omega_c^2}{\nu_1^2}\frac{\partial^2\varphi}{\partial z^2} = -\frac{\nabla\cdot\left(\varkappa\,\vec{a}_1\times\vec{\omega}_c/\nu_1\right)}{\varkappa} \tag{9}$$

where $\varkappa$ is defined by

$$\varkappa = \frac{\omega_p^2\,\nu_1}{\omega_c^2 + \nu_1^2/4} \,.$$

Since the neutral drag term has only r and z components, the right-hand side of Eq. 9 may be written in the form

$$-\frac{1}{xr}\frac{\partial}{\partial\theta}\left(x a_{1_\perp}\,\omega_e/\nu_i\right)$$

where $a_{1_\perp}$ is the radial component of the drag term. Thus, when the neutral flow and the plasma properties are axially symmetric the polarization electric fields vanish. In this case the analysis described in Section V-6 may be applied to the motion.

An azimuthal variation in either the ion density or the neutral drag may result in a non-zero charge density. The resulting electric fields may considerably alter the ion motion from that expected in the absence of polarization fields.

Substitution of Eq. 5 into 4 yields the following expression for the momentum velocity $\vec{u}$:

$$\vec{u} = \left(\frac{\vec{a}_i}{\nu_i}\right)_{\parallel} + \frac{\vec{a}_{i_\perp}}{\nu_i}\left(\frac{\nu_i^2}{4\omega_e^2+\nu_i^2}\right) + \frac{4\vec{\mathcal{E}}\times\vec{\omega}_e}{4\omega_e^2+\nu_i^2} \qquad (10)$$

As expected, the motion parallel to the magnetic field is unaffected. The motion perpendicular to the field lines is the sum of the diffusion term $\vec{u}_D$ in the direction of the driving force and a term due to the polarization fields $\vec{u}_E$. In the general case there will also be a term due to the induced field which we are not considering here. Thus the velocity in Eq. 10 is really the velocity relative to the field lines. The diffusion term is the same as that given in Section III-1. (Note that the Larmor frequency in Eq. 10 is defined in terms of $(m_i + m_e)$ whereas in Section III-1 it is defined in terms of m_i only).

In this section we want to examine the polarization term $\vec{u}_E$. First

we note that

$$\operatorname{div} \vec{u} = (\nabla \times \vec{\mathcal{E}}) \cdot \vec{\omega}_c \Big/ \left(\omega_c^2 + \nu_i^2/4\right) . \qquad (11)$$

Thus the motion induced by the polarization fields ($\nabla \times \vec{\mathcal{E}} = 0$) is incompressible ($\operatorname{div} \vec{u} = 0$).

We now want to examine the nature of solutions of Eq. 9 in the special case when the azimuthal variations of both the electron density (i.e., ω_p^2) and the perpendicular acceleration are small. Before proceeding to this, however, it will prove convenient to express the results of this section in terms of the current density $\vec{J}$ and the parallel and perpendicular conductivities, $\sigma_\parallel$ and $\sigma_\perp$. The current parallel to the magnetic field is given by

$$\vec{J}_\parallel = e n_e \vec{v}_\parallel / c = 4 e^2 n_e \vec{\mathcal{E}}_\parallel / c \nu_i . \qquad (12)$$

Thus, since the conductivity is defined by the relation $\sigma = e\vec{J}/m\vec{\mathcal{E}}$, the conductivity parallel to the field is given by

$$\sigma_\parallel = 4 e^2 n_e / m c \nu_i . \qquad (13)$$

From Eq. 5 the current perpendicular to the field lines is

$$\vec{J}_\perp = e \nu_i n_e \left(\vec{\mathcal{E}}_\perp + \frac{\vec{a}_i \times \vec{\omega}_c}{\nu_i} \right) \Big/ c\left(\omega_c^2 + \nu_i^2/4\right) . \qquad (14)$$

Thus, the perpendicular conductivity is given by

$$\sigma_\perp = 4 e^2 n_e / m c \nu_i \left(1 + 4\omega_c^2/\nu_i^2\right) . \qquad (15)$$

The condition that div $\vec{J} = 0$ in the steady state (Eq. 6) may be now expressed in the form

$$\operatorname{div}\left(\sigma_\perp \vec{\mathcal{E}}_\perp + \sigma_\parallel \vec{\mathcal{E}}_\parallel\right) = -\operatorname{div}\left(\sigma_\perp \vec{a}_i \times \vec{\omega}_c/\nu_i\right) . \qquad (16)$$

According to this relation the force exerted by the neutrals on the ions in the direction perpendicular to the magnetic field may be thought of as inducing a current $\vec{J}_n$ across the field:

$$\vec{J}_n = \sigma_\perp \vec{a}_i \times \vec{\omega}_c/\nu_i . \qquad (17)$$

Since the total current must be divergence-free these wind-induced currents cause polarization electric fields to be set up in order to create additional currents $\vec{J}_p (= \sigma_\perp \vec{\mathcal{E}}_\perp + \sigma_\parallel \vec{\mathcal{E}}_\parallel)$ such that

$$\operatorname{div}\left(\vec{J}_n + \vec{J}_p\right) = 0 \qquad (18)$$

The solution of Eq. 9 in the general case is difficult because of the anisotropy of the conductivity. However, when both the magnetic field and the collision frequency are constant, the anisotropic Poisson's equation resulting from Eq. 9 may be reduced to the more familiar isotropic form by a simple transformation of coordinates. To accomplish this we first introduce the potential φ ($\vec{\mathcal{E}} = \nabla\varphi$) with the z axis aligned parallel to $\vec{B}$.

By transforming from the real space coordinates (r, θ, z) to a set (r, θ, z′) in which the coordinate parallel to the magnetic field is shrunk by the factor $\sqrt{\sigma_\perp/\sigma_\parallel}$, Eq. 9 may be reduced to the isotropic form

$$\nabla'\cdot\left(\sigma_\perp \nabla'\varphi\right) = -\nabla'\cdot\left(\sigma_\perp \vec{a}_i \times \vec{\omega}_c/\nu_i\right) . \qquad (19)$$

Here ∇' is the gradient operator in the r, θ, z′ coordinates and

$$z' = z\sqrt{\sigma_\perp/\sigma_0} = z\Big/\sqrt{1+\frac{4\pi\sigma_0^2}{\nu_1^2}} \quad . \tag{20}$$

In order to gain a better understanding of the nature of the solutions to Eq.19 we now limit ourselves to the case in which the fractional azimuthal variations in the ion density (i.e., in $\sigma_\perp$) and in the perpendicular acceleration ($\vec{a}_{1\perp}$) are both small. Then, retaining only the first order terms in these quantities, we may reduce Eq. 19 to the form

$$\nabla'^2\varphi = -\frac{a_{1\perp}\omega_c}{\nu_1 r}\frac{\partial}{\partial\theta}\left(\frac{n_e-\bar{n}_e}{\bar{n}_e}\right) - \frac{\omega_c}{\nu_1 r}\frac{\partial}{\partial\theta}(a_{1\perp}) \quad . \tag{21}$$

where $\bar{n}_e$ is the mean value of the ion density (averaged over the azimuthal angle):

$$\bar{n}_e(r,z) = \frac{1}{2\pi}\int_0^{2\pi} n_e(r,z,\theta)\,d\theta \quad .$$

Since solutions to the inhomogeneous Laplace equation are familiar and relatively easy to visualize, it is useful to interpret Eq. 21 as Poisson's equation for the (psuedo-) electric field $\vec{E}'$ $\left(\frac{e}{m}\vec{E}' = \nabla'\varphi\right)$ due to a (psuedo-) charge distribution ρ', defined by

$$\frac{e}{m}\rho' = -\frac{\bar{a}_{1\perp}\omega_c}{4\pi\nu_1 r}\frac{\partial}{\partial\theta}\left(\frac{n_e a_{1\perp}}{\bar{n}_e\bar{a}_{1\perp}}\right) \tag{22}$$

The psuedo-field $\vec{E}'$ is related to the real electric field $\vec{E}$ by

$$E_r = E'_r$$
$$E_\theta = E'_\theta \qquad (23)$$

and

$$E_z = \sqrt{\frac{\sigma_\perp}{\sigma_\parallel}}\, E'_z$$

This psuedo-charge distribution , ρ', may be thought of as a superposition of a number of charged rings, on each of which r and z are constant and on each of which the total charge is zero. At each point the charge density is proportional to the magnetic field strength $(\vec{\omega}_c)$, to the drag term $(\vec{a}_{l_\perp}/\nu_l)$ due to the neutral wind (this drag term is roughly of the order of the perpendicular component of the velocity of the neutrals across the field lines) and to the fractional variation of the product $n_e\, a_{l_\perp}$.

Azimuthal variations in n_e or $a_{l_\perp}$ may result from random inhomogeneities in the neutral wind or in the ambient ion density and from atmospheric stratification of the neutral or the ambient ion density. Quite large variations in these quantities may be expected as the flow develops if the axis of symmetry of the neutral flow is not aligned with the magnetic field. In general, we expect non-zero values of ρ' whenever the neutral wind velocity across the field lines is significantly different from zero.

In order to obtain a feeling for the resultant motion of the ion fluid let us consider first the special case in which the neutral flow field is axially symmetric with the axis of symmetry parallel to the magnetic field $(\partial\, a_{l_\perp}/\partial\theta = 0)$ and in which the ratios of the characteristic longitudinal

dimensions (parallel to the field) to the lateral dimensions for both the neutral flow and for the ion density inhomogeneities are much larger than $\sqrt{\sigma_\parallel / \sigma_\perp}$. At high altitudes in the ionosphere this requirement is expected to be difficult to meet in practical situations because of the typically large ratios that usually obtain for $\sigma_\parallel / \sigma_\perp$ (see Table V-2).* However, the simplicity of this case warrants its treatment first.

Since, in this case, the characteristic longitudinal dimension is large compared to the lateral dimensions, even in the r', ϑ', z' coordinate system, the resultant potential distribution in this coordinate system, as well as in the real space coordinate system, is approximately two-dimensional (r, θ only).

Let us ask what happens to randomly distributed inhomogeneities in the ion density. The total electric field at any point may be thought of as a superposition of contributions from individual irregularities. Suppose that the ion density distribution may be represented as a sum of contributions of the form, for example

$$n_e - \bar{n}_e = \Delta n_{e_i} \exp\left[- (\vec{r} - \vec{r}_i)^2 / r_{0_i}^2 \right] \qquad (24)$$

*The present discussion has been based on the assumption of equal masses for the positive and negative ions. However, it is shown later that the appropriate parameter for non-equal masses is still the ratio of the two conductivities.

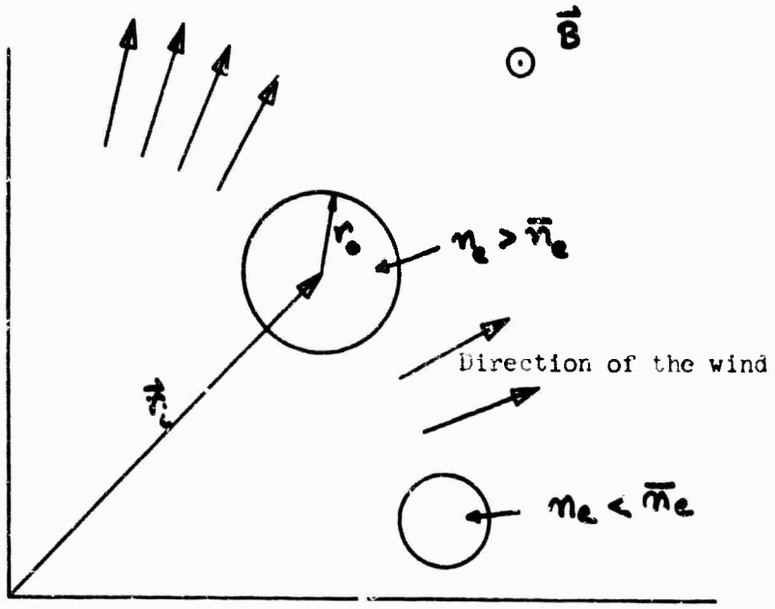

Fig.V-1a. Radial Neutral wind interacting with plasma inhomogeneities.

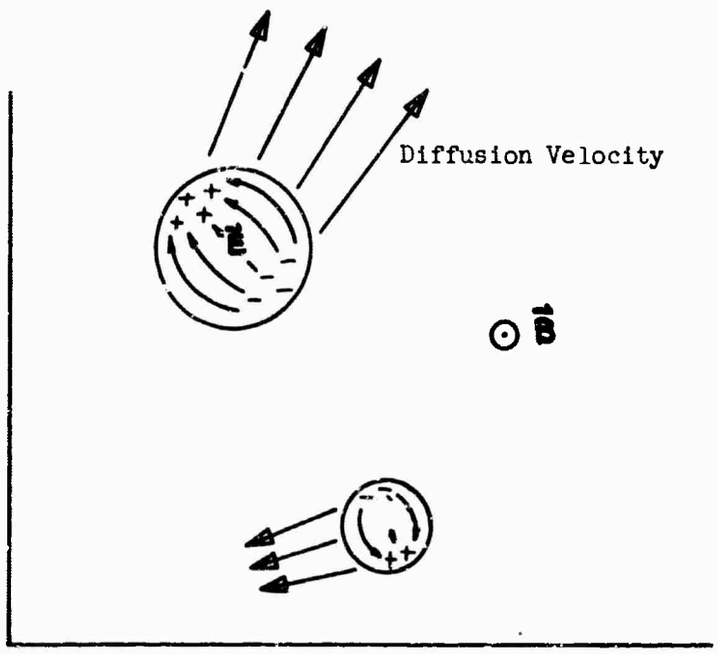

Fig. V-1b Resulting diffusion of the inhomogenieties.

and that the characteristic dimensions (r_{o_i}) of the irregularities are small compared to those of the neutral flow field. As a result of the variations in n_e in the direction of $\vec{a}_1 \times \vec{\omega}_c$, polarization charge distributions will be set up (see Fig. V-1). The resultant electric field near the center of an irregularity ($\vec{r} \simeq \vec{r}_i$) will be of the order

$$\frac{e\vec{\mathcal{E}}}{m} \lesssim - \frac{\vec{a}_{1_\perp} \times \vec{\omega}_c}{\nu_1} \frac{\Delta n_e}{n_e} + \frac{e\vec{\mathcal{E}}''}{m} \qquad (25)$$

where $\vec{\mathcal{E}}''$ is the field due to all the other irregularities. Since these are randomly distributed we expect $\vec{\mathcal{E}}'' \simeq 0$. Equation 25 will approximately represent the electric field in the immediate vicinity of the irregularity only. The drift velocity induced by this field will be of the order

$$\vec{u} \lesssim \frac{\vec{\mathcal{E}} \times \vec{\omega}_c}{\omega_c^2} \lesssim \frac{\vec{a}_{1_\perp}}{\nu_1} \frac{\Delta n_e}{n_e} . \qquad (26)$$

Thus, regions in which the ion density is greater than the average tend to move in the direction of the neutral wind and those having a lower density move against the wind (Note that the velocity is not sensitive to the dimensions of the inhomogeneity, nor to the value of the magnetic field). Since this motion is incompressible (Eq. 11), the motion is simply a rearrangement of the plasma, the regions of higher density being blown outward in the direction of the neutral wind. A mean radial velocity,

$\bar{u}_r$, may be evaluated from

$$\bar{n}_e \bar{u}_r \simeq \frac{1}{2\pi r} \int n_e \vec{u} \cdot d\vec{A} \quad . \tag{27}$$

Thus the mean outward velocity is given by

$$\bar{u}_r \simeq \frac{a_{i\perp}}{\nu_i} \overline{\left(\frac{\Delta n_e}{n_e} \right)^2} \quad . \tag{28}$$

The fact that the drift velocity is independent of the magnetic field cannot be true in the limit of $\vec{B} \to 0$. The restrictions on Eq. 26 are that the characteristic dimensions of the inhomogeneities be small compared to that of the neutral flow field but large compared to a Larmor radius. Thus when the Larmor radius is comparable to the flow field dimensions Eq. 28 fails. When the characteristic dimension of the inhomogeneity is comparable to that of the neutral flow field the mean outward velocity cannot be obtained from Eq. 28 . The general nature of the motion in this case, however, should be similar; the high density regions moving with the wind, the low density regions against it.

Equations 10 and 28 thus show that there are two modes by which the plasma may diffuse across the field lines. In the first, the diffusion velocity is given by

$$\vec{u}_{D_1} = \frac{\vec{a}_{i\perp} / \nu_i}{1 + \frac{4\omega_i^2}{\nu_i^2}} \quad . \tag{29}$$

This is normal diffusion in which the diffusion velocity decreases with increasing magnetic field as B^{-2} for strong fields. In the second, the diffusion velocity is

$$\vec{u}_{D_2} = \frac{\vec{a}_{\perp}}{\nu_i} \overline{\left(\frac{en_e}{m_e}\right)^2} . \qquad (30)$$

This is the so-called anomalous diffusion and is due to varying polarization electric fields set up as a result of inhomogeneities in the plasma density. In this case of cylindrical symmetry it is independent of $\vec{B}$ so long as the Larmor radius is sufficiently small.

We will now examine the case which we expect to be more realistic, in which the longitudinal dimensions of the neutral flow field and of the inhomogeneities are small compared to $\sqrt{\sigma_{\parallel}/\sigma_{\perp}}$ times their lateral dimensions. In the r', θ', z' space the regions of non-zero charge density are thus disc-shaped, the thickness in the direction of the field being much less than the radial dimension. The magnitude of the charge density is the same as before but now the volume is much reduced. Thus we expect weaker electric fields and reduced diffusion velocities. In order to estimate the magnitude of the reduction we compare the value of the radial electric field on the mid-plane of disc of thickness ℓ and radius R to the value expected for infinite cylinder of the same radius. Rough calculations indicate that a reduction factor of the order of

$$f = \frac{\ell}{3R}\left(1 + \ell n \frac{2R}{\ell}\right) \qquad (31)$$

is expected when $R \gg \ell$. If the actual longitudinal dimension is L, then we expect the radial electric field to be reduced by a factor of the order

$$f = \frac{1}{3}\beta^*\left(1 + \ell n \frac{2}{\beta^*}\right)$$

where $\beta^* = \frac{L}{R}\sqrt{\frac{\sigma_{\perp}}{\sigma_{\parallel}}}$.

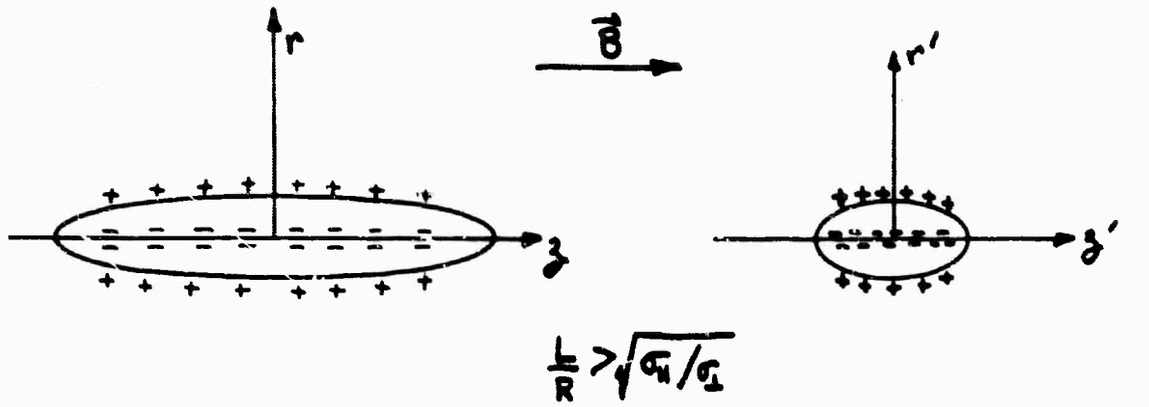

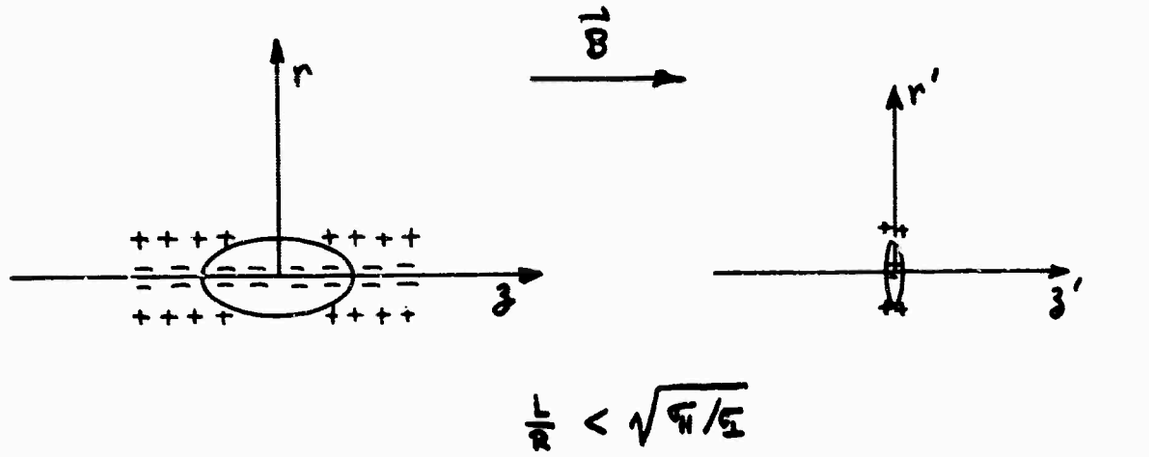

Fig. V-2a Charge distributions in the real and transformed space.

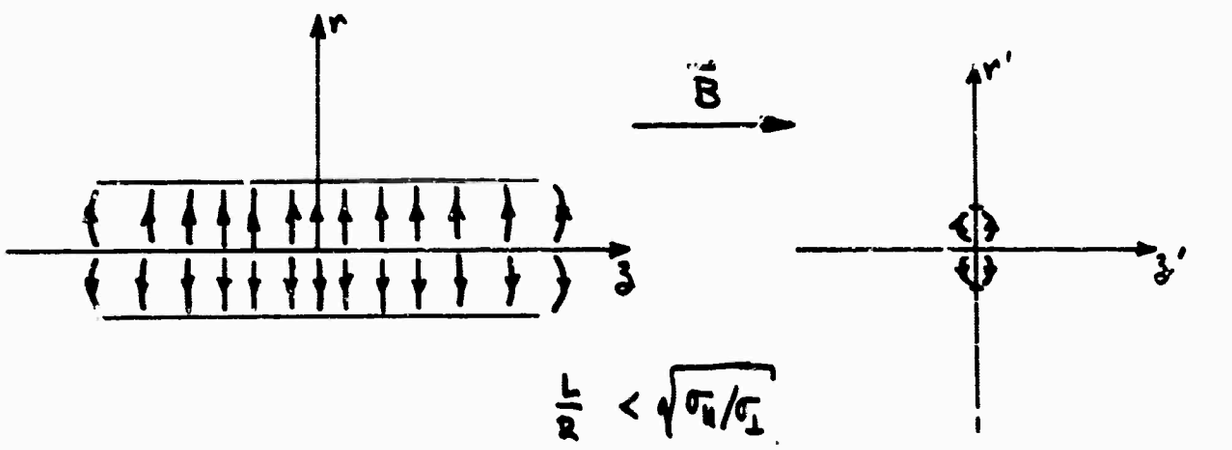

Fig. V-2b Electric field distribution in the real and transformed space.

In the r', θ', z' coordinates this radial field will be relatively uniform (within a factor of 2 to 4) for $|z'| \leq R$. In real space, therefore, the radial field is more or less uniform for $|z| \leq \sqrt{\frac{\sigma_\parallel}{\sigma_\perp}}\, R$. In other words, the high conductivity along the field lines causes the charge distribution to spread out more or less uniformly along the field lines over a width $\approx \pm \sqrt{\frac{\sigma_\parallel}{\sigma_\perp}}\, R$.

We now consider what happens to a field-aligned inhomogeneity in the plasma whose length is L and width is R. Here we assume that the neutral flow also has at least the length L. The drift velocity induced by the electric field will be of the order

$$\vec{u}_D \approx \frac{\Delta n_e}{n_e} \frac{\sigma_\perp}{\nu_i} \frac{\beta^*}{3} \left(1 + \ln \frac{2}{\beta^*}\right) \qquad (33)$$

where $\beta^* = \frac{L}{R}\sqrt{\frac{\sigma_\perp}{\sigma_\parallel}}$. This drift motion will be present not only in the inhomogeneity ($|z| \leq L/2$) but also beyond it (out to $z \simeq \sqrt{\frac{\sigma_\parallel}{\sigma_\perp}}\, R$). Within the inhomogeneity, where the drift velocity is correlated with the ion density, this motion results in a mean diffusion velocity across the field lines given by

$$\overline{\vec{u}_D} \approx \frac{\vec{\sigma}_\perp}{\nu_i} \overline{\left(\frac{\Delta n_e}{n_e}\right)^2} \frac{\beta^*}{3} \left(1 + \ln \frac{2}{\beta^*}\right). \qquad (34)$$

Beyond the inhomogeneity $\left(L < z < \sqrt{\frac{\sigma_\parallel}{\sigma_\perp}}\, R\right)$, the electric fields cause the same type of incompressible rearrangement of the plasma but, because the drift velocity is uncorrelated with the ion density, no mean transport of ions occurs.

In this case, where the longitudinal extent of the inhomogeneities is not too large, the anomalous diffusion velocity varies as B^{-1} for strong fields and is dependent on both the degree of inhomogeneity in the ion

density and the ratio of length to width of the individual irregularities. In general we would expect the irregularities in the ambient ionosphere to be field-aligned but we do not presently have estimates of their strength or shape.

In Table V-2, we have listed estimates for the magnetic field dependent factors for the normal diffusion and the anomalous diffusion velocities as a function of altitude. For the normal diffusion term the factor listed is the ratio of the diffusion velocity to the velocity that would obtain in the absence of the magnetic field. The same quantity is listed for the anomalous diffusion velocity in the special cases when the parameter γ has the values 1 or 10. Here γ is defined as

$$\sqrt{\left(\frac{\Delta n_e}{n_e}\right)^2 \frac{\beta^*}{3}\left(1 + \ell n \frac{2}{\beta^*}\right)} \quad .$$

Values for this quantity between 1 and 10 might be expected to be induced by a neutral flow field whose longitudinal dimensions are of the order of 10 times its lateral dimensions (a typical configuration) and whose axis of symmetry is not aligned with the magnetic field. In this case we would expect values for $\left(\frac{\Delta n_e}{n_e}\right)^2$ of the order of unity to arise as a result of the predominantly one-dimensional motion of the plasma along the field lines. Although the preceeding analysis is not valid for such strong variations in the plasma density we assume the effects will be qualitatively similar. Also, when the neutral flow axis and magnetic field do not coincide, polarization fields will develop due to the second term in Eq. 21: this has been ignored here.

Subject to these approximations we would expect values of γ of the order of unity when the neutral flow axis is perpendicular to the magnetic

field and of the order of 10 when the flow axis is close to but not precisely aligned with the field. When the angle between the flow axis and the field is less than the width to length ratio of the neutral flow it is not clear what order of magnitude might be expected for $\overline{\left(\Delta n_e/n_e\right)^2}$.

Table 1-2. Steady state ratios of diffusion velocity to the values expected for zero magnetic field

Altitude km	Anomalous diffusion $\sqrt{\sigma_\perp/\sigma_\parallel}$		Normal Diffusion $\left[1+\left(\frac{\omega_{c_i}}{\nu_i}\right)^2\right]^{-1}$		Longitudinal Spreading Ratio $\sqrt{\sigma_\parallel/\sigma_\perp}$
	$\gamma = 1$	$\gamma = 10$	Ambient	Shock	Ambient
100	0.70		1.0	1.0	1.4
120	.06		0.64	0.98	17
150	.008	.08	0.01	0.5	125
200	(.0015)	(.015)	0.0004	0.04	(670)
250	(.0006)	(.006)	0.00006	0.006	(1700)
300	(.0002)	(.002)	0.000006	0.0006	(5000)

In Table V-2 we also list the spreading ratio, $\sqrt{\sigma_\parallel / \sigma_\perp}$, - the ratio of the distance along the field lines that the polarization charges are spread to the lateral dimensions of the flow in the steady state. Above 200 km altitude the values are of the order of 500 or greater. These very high values are not expected to be obtained in practice for two reasons. First, since the lateral flow dimensions at 200 km altitude are of the order of a few kilometers, this ratio corresponds to spreading distances of the order of thousands of kilometers. Over these distances along the field lines the collision frequencies cannot be assumed to remain even approximately constant. As the field lines penetrate to lower altitudes the perpendicular conductivity increases, effectively tending to neutralize the charge distributions more rapidly. In the other direction, as the field lines climb to higher altitudes, the cross conductivity decreases, reducing the leakage current. This altitude effect predominantly determines the manner in which the charges are finally neutralized far from the neutral flow perturbation but is not expected to have much influence on the electric fields in the immediate neighborhood of the neutral disturbance.

A more important effect is the result of the fact that the neutral flow is not a steady-state phenomena and, under these high altitude conditions, the quasi-steady approximation may fail as far as the anomalous diffusion is concerned. The argument is as follows: We visualize the neutral motion as a primarily lateral expansion with characteristic expansion velocity V and starting at time t = 0. Due to various plasma or neutral flow inhomogeneities or to positive-negative ion asymmetries (see Section), charge separation occurs within the confines of the neutral flow field. Because of the high conductivity along the field lines there is a tendency for these

charges to spread out rapidly in the direction of the field. We expect that this spreading is accomplished as a disturbance propagating at the Alfvén speed C_A along the field lines. The nature of this Alfvén motion is discussed in Section V-6. Thus the maximum extent over which the charges may be spread by the time t is $C_A t$. Since, at this time, the lateral flow dimensions are of the order of Vt we expect that the maximum value of the spreading ratio is C_A/V. During the initial expansion of the neutral flow we expect values of V between 1 and 4 km/sec (say a mean value of 2 km/sec). Thus, maximum spreading ratios during the first several seconds of the motion are expected to be of the order of 100. (Here we are referring only to the spreading of disturbances whose lateral dimensions are comparable to those of the neutral flow field. Smaller disturbances will attain their quasi-steady state values more quickly.)

According to the above argument we expect that the appropriate values for the anomalous diffusion velocities above an altitude of 150 km are not as low as those shown in Table V-2 but may remain more comparable to the values at 150 km. Thus it appears that below about 200 km the normal diffusion mechanism can account for most of the motion across the field lines in the region of the neutral flow. Above about 200 km the electric fields due to polarization charges may contribute much of the cross field motion. The relative importance of each mechanism depends on several parameters (shock strengths and velocities, ambient ion density, angle between trajectory and magnetic field, degree of inhomogeneity, etc.) so that these values can only be expected to be indicative. More detailed examination of specific situations will be required to get quantitative results.

The present considerations indicate that at some altitude between 120 and 150 km the motion of the ions across the magnetic field begins to be appreciably reduced below the neutral velocity. Above 200 km altitude the lateral velocity of the ions may be expected to be between 1 and 10% of the neutral velocity during the first few seconds or tens of seconds of the neutral motion.

At late times, when the neutral density is comparable to the ambient density and the polarization fields have reached their quasi-steady values, the cross-field motion will be even further suppressed.

V-3b. Linearized Steady State Approximation for Non-Identical Ions

When the positive and negative ions do not have identical properties, charge separations can result from this asymmetry. In this section we develop the steady state equations in the approximation that the electron mass is small compared to the ion mass. For small values of m_e/m_i, Eqs. V-2-5 and 6 may be recast in the form (for $\vec{u} = \vec{v} = 0$)

$$\vec{u} = \left(\vec{v} \times \vec{\omega}_c + \vec{a}_1 + \beta^2 \nu_{12} \vec{v} \right) / \nu_1 \qquad (1)$$

and

$$\vec{\mathcal{E}} = -\left(\frac{\vec{a}_1}{\nu_1} - \vec{v} \right) \times \vec{\omega}_c + \vec{A}_2 + \vec{v} \left(\omega_c^2 + \beta^2 \nu_1 \nu_2 \right) / \nu_1 - \vec{v}_\parallel \omega_c^2 / \nu_1 \quad . \qquad (2)$$

Here we have defined a source term $\vec{A}_2$ according to

$$\vec{A}_2 = \beta^2 \left(\nu_{12} \vec{a}_1 - \nu_1 \vec{a}_2 \right) / \nu_1 \qquad (3)$$

This term represents a current source and is non-zero in general because of the asymmetry between the interactions of neutrals with the ions and neutrals with the electrons.

Equation 2 may be rewritten to express the current velocity $\vec{v}$ in terms of the driving forces:

$$\vec{v} = \frac{4\pi c}{\omega_p^2} \left[\sigma_P \vec{F}_\perp + \sigma_H \vec{\omega}_c \times \vec{F}_\perp / \omega_c + \sigma_\parallel \vec{F}_\parallel \right] , \qquad (4)$$

where $\vec{F}$ is an effective electric field defined by

$$\vec{F} = \vec{\mathcal{E}} + \vec{a}_1 \times \vec{\omega}_c / \nu_1 - \vec{A}_2 \quad . \qquad (5)$$

Here

$$\sigma_P = \frac{\omega_p^2}{4\pi c} \frac{\nu_1}{\omega_c^2} \left[\frac{1 + \beta^2 \nu_1 \nu_2 / \omega_c^2}{\left(1 + \beta^2 \nu_1 \nu_2 / \omega_c^2 \right)^2 + \left(\nu_1 / \omega_c \right)^2} \right] , \qquad (6)$$

$$\sigma_H = \frac{\omega_p^2}{4\pi c}\,\frac{\nu_1}{\omega_c^2}\left[\frac{\nu_1/\omega_c}{\left(1+\beta^2\nu_1\nu_2/\omega_c^2\right)^2+\left(\nu_1/\omega_c\right)^2}\right], \quad (7)$$

and

$$\sigma_\parallel = \omega_p^2/4\pi c\beta^2\nu_2 . \quad (8)$$

The steady state condition that div $\vec{J}=0$ and curl $\vec{E}=0$ yield an equation for the electric potential due to the polarization charges:

$$\operatorname{div}\left[\sigma_P\nabla_\perp\varphi + \sigma_\parallel\nabla_\parallel\varphi + \sigma_H\frac{\vec{\omega}_c\times\nabla_\perp\varphi}{\omega_c}\right] = -\operatorname{div}\vec{G} \quad (9)$$

where the source function $\vec{G}$ is defined by

$$\vec{G} = \sigma_P\left(\frac{\vec{a}_1\times\vec{\omega}_c}{\nu_1}-\vec{A}_{2\perp}\right)+\sigma_H\left(\frac{\omega_c\vec{a}_{1\perp}}{\nu_1}-\frac{\vec{\omega}_c\times\vec{A}_{1\perp}}{\omega_c}\right)-\sigma_\parallel\vec{A}_{2\parallel} \quad (10)$$

As was done in Section V-3a we assume first that the ratio of the parallel conductivity $\sigma_\parallel$ to the perpendicular (Pedersen) conductivity σ_P is independent of position. We also, as before, transform to the space r', θ', z' in which

$$r' = r$$
$$\theta' = \theta \quad (11)$$
$$z' = \sqrt{\frac{\sigma_P}{\sigma_\parallel}}\,z$$

If ∇' represents the gradient operator in the r', θ', z' space, we may rewrite Eq. in the form

$$\nabla'\cdot\left(\sigma_P\nabla'\varphi\right)+\left(\nabla'\varphi\times\nabla'\sigma_H\right)_\parallel = -\nabla\cdot\vec{G} \quad (12)$$

If we assume that the spatial variations in the Pedersen and Hall conductivities are small, then the first order approximation to the potential equation becomes:

$$\nabla'^2\varphi = -\frac{1}{\sigma_P}\,\mathrm{div}\left\{\sigma_P\left(\frac{\vec{a}_1\times\vec{\omega}_c}{\nu_1}-\vec{A}_{2\perp}\right)+\sigma_H\left(\frac{\omega_c}{\nu_1}\vec{a}_1-\frac{\vec{\omega}_c\times\vec{A}_2}{\omega_c}\right)-\sigma_\parallel A_{2\parallel}\right\} \quad (13)$$

When both the plasma and the driving neutral-ion interaction are axially symmetric (we always assume that the driving forces have r and z components only), Eq. 13 reduces to the form:

$$\nabla'^2\varphi = -\frac{1}{\sigma_P}\,\mathrm{div}\left\{\sigma_H\,\frac{\omega_c}{\nu_1}\vec{a}_{1\perp}-\sigma_P\vec{A}_{2\perp}-\sigma_\parallel A_{2\parallel}\right\} . \quad (14)$$

Throughout most of the ionosphere the term $\beta^2\nu_1\nu_2/\omega_c^2$ is small compared to unity (see Table III-1)* In this case $\sigma_H \simeq \frac{\nu_1\sigma_P}{\omega_c}$, and

$$\sigma_P \simeq \frac{\omega_p^2}{4\pi c}\,\frac{\nu_1}{\omega_c^2}\,\frac{1}{1+\left(\nu_1/\omega_c\right)^2} . \quad (15)$$

The ratio of perpendicular to parallel conductivities is given by

$$\frac{\sigma_P}{\sigma_\parallel} = \frac{\beta^2\nu_1\nu_2}{\omega_c^2+\nu_1^2} \quad (16)$$

Since we expect values for $\vec{A}_2$ to be smaller than those for $\vec{a}_1$ by a factor of the order of $\sqrt{m_e/m_i}$, the source function $\vec{G}$ in Eq. 10 is approximately

*This assumption is made throughout the remainder of this section.

represented by

$$\vec{G} \simeq \sigma_P \left(\vec{a}_{1\perp} + \vec{a}_{1\perp} \times \frac{\vec{\omega}_e}{\nu_1} \right) - \sigma_\parallel \vec{A}_{2\parallel} \cdot \qquad (17)$$

For the axially symmetric case, the potential equation then takes the form:

$$\nabla^2 \varphi = - \frac{1}{\sigma_P} \operatorname{div} \left(\sigma_P \vec{a}_{1\perp} - \sigma_\parallel \vec{A}_{2\parallel} \right). \qquad (18)$$

The first term on the right-hand side of Eq. 18 results from the fact that the ions move more easily across the field lines than do the electrons. The second term is independent of the magnetic field and is a result of the difference between the accelerations imparted by the neutrals to the ions and to the electrons.

The drift motion due to the radial variations of the driving term $\vec{a}_1$ may be evaluated as follows. Due to this term, the electric field has value, within the confines of the neutral flow field, of the order of

$$\vec{\mathcal{E}}_r \simeq - f \vec{a}_{1r}$$

where f is the reduction factor (defined in Section III-3a due to the spreading of the charge distribution along the field lines:

$$f \simeq \frac{\beta^*}{3} \left(1 + \ln \frac{2}{\beta^*} \right).$$

Using Eqs. 1, 2 and 4 we may roughly evaluate the magnitude of the outward drift velocity. Neglecting terms of the order $\sqrt{m_e/m_i}$ compared to unity, we have

$$\vec{u} = \frac{a_{1\parallel}}{\nu_1} + \left[\frac{\vec{a}_{1\perp}}{\nu_1} + \frac{\vec{a}_{1\perp} \times \vec{\omega}_e}{\nu_1^2} + \frac{\vec{\mathcal{E}}_\perp - \vec{A}_{2\perp}}{\nu_1} + \frac{(\vec{\mathcal{E}}_\perp - \vec{A}_{2\perp}) \times \vec{\omega}_e}{\nu_1^2} \right] \left[\frac{\nu_1^2}{\nu_1^2 + \omega_e^2} \right] \cdot \qquad (19)$$

We may estimate the outward drift to be

$$\vec{u}_r = \frac{\nu_1^2}{\nu_1^2+\omega_c^2}\frac{\vec{a}_i}{\nu_1}\left(1-f+O(f\beta^2\nu_2/\nu_1)\right). \qquad (20)$$

Thus, when the reduction of the polarization field by anisotropic conduction along the field lines is considerable, ($f \ll 1$) the outward drift motion is determined by the ions alone and has the same value as in the identical particle model (Section V-3a). For cylindrical symmetry, however, there is no conduction along the field lines ($f=1$). In this case the outward drift velocity, although only evaluated by Eq. to order of magnitude, is much smaller (c.f. Eq. III-1-2) due to the fact that the electrons now have to be dragged across the field lines.

When the variations of the plasma density in space are appreciable, additional polarization fields will arise. As was shown in Section V-3a these can result in an appreciable increase in the rate of diffusion of the plasma across the field lines. We will not attempt a detailed evaluation of these motions here but simply identify the terms giving rise to the drift motion. This case is somewhat different than when the ions are identical since here a polarization field exists even when the plasma is uniform.

In the linear approximation we may separate the electric field into two terms $\vec{\mathcal{E}}_0(=\nabla\varphi_0)$ and $\vec{\mathcal{E}}_1(=\nabla\varphi_1)$. $\vec{\mathcal{E}}_0$ is the field that would exist in a uniform plasma and $\vec{\mathcal{E}}_1$ is the contribution due to variations in the plasma density and (azimuthal only) in the neutral flow. Here φ_0 may be evaluated from

$$\nabla^2\varphi_0 = -\nabla\cdot\vec{a}_{i\perp} + \frac{\sigma_\parallel}{\sigma_P}\nabla\cdot\vec{A}_{n\parallel} \qquad . \qquad (21)$$

The potential due to the variations in plasma density is determined by

$$\nabla'^2\varphi_1 = -\frac{1}{\sigma_{P_r}}\frac{\partial}{\partial\theta}\left(\frac{\sigma_P a_{1r}\omega_e}{\nu_i}\right) - \frac{\varepsilon_{o_r}}{\sigma_{P_r}}\frac{\partial\sigma_n}{\partial\theta} - \frac{a_{1r}}{\sigma_P}\frac{\partial\sigma_P}{\partial r} - \frac{\nabla'\sigma_P}{\sigma_P}\cdot\varepsilon_o' - \frac{a_{1\theta}}{\sigma_P}\frac{\partial\sigma_n}{\partial\theta'} \qquad (21)$$

The first term in Eq. 21 is the only one appearing in the identical ion model (Eq. 9). The other terms result from the fact that the positive and negative ions are different. The first two terms in Eq. 21 give rise to electric fields which cause predominantly radial drift motions. The third and fourth term result in predominantly azimuthal drifts and the last term does not give rise to a drift motion (to a first approximation).

More detailed considerations similar to those in Section V-3a would be required to evaluate the effect of these additional terms. In any case it is clear that the electrons affect the plasma motion primarily through the polarization fields, and that the importance of the electron-neutral and electron-ion interactions depends on the extent to which the electrons can neutralize the polarization charges by conduction along the field lines. In general, this question can only be answered by considering the geometry and time dependence of the specific problem of interest in some detail. In the following paragraphs we restate this conclusion in more general terms.

The first term on the right-hand side of Eq. 21 is the (pseudo) charge density that results from the fact that the electrons are more strongly bound to the field lines than are the ions. In the cylindrically symmetric case, the charge neutral condition requires that the radial velocities of ions and electrons be approximately equal. Rather strong radial fields must then be set up to pull the electrons across the field lines with the ions.

When the flow dimension in the direction parallel to the field is not too large, the electrons do not necessarily have to move with the ions. In this case, when no azimuthal polarization electric fields are present, the motion across the field lines is primarily of the ions only. The electrons move relatively freely along the field lines in an attempt to maintain their density approximately equal to the ion density.

When the distance the electrons have to move to compensate for a given lateral ion motion is not too large (i.e., small compared to $\sqrt{\sigma_e/\sigma_p}$ times the ion displacement), the forces required to move the electrons are small compared to those required for the ions. Since, in the absence of an externally applied electric field, the driving forces exerted on the electrons are small compared to those exerted on the ions, the motion of the plasma is largely controlled by the properties of the heavy ions and their interactions with the neutrals and is insensitive to the electronic properties. However, in certain situations the electrons can have a considerably stronger influence on the plasma motion than simply the mass ratio would indicate. For example, when the symmetry of the neutral flow field is such that the electric fields induced by the ion motion are nearly perpendicular to the magnetic field lines, relatively large electric fields have to be set up in order to get significant motion of the electrons. Also, when the distances the electrons have to travel in order to compensate for a given ion motion are much larger than the ion displacements, the electrons must be accelerated to considerably higher velocities than do the ions. These effects will tend to increase the influence of the electronic properties on the motion of the plasma.

Formulation of the Nonlinear Equations for Simplified G etries

In the region of the ionosphere under consideration, neutral particles are about 10^4 times more numerous than charged particles. On the other hand, the Larmor cyclotron frequency of each charged species is considerably higher than its collision frequency. In this situation, since the earth's magnetic field is rather weak, a one-fluid hydrodynamic calculation of the motion of the neutral particles may be carried out without regard to the currents or ponderomotive forces which this motion induces. The ions and electrons, however, describe a number of Larmor cycles in the geomagnetic field between collisions, and their motion is therefore strongly affected by the magnetic field. The following simple example provides some insight into the situation.

Consider a charged particle with charge $q = \pm e$, immersed in a uniform magnetic field and a bath of neutral particles. If collisions are infrequent compared with the rate of Larmor gyration in the magnetic field, we may view the collision as a displacement of the guiding center of the particle. A collision will move the guiding center by at most $2\ r_L$ ($r_L = mVC/eB$ is the Larmor radius). We expect the average "drift" velocity

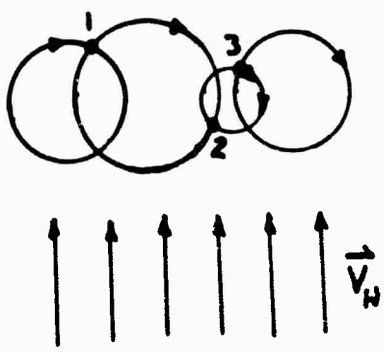

⊗ ($\vec{B}$ field out of paper)

Fig. 1 Ion in a Neutral-Particle Bath

of the guiding center to be of the order of $(\nu/\omega_L)\, V_N$, where ν is the collision frequency with the neutrals. The collisions will predominantly occur in the portion of the cycle when the ion is moving against the neutral stream, and the collisions will tend to make the particle drift to the right (in Fig. 1) if it is positively charged and to the left if it is negative. A calculation of the drift motion, taking averages over all collisions (Appendix II), will reveal that the lateral average velocity (in the direction $q\, \vec{V}_N \times \vec{B}$) is $\nu\omega_L(\nu^2 + \omega_L^2)^{-1}\, V_N$, and the drift parallel to V_N is at the speed $\nu^2(\nu^2 + \omega_L^2)^{-1}\, V_N$. The drift velocity is always perpendicular to the direction from which the neutrals appear to come, but to the ion in its drifting motion the apparent direction of the neutral stream changes; hence the component parallel to V_N arises. The above simple picture neglects electric fields.

Since the sign of the component of drift motion perpendicular to V_N is dependent on the sign of the charge, an electric current will arise. This current will cause a change in $\vec{B}$ (though slight), and the time-rate of this change will induce an electric field, according to Ampere's law. This electric field will bring about an additional drift of the charged particles, according to the well-known expression

$$\vec{V}_d = c\, \vec{E} \times \vec{B}/B^2 ,$$

which is independent of charge. The simple picture of figure 1 will hold if we perform a Lorentz transformation to the frame of reference in which $\vec{E} = 0$ if $\vec{E}$ does not vary significantly over a Larmor radius.

In the following sections, we will undertake a detailed solution of the ion and electron motion, including the influence of the magnetic and induced

electric fields and the neutral flow field, in the vicinity of a missile traversing the ionosphere. The philosophy will be to understand one simple geometry, namely that of cylindrically symmetric neutral flow with the geomagnetic field along the axis of symmetry. We will also discuss preliminary attempts to apply these results to more general neutral flow fields, for example the spherically symmetric motion of the neutral gas in a uniform magnetic field.

In the analysis, it will be assumed that ions and electrons collide only with neutrals. This approximation will be justified on the basis of the relative number densities and cross sections. It will also be shown that the relative change of the geomagnetic field induced by the flow is very small. Any ionization or recombination occurring during characteristic flow times will be neglected, as they have little bearing on the plasma motion and are very difficult to include.

A number of other simplifications arise from the large time scale peculiar to the flows under consideration. For example, since the mean free time and mean free path of the neutrals are of the order of 0.1 to 1 sec and 1 km, the passage of the neutral flow past a point in space excites plasma oscillations (whose frequency is of the order of 10 mc/sec) only very weakly.

In addition to these effects, it is expected that the electron motion is coupled to the ion motion through the magnetic field, effectively limiting the speed at which divergence-free current disturbances in the electron fluid can propagate through the plasma. This limiting velocity is expected to be of the order of the ion Alfvén speed.

Basic Equations

The motion is governed by the following equations (using c. g. s. Gaussian units) , with subscripts i and e referring to ions (of various species) and electrons:

$$\nabla \times \vec{E} = -\frac{1}{c}\dot{\vec{B}} \tag{1}$$

$$\nabla \times \vec{B} = \dot{\vec{E}}/c + 4\pi \vec{J} \tag{2}$$

$$\vec{J} = \frac{e}{c}(n_i \vec{v}_i - n_e \vec{v}_e) \tag{3}$$

$$\dot{n}_i + \nabla \cdot (n_i \vec{v}_i) = 0 \tag{4}$$

$$\dot{n}_e + \nabla \cdot (n_e \vec{v}_e) = 0 \tag{5}$$

$$n_i m_i \left(\frac{\partial \vec{v}_i}{\partial t} + \vec{v}_i \cdot \nabla \vec{v}_i \right) = -\nabla \cdot \vec{P}_i + e n_i \left(\vec{E} + \frac{\vec{v}_i \times \vec{B}}{c} \right) + n_i \vec{I}_i \tag{6}$$

$$n_e m_e \left(\dot{\vec{v}}_e + \vec{v}_e \cdot \nabla \vec{v}_e \right) = -\nabla \cdot \vec{P}_e - e n_e \left(\vec{E} + \frac{\vec{v}_e \times \vec{B}}{c} \right) + n_e \vec{I}_e \tag{7}$$

The collision integral for momentum exchange of the jth species with all other species is:[1]

$$\vec{I}_j = \sum_{k \neq j} \frac{m_k}{m_j + m_k} \int (\vec{c}_k - \vec{c}_j) f_j(\vec{c}_j) f_k(\vec{c}_k) \sigma_m \left| \vec{c}_j - \vec{c}_k \right| d\vec{c}_j \, d\vec{c}_k \tag{8}$$

where $\vec{c}_k$ is the velocity of a single particle of the kth species and f_k is the velocity distribution function for the kth species. $\vec{c}'$ represents the velocity after a collision. The momentum transfer cross section used here is defined as

$$\sigma_m = 2\pi \int_0^{\pi} \sigma(\theta)(1-\cos\theta)\sin\theta\, d\theta \quad . \tag{9}$$

$\vec{V}_j$ is the mean velocity of the jth species and $\mathbf{P}_j$ is its pressure tensor. We will consider only cases where there is a single ion species, for simplicity. The energy-conservation equation is omitted since, in all cases considered, the pressure gradient term in Eqs. (6) and (7) will be neglected* in comparison with the momentum-exchange integrals $\vec{I}_i$, $\vec{I}_e$. In this approximation Eqs. (1) to (7) form a closed system. No chemical reactions have been included. However, charge exchange between an ion and a parent atom (same species), which is the dominant charge-transfer process, will be included as part of the momentum-exchange integral, since for such a pair the results of charge-exchange and momentum-exchange are equivalent.

Formidable difficulties arise in the evaluation of the collision integral in (8). The distribution functions f_j, f_k can hardly be called Maxwellian with any confidence since we must allow for the possibility of quite large ion "slip" relative to the neutrals; a three-fluid model using Maxwellian distributions could be used as a good approximation in the event that the fluid were in quasi-equilibrium. However, the criterion for the validity of this approach is not clear when the mean relative velocities are not small compared with thermal velocities. It would be very inaccurate to approximate the f_j's with δ-functions, since the thermal velocity of the molecules and ions behind the shock is of the same order as the velocity of propagation of the shock into the undisturbed surrounding.

Even if the f_j's were known, σ_m is usually not a convenient function of the relative speed of the interacting particles. The integration of Eq. (8)

*See Section III-2.

is quite complicated even if we assume some r^{-n} potential law between particles. Therefore we will simply lump all of the uncertain factors in the integral in (8) into a collision frequency, ν, which we may assume to be constant to a reasonable approximation:

$$\vec{I}_j = \sum_{k \neq j} n_j \nu_{jk} (\vec{V}_k - \vec{V}_j) \qquad (10)$$

(ν_{jk} is proportional to the density n_k.)

Equation (10) is exact for an interaction potential which varies as r^{-4}, (the so-called "Maxwellian-molecule" force law). In this case σ_m varies as $(V_{rel})^{-1}$, and the integrations over arbitrary f_j, f_k become trivial. Dalgarno[2] has shown that the r^{-4} interaction potential is a rather good approximation for ion-neutral encounters at low energies ($\lesssim$ 1 eV). For hard-sphere potentials ($n = \infty$, σ_m independent of energy), Zhdanov[3] has shown that for the quasi-equilibrium case $\left[(\vec{V}_k - \vec{V}_j) \ll V_{Thermal} \right]$ the collision integral $\vec{I}$ again takes the form shown in (10).

Since a large part of the subsequent analysis will involve the simple case of flow which is cylindrically symmetric about the geomagnetic field direction, we now obtain the form of Eqs. (1) to (7) in this special case. In cylindrical coordinates, with $\frac{\partial}{\partial z} = \frac{\partial}{\partial \theta} = 0$, and dropping ∇-[illegible],

$$\frac{1}{r} \frac{\partial}{\partial r} (r E_\theta) = -\frac{1}{c} \frac{\partial B_z}{\partial t} \qquad (11)$$

$$-\frac{\partial B_z}{\partial r} = \frac{4\pi e}{c} (n_i v_i - n_e v_e) + \frac{1}{c} \frac{\partial E_\theta}{\partial t} \qquad (12)$$

$$0 = \frac{4\pi e}{c} (n_i u_i - n_e u_e) + \frac{1}{c} \frac{\partial E_r}{\partial t} \qquad (13)$$

$$\frac{\partial n_i}{\partial t} + \frac{1}{r}\frac{\partial}{\partial r}(r n_i u_i) = 0 \tag{14}$$

$$\frac{\partial n_e}{\partial t} + \frac{1}{r}\frac{\partial}{\partial r}(r n_e u_e) = 0 \tag{15}$$

$$\frac{\partial u_i}{\partial t} + u_i\frac{\partial u_i}{\partial r} - \frac{v_i^2}{r} = \frac{e}{m_i}\left(E_r + \frac{v_i B_z}{c}\right) - \nu_i(u_i - V_N) \tag{16}$$

$$\frac{\partial u_e}{\partial t} + u_e\frac{\partial u_e}{\partial r} - \frac{v_e^2}{r} = -\frac{e}{m_e}\left(E_r + \frac{v_e B_z}{c}\right) - \nu_e(u_e - V_N) \tag{17}$$

$$\frac{\partial v_i}{\partial t} + u_i\frac{\partial v_i}{\partial r} - \frac{u_i v_i}{r} = \frac{e}{m_i}\left(E_\theta - \frac{u_i B_z}{c}\right) - \nu_i v_i \tag{18}$$

$$\frac{\partial v_e}{\partial t} + u_e\frac{\partial v_e}{\partial r} + \frac{u_e v_e}{r} = -\frac{e}{m_e}\left(E_\theta - \frac{u_e B_z}{c}\right) - \nu_e v_e \tag{19}$$

Here u, v are radial and azimuthal components of velocity. The neutrals have only a radial velocity V_N. All species of neutrals are assumed to have the same mean velocity, when averaged over a few collision times or mean free paths. Since $E_z = 0$, there being no motion along the z-direction, the r & θ components of Eq. (1) yield $\partial B_r/\partial t = 0$, $\partial B_\theta/\partial t = 0$; hence $B_r = B_\theta = 0$ for all time.

We have elected to work with the equations of motion of the ions and electrons, since it is more direct than to think of such motion in terms of an "Ohm's Law" which includes Hall current and ion slip. The Ohm's Law approach results in a simplification only if a steady state is assumed. It is shown subsequently that Eqs. (6) and (7) lead to the usual form of the generalized Ohm's Law in a steady, uniform state.

Before proceeding to numerical calculations, we will learn what we can from a linearized approximation to the governing equations. We will consider the general axially symmetric case, since the assumption of cylindrical symmetry is needlessly restrictive in the linearized approximation and since we will want to discuss more general axial symmetry later.

The object of the present section is to determine the accuracy of several levels of simplicity in the governing equations. This is done in the hope that it will be possible to neglect terms which are related to high-frequency oscillations of the plasma, and thus make possible numerical calculations with reasonably long time steps. For example, if $n_e = 10^6$ cm^{-3}, the plasma angular frequency is 5.5×10^7 sec^{-1}, whereas we will be concerned with flow times of the order of one second.

Assuming a constant density of neutrals, n_N, constant ion and electron collision frequencies with neutrals, ν_i and ν_e, and treating $\vec{v}_e$, $\vec{v}_i$ $(n_e - n_{eo})$, $(n_i = n_{io})$ and $(\vec{B} - \vec{B}_o)$ as first-order quantities and neglecting $\nabla \cdot \mathbf{P}$ we obtain from Eqs. (1) to (7) in the axially symmetric case the following equations (with cylindrical coordinates and $\partial/\partial\theta = 0$):

$$-\frac{\partial E_\theta}{\partial z} = -\frac{1}{c}\frac{\partial B_r}{\partial t} \tag{20}$$

$$\frac{\partial E_r}{\partial z} - \frac{\partial E_z}{\partial r} = -\frac{1}{c}\frac{\partial B_\theta}{\partial t} \tag{21}$$

$$\frac{1}{r}\frac{\partial}{\partial r}(r E_\theta) = -\frac{1}{c}\frac{\partial B_z}{\partial t} \tag{22}$$

$$-\frac{\partial B_\theta}{\partial z} = \frac{4\pi n_{e_0}}{c}(u_i - u_e) + \frac{1}{c}\frac{\partial E_r}{\partial t} \tag{24}$$

$$\frac{\partial B_r}{\partial z} - \frac{\partial B_z}{\partial r} = \frac{4\pi e n_{e_0}}{c}(v_i - v_e) + \frac{1}{c}\frac{\partial E_\theta}{\partial t} \tag{25}$$

$$\frac{1}{r}\frac{\partial}{\partial r}(rB_\theta) = \frac{4\pi e n_{e_0}}{c}(w_i - w_e) + \frac{1}{c}\frac{\partial E_z}{\partial t} \tag{26}$$

$$\frac{\partial n_i}{\partial t} + n_{i_0}\left(\frac{1}{r}\frac{\partial}{\partial r}(r u_i) + \frac{\partial w_i}{\partial z}\right) = 0 \tag{27}$$

$$\frac{\partial n_e}{\partial t} + n_{e_0}\left(\frac{1}{r}\frac{\partial}{\partial r}(r u_e) + \frac{\partial w_e}{\partial z}\right) = 0 \tag{28}$$

$$\frac{\partial \vec{v}_i}{\partial t} = \frac{e}{m_i}\left(\vec{E} + \frac{\vec{v}_i \times \vec{B}_0}{c}\right) - \nu_i(\vec{v}_i - \vec{V}_N) \tag{29}$$

$$\frac{\partial \vec{v}_e}{\partial t} = -\frac{e}{m_i}\left(\vec{E} + \frac{\vec{v}_e \times \vec{B}_0}{c}\right) - \nu_e(\vec{v}_e - \vec{V}_N) \tag{30}$$

Taking the curl of Eqs. (23) to (25) and $\partial/\partial t$ of (26) to (28), we obtain

$$-\frac{\partial^2 E_r}{\partial t^2} + \frac{\partial^2 E_z}{\partial r \partial z} = -\frac{4\pi e n_{e_0}}{c^2}\frac{\partial}{\partial t}(u_i - u_e) - \frac{1}{c^2}\frac{\partial^2 E_r}{\partial t^2} \tag{31}$$

$$\frac{\partial^2 E_\theta}{\partial z^2} + \frac{\partial}{\partial r}\left(\frac{1}{r}\frac{\partial}{\partial r}(rE_\theta)\right) = \frac{4\pi e n_{e_0}}{c^2}\frac{\partial}{\partial t}(v_i - v_e) + \frac{1}{c^2}\frac{\partial^2 E_\theta}{\partial t^2} \tag{32}$$

$$\frac{1}{r}\frac{\partial}{\partial r}\left(r\left[\frac{\partial E_r}{\partial z} - \frac{\partial E_z}{\partial r}\right]\right) = -\frac{4\pi e n_{e_0}}{c^2}\frac{\partial}{\partial t}(w_i - w_e) - \frac{1}{c^2}\frac{\partial^2 E_z}{\partial t^2} \tag{33}$$

Thus $\vec{B}$ is uncoupled, as are n_i and n_e, and there remain 9 scalar equations in the unknowns $\vec{v}_i, \vec{v}_e$, and $\vec{E}$.

The plasma motion may be viewed as a forced oscillation with a forcing function $\vec{V}_N(t)$ independently prescribed. In problems of concern here, significant variations of the flow field require significant fractions of one second to take place; thus we expect the Fourier components of $\vec{V}_N(t)$ at the plasma frequency to be small. An important simplification will therefore be the assumption that $n_i = n_e$, which, as we shall see, eliminates the unimportant high frequency oscillations. In this analysis we restrict ourselves to the condition that the radial and longitudinal motions of the positive and negative ions are identical. This result follows from the assumption $n_i = n_e$ when the particles are identical in general or when the driving interactions have cylindrical symmetry if the particles have different masses. In the general axially symmetric configuration for differing particles, longitudinal electron currents may radically alter the coupling of the ions with the magnetic field. However, for the present analysis, we are concerned with examining the non-linear effects and we shall make the assumption that $u_e = u_i = u$ and $w_e = w_i = w$ (Eqs. 29, 30) in order to get a tractable first approach. This permits only azimuthal currents, which do not change the Coulomb E-field. In order that this model be self-consistent, it becomes necessary to drop Eqs. (33) and (35), and to determine E_r, E_z by the requirements that $u_e = u_i$ and $w_e = w_i$ in the r, z components of Eqs. (31) and (32). We then have four coupled equations (assuming $v_N = 0$, a non-rotating neutral flow field):

$$\frac{\partial^2 E_\theta}{\partial z^2} + \frac{\partial}{\partial r}\left(\frac{1}{r}\frac{\partial}{\partial r}(rE_\theta)\right) = \frac{4\pi e n_0}{c^2}\frac{\partial}{\partial t}\left(v_i - v_e\right) + \frac{1}{c^2}\frac{\partial^2 E_\theta}{\partial t^2} \qquad (36)$$

$$\left(1+\frac{m_e}{m_i}\right)\frac{\partial u}{\partial t} = \omega_i (v_i - v_e) - (\nu_i + m_e \nu_e / m_i)(u - u_n) \tag{37}$$

$$\frac{\partial v_i}{\partial t} = \frac{e}{m_i}\left(E_\theta - u\frac{B_0}{c}\right) - \nu_i v_i \tag{38}$$

$$\frac{\partial u_e}{\partial t} = -\frac{e}{m_e}\left(E_\theta - u\frac{B_0}{c}\right) - \nu_e v_e \tag{39}$$

In addition, there are the uncoupled equations:

$$\left(1+\frac{m_e}{m_i}\right)\frac{\partial w}{\partial t} = -\left(\nu_i + m_e \nu_e / m_i\right)(w - w_n) \tag{40}$$

$$E_z = \frac{m_i}{e}\left(\frac{\partial w}{\partial t} + \nu_i (w - w_n)\right) \tag{41}$$

$$E_r = -\frac{\nu_i B_0}{c} + \frac{m_i}{e}\left(\frac{\partial u}{\partial t} + \nu_i (u - u_n)\right) \tag{42}$$

In the identical particle model, the electrons and ions have equal masses, and equal but opposite charges. In this case (from (38) and (39)), $v_i = v_e \equiv v$, and one more dependent variable is eliminated. Furthermore, substituting Eqs. (37) and (40) into (41) and (42) this limit yields $E_r = E_z = 0$. We obtain a similar form of the equations when $m_e \neq m_i$, by introducing the variables:

$$w = v_i - v_e$$

$$\bar{v} = v_i + m_e \nu_e / m_i \tag{43}$$

Then, from (38) and (39),

$$\frac{\partial v}{\partial t} = \frac{e m}{m_i m_e}\left(E_\theta - u\frac{B_\theta}{c}\right) - \nu' v - \bar{v}\frac{m_i}{m}(\nu_i - \nu_e) \qquad (44)$$

$$\frac{\partial \bar{v}}{\partial t} = \frac{m_e}{m}(\nu_e - \nu_i)v - \nu_i' \bar{v} \qquad (45)$$

where $m = m_i + m_e$, $\nu_e' = (m_i\nu_e + m_e\nu_i)/m$ and $\nu_i' = (m_i\nu_i + m_e\nu_e)/m$. From (45), we estimate $\bar{v}$ to be of the order of

$$\bar{v} \approx m_e(\nu_e - \nu_i)v/m\nu_i' .$$

Since we expect $\nu_e/\nu_i \approx (m_i/m_e)^{\frac{1}{2}}$, the term involving $\bar{v}$ in (44) is smaller than the term involving v by $(m_e/m_i)^{\frac{1}{2}}$. Thus for $m_e \ll m_i$, equation (44) takes the form:

$$\frac{\partial v}{\partial t} \approx \frac{e m}{m_i m_e}\left(E_\theta - u\frac{B_\theta}{c}\right) - \nu_e' v. \qquad (46)$$

Equation (46) has the same form as does the combination of (38) and (39) for ions of equal mass and opposite charge. The resulting simplification will be used extensively.

We now have three models of the linearized problem, which we wish to compare in detail. These are represented by:

a) Equations (31) to (35), the general problem, which we shall be able to handle only for cylindrical symmetry.

b) The "electrical neutrality" model, $n_i = n_e$, which employs Eqs. (36) to (39), and which holds for arbitrary axial symmetry for identical particles in general and for non-identical particles

when it can be shown that the r and z motions are the same.

c) The "very unequal mass" model ($m_e \ll m_i$ and $n_i = n_e$), in which Eqs. (38) and (39) are replaced by (46), and which has the same mathematical form as the "equal mass" model; it also permits a formal axial symmetry.

We now wish to express the equation for the electric field in terms of a source function. To do this, we first perform a Fourier-transformation in time of the equations governing each model. In each of the three models, we substitute into Eq. (34) from the other pertinent equations to obtain a differential equation in space for the transform $\mathcal{E}$, which has the form

$$\nabla^2 \mathcal{E} + \mathcal{E}\left(k^2(\omega) - \frac{1}{r^2} \right) = A(\omega)\, u_N(\vec{r}, \omega)$$

where

$$\mathcal{E}(\vec{r}, \omega) = \frac{1}{\sqrt{2\pi}} \int_{-\infty}^{\infty} E_\theta(\vec{r}, t)\, e^{i\omega t}\, dt.$$

The functions $A(\omega)$ and $k^2(\omega)$ are shown below for each model.

(a) General Case (cylindrical symmetry).

$$k^2 = \frac{\omega^2}{c^2} + \frac{i\omega\omega_p^2}{\omega_e c^2}\left[\frac{g(1+g_H^2) - \frac{\omega_p^2}{i\omega\omega_e} g^2}{1 + g^2 - g_H^2 - \frac{\omega_p^2}{i\omega\omega_e} g(1+g_H^2)} \right] \qquad (48)$$

$$A(\omega) = \frac{i\omega 4\pi e n_{e_0}}{c^2} \left\{ \frac{\frac{\nu_i}{\nu_i - i\omega}\left[g_i(1+g_e^2) - \frac{\omega_p^2}{i\omega\omega_e} g g_e \right] + \frac{\nu_e}{\nu_e - i\omega}\left[g_e(1+g_i^2) - \frac{\omega_p^2}{i\omega\omega_e} g J_i \right]}{1 + g^2 - g_H^2 - \frac{\omega_p^2}{i\omega\omega_e} g(1+g_H^2)} \right\} \qquad (49)$$

(b) Electrical Neutrality (axial symmetry)

$$k^2 = \frac{\omega^2}{c^2} + \frac{i\omega\omega_p^2 g}{\omega_e c^2 (1+g_H^2)} \tag{50}$$

$$A(\omega) = \frac{i\omega 4\pi e n_{e_0}}{c^2} \cdot \frac{\nu_i'}{\nu_i' - i\omega} \cdot \frac{g}{1+g_H^2} \tag{51}$$

(c) "Very unequal masses" (axial symmetry)

$$k^2 = \frac{\omega^2}{c^2} + \frac{i\omega\omega_p^2}{\omega_e c^2} \frac{m}{m_i} \frac{g_e'}{1+g_H'^2} \tag{52}$$

$$A(\omega) = \frac{i\omega 4\pi e n_{e_0}}{c^2} \frac{m}{m_i} \frac{\nu_i'}{\nu_i' - i\omega} \frac{g_e'}{1+g_H'^2} \tag{53}$$

Here we have used the notation $g_e = \frac{\omega_e}{\nu_e - i\omega}$, $g_i = \frac{\omega_i}{\nu_i - i\omega}$, $g_H = g_i g_e$, $g = g_i + g_e$, and g_e', g_i' mean that ν_e, ν_i are replaced by ν_e', ν_i' in the expressions for g_e, g_i. Also, $\omega_p^2 = 4\pi n_{eo} e^2/m_e$, $\omega_e = eB_o/m_e$, $\omega_i = eB_o/m_i$, and we denote $\omega_H = \sqrt{\omega_i \omega_e'}$ as the "hybrid" Larmor frequency.

V-4. Analysis of the Nonlinear Equations for Cylindrical Geometry

In the numerical analysis, we will be restricted to the cylindrically symmetric case except for several simple examples discussed in Section For simplicity we will again take n_N, ν_i and ν_e as constants, but here we will include the nonlinear terms in the equations.

The equations employed are Eqs. (14) to (22). We know that the equations are hyperbolic in nature and therefore that solutions may be obtained by marching forward in time. This is shown by combining Eqs. (1) to (3) to obtain:

$$\nabla(\nabla\cdot\vec{E}) - \nabla^2\vec{E} + \frac{4\pi e}{c^2}\frac{\partial}{\partial t}\left(n_i\vec{v}_i - n_e\vec{v}_e\right) + \frac{1}{c^2}\frac{\partial^2 E}{\partial t^2} = 0 \quad . \tag{66}$$

In the cylindrically symmetric case at hand, for one ion species present, this equation takes the form (for the azimuthal component):

$$\frac{\partial}{\partial r}\left(\frac{1}{r}\frac{\partial}{\partial r}(rE_\theta)\right) = \frac{4\pi e}{c^2}\frac{\partial}{\partial t}\left(n_i v_i - n_e v_e\right) + \frac{1}{c^2}\frac{\partial^2 E_\theta}{\partial t^2} \cdot \tag{67}$$

The treatment of the equations numerically is considerably different, depending on whether or not the displacement current term in Eq. (67) is neglected. To gain insight into this question, we refer to the linearized approximations studied in the preceding section. Requiring all the dependent variables to vary as $\exp(iKr - i\omega t)$ and taking the limit of large Kr, we find that the dispersion relations for the three models considered are given, respectively, by Eqs. (48), (50) and (52).

For $\omega^2 \ll \omega_H^2$, $\mathbf{k}$ is given by Eq. (62). For $\omega \gtrsim \omega_H$, and $\omega^2 \gg \nu_i \nu_e$, from (48),

$$n^2 = \frac{c^2 k^2}{\omega^2} \simeq 1 + \frac{\omega_p^2 \left(\omega_p^2 + \omega_H^2 - \omega^2 \right)}{\omega^4 - \omega^2 \left(\omega_p^2 + \omega_e^2 - \omega_H^2 \right) + \omega_H^2 \omega_p^2} \tag{68}$$

gives the index of refraction.

From Eq. (68), we see that if we use Model "a", oscillatory solutions are possible for $\omega \lesssim \omega_H$, $\omega^2 \gtrsim \omega_p^2 + \omega_e\omega_p$, and in a narrow band $\omega_p^2 - \omega_e\omega_p \lesssim \omega^2 \lesssim \omega_p^2 + \omega_e^2$. (We have used the fact that $\omega_p^2/\omega_p^2 \ll 1$.)

On the other hand, if we use the dispersion relations (50) and (52), again neglecting collisions, we obtain

$$n^2 \approx 1 + \frac{\omega_p^2}{\omega_H^2 - \omega^2} \quad . \tag{69}$$

We find oscillatory solutions for $\omega \lesssim \omega_H$ and $\omega \gtrsim \omega_p$. If the displacement current is neglected ("1" in Eqs. (68) and (69), all solutions are exponentially decaying for $\omega > \omega_H$ in Models (b) and (c) (electrically neutral plasma), although there remains a narrow band of oscillatory solutions near $\omega = \omega_p$ in Model (a).

Thus if we employ the assumption of electrical neutrality and neglect the displacement current, only the frequencies $\omega \gtrsim \omega_p$ are significantly misrepresented. Since, as we have shown in Section , phenomena of interest occur at characteristic frequencies far below ω_p, we may neglect the displacement current with very little error. For example, for $\omega \ll \omega_H$, (68) or (69) yields $n^2 \approx 5 \times 10^6$ for $n_e \approx 10^6/cm^3$ and B = 0.3 gauss (typical values in the ionosphere).

It proves very convenient to omit the displacement current in performing numerical computations. If we do so, we cannot arbitrarily specify the electric field at some initial time, but rather we must calculate it from

$$\frac{\partial}{\partial r}\left(\frac{1}{r}\frac{\partial}{\partial r}(rE_\theta)\right) = \frac{4\pi e}{c^2}\frac{\partial}{\partial t}(n_e v) \tag{70}$$

where, as in Section V-F, $v = v_i - v_e$. Setting $u_i = u_e = u$, the remaining equations are obtained by the arguments used to obtain Eq. (47). We find

$$\frac{\partial v}{\partial t} + u\frac{\partial v}{\partial r} = \frac{em}{m_i m_e}\left(E_\theta - \frac{uB}{c}\right) - \frac{uv}{r} - \nu_e' v. \qquad (71)$$

Combining Eqs. (19) and (20), and approximating the centrifugal term by

$$m_i v_i^2 + m_e v_e^2 \simeq m_i m_e v^2/m,$$

we find

$$\frac{\partial u}{\partial t} + u\frac{\partial u}{\partial r} - \frac{m_i m_e}{m^2}\frac{v^2}{r} = \frac{eB}{mc}v - \nu_i'(u - u_n). \qquad (72)$$

To close the system, we use Eqs. (14) and (18):

$$\frac{\partial B}{\partial t} = -\frac{c}{r}\frac{\partial}{\partial r}(rE_\theta), \qquad (73)$$

$$\frac{\partial n_e}{\partial t} + \frac{1}{r}\frac{\partial}{\partial r}(run_e) = 0. \qquad (74)$$

Sample Calculation

The procedure outlined in the preceding section has been incorporated into a numerical program for the evaluation of the current distribution and plasma motion induced by a cylindrical neutral wind. The principal objective is to be able to study the non-linear motion of the plasma during the early stages of the expansion of a dense cloud of gas when the collision frequencies are moderately large. We expect the maximum field disturbances to occur when the neutral ion collision frequencies are comparable to the ion cyclotron frequencies. The calculation is set up to take a neutral wind calculated in the small disturbance approximation and will evaluate the plasma motion in a parallel magnetic field under the influence of this driving force. In attempting to treat the neutral flow field corresponding to a vacuum expansion, difficulties were experienced because of the severe ion density gradients that result at the edge of the sweeping region in this situation (see Fig. III-4).

This problem has not been adequately resolved to date. A simpler but rather hypothetical situation has been treated. Here the neutral flow velocity was chosen to have a form similar to that obtained in the collisionless representation but the ion-neutral collision frequency was taken to be constant. Specifically the neutral radial velocity was assumed to have the form

$$V = (r/t)/\left(1 + e^{A(r/R_o - 1)}\right)$$

where $R_o = V_o t$ and A is typically a number between 5 and 10. Typical results are shown in Figures V-3 to V-6. In this example the calculation was started after the neutral flow had reached a certain size (i.e., the interaction

between the ions and the neutrals was switched on suddenly after the neutral flow had developed). The current distribution and electric and magnetic fields undergo a transient stage as the quasi-steady solution is approached. This sudden transient motion generates an Alfvén wave which propagates away from the source of the disturbance as a compression pulse in the magnetic field. (See Figure V-3.) Of course this pulse is solely due to the switching on of the interaction and has no real physical counterpart.

Relationship of Present Model to General Ohm's Law

Neglecting pressure gradients, we may write the electron and ion momentum equations (6) and (7), employing (10), as follows:

$$\dot{\vec{V}}_i = \frac{e}{m_i}\left(\vec{E} + \frac{\vec{V}_i \times \vec{B}}{c}\right) + \nu_i\,(\vec{V}_N - \vec{V}_i) \tag{75}$$

$$\dot{\vec{V}}_e = -\frac{e}{m_e}\left(\vec{E} + \frac{\vec{V}_e \times \vec{B}}{c}\right) + \nu_e\,(\vec{V}_N - \vec{V}_e) \tag{76}$$

In the steady uniform state, the left-hand sides of the above equations vanish. It is simple to show that the remaining terms lead to the customary steady-state Ohm's Law for a weakly ionized gas, including Hall effect and ion slip. To do this, we introduce the notation:

$$\begin{aligned} m\vec{u} &= m_i \vec{V}_i + m_e \vec{V}_e \\ \vec{v} &= \vec{V}_i - \vec{V}_e \\ m &= m_i + m_e \\ m\nu_1 &= m_i \nu_i + m_e \nu_e \\ m\nu_2 &= m_i \nu_e + m_e \nu_i \end{aligned} \tag{77}$$

Equations (75) and (76) may be written (with d/dt = 0):

$$\frac{e}{c}\vec{v}\times\vec{B} + m\nu_1(\vec{V}_N - \vec{u}) + (\nu_e - \nu_i)\frac{m_e m_i}{m}\vec{v} = 0 \tag{78}$$

$$-\nu_2\vec{v} + \frac{e m \vec{E}}{m_i m_e} + (\nu_i - \nu_e)(\vec{V}_N - \vec{u}) + \frac{e m}{m_i m_e}\frac{\vec{u}\times\vec{B}}{c} + \frac{e(m_i - m_e)}{m_e m_i}\frac{\vec{J}\times\vec{v}}{c} = 0 \tag{79}$$

Noting that $\vec{J} = en_e\vec{V}/c$, and substituting for $\vec{v}$ in (79) from (78) (80)

as a function of $\vec{V}$ and $\vec{V}_N$, we obtain

$$\vec{J} = \frac{e^2 m n_e}{\alpha m_i m_e c}\left(\vec{E} + \frac{\vec{V}_N \times \vec{B}}{c}\right) + \beta\,\vec{J}\times\vec{B} + \frac{e^2(\vec{J}\times\vec{B})\times\vec{B}}{\alpha\nu_1 m_i m_e c^2} \tag{90}$$

where

$$\alpha = \nu_2 - (\nu_e - \nu_i)^2 m_i m_e / \nu_1 m^2 \simeq \nu_e,$$

$$\beta = \frac{c}{\alpha m c}\left(\frac{2(\nu_e - \nu_i)}{\nu_1} - \frac{m_i}{m_e} + \frac{m_e}{m_i}\right).$$

This is completely equivalent to the well-known result (e.g., Ref. 11, appendix), where the result is given as

$$\vec{j} = \sigma\left[\vec{E} + \frac{\vec{v}_N \times \vec{B}}{c} - \varkappa \vec{j} \times \vec{B} + \lambda(\vec{j} \times \vec{B}) \times \vec{B}\right] \tag{91}$$

and, to dominant terms (and using our own notation),

$$\sigma \simeq \frac{e^2 n_e}{m_e \nu_e c}, \quad \varkappa = \frac{1}{e n_e}, \quad \lambda = \frac{1}{\nu_i n_i m_i c}. \tag{92}$$

The following useful expressions for the particle drift velocities in the steady uniform state are obtained from (75) and (76) in the same manner, with subscripts $\parallel$ and $\perp$ referring to components parallel and perpendicular to $\vec{B}_o$:

$$\vec{v}_{i\parallel} = \vec{v}_{e\parallel} = \vec{v}_{N\parallel}, \tag{93}$$

$$\vec{v}_{i\perp} = \frac{\left[\nu_i^2 \vec{v}_{N\perp} + \nu_i \omega_i \left[\frac{c\vec{E}}{B} + \frac{\vec{v}_N \times \vec{B}}{B}\right] + \omega_i^2 \frac{c\vec{E} \times \vec{B}}{B^2}\right]}{\left[\nu_i^2 + \omega_i^2\right]}, \tag{94}$$

$$\vec{v}_{e\perp} = \frac{\nu_e^2 \vec{v}_{N\perp} - \nu_e \omega_e \left[\frac{c\vec{E}}{B} + \frac{\vec{v}_N \times \vec{B}}{B}\right] + \omega_e^2 \frac{c\vec{E} \times \vec{B}}{B^2}}{\left[\nu_e^2 + \omega_e^2\right]}. \tag{95}$$

It is usually convenient to rewrite Equation (91) in terms of the Hall and Pedersen conductivities, σ_H and σ_p. Here

$$\vec{j} = \sigma_p\left(\vec{E}_\perp + \frac{\vec{v}_N \times \vec{B}}{c}\right) - \sigma_H\left(\vec{E}_\perp + \frac{\vec{v}_N \times \vec{B}}{c}\right) \times \frac{\vec{B}}{B} + \sigma_\parallel \vec{E}_\parallel \tag{96}$$

where the conductivities are given by

$$\sigma_p = \frac{\sigma\left(1+\sigma\lambda B^2\right)}{\left(1+\sigma\lambda B^2\right)^2+(\mu\sigma B)^2}\,, \tag{97}$$

$$\sigma_H = \frac{\mu B \sigma^2}{\left(1+\sigma\lambda B^2\right)^2+(\mu\sigma B)^2}\,,$$

$$\sigma_{\parallel} = \sigma\,.$$

V-5. Numerical Values of Cross Sections and Collision Frequencies

We consider first the encounters between ions and neutrals. Following Dalgarno,[2] the interaction potential at large separations is

$$\phi(r) = -\tfrac{1}{2}\alpha e^2/r^4 \tag{1}$$

and the corresponding momentum-exchange cross section, defined by Eq. (9), is

$$\sigma_m = 2.21\pi\left(\alpha e^2/\mu V^2\right)^{1/2} \tag{2}$$

where α is the polarizability of the neutral atom, $\mu = m_i m_a (m_i + m_a)^{-1}$ is the reduced mass, and V is the relative speed of the ion and neutral particle. The collision frequency is thus independent of temperature or relative velocity:

$$\nu_{ia} = 2.21\pi n_a \left(\alpha e^2/\mu\right)^{1/2}. \tag{3}$$

At the lower altitudes of interest, say 150 km, the ions and neutrals are mostly diatomic.[7] Taking them to be N_2, O_2, N_2^+, O_2^+ and NO^+, the reduced mass and polarizability vary only slightly between the various possible ion-neutral pairs, and we find

$$\nu_{ia} \simeq 4\times10^{-10} n_a \ \text{sec}^{-1} \quad \text{[diatomic molecules and ions]} \tag{4}$$

where n_a is now the total number density of neutrals, and we have used $\alpha = 1.5 \times 10^{-24}$ cm^3.

At the higher altitudes of interest, say 300 km, the ions and neutrals are mostly monatomic:[7] N, O, N^+, O^+ (mostly O and O^+). Again $\mu^{1/2}$ and α are very insensitive to the choice of pairs, and we find

$$\nu_{ia} \simeq 5.6\times10^{-10} n_a \ \text{sec}^{-1} \quad \text{[monatomic molecules and ions]} \tag{5}$$

Since V is in the range 1 to 5 km/sec, we are dealing with cross sections of the order of 2 to 6 × 10^{-15} cm^2.

There is in addition an effective momentum exchange between ions and neutrals brought about by charge exchange. This is much more complicated, inasmuch as there is often an exchange between unlike particles. However, exchange between unlike particles appears to be unimportant for the following reasons.

Following the discussion by Hasted[8], σ_c is a maximum when the relative velocity corresponds roughly to resonance:

$$V_{res} \simeq a|\Delta E|\hbar^{-1} \qquad (6)$$

where the length parameter $a \approx 7 \times 10^{-8}$ cm and ΔE is the energy difference between the two ionization states. For $V \ll V_{res}$, σ_c obeys approximately the relation

$$\sigma_c \simeq \sigma_c(max) \exp(-a|\Delta E|/4\hbar V) \qquad (7)$$

where $\sigma_c(max)$ is usually of the order of 10^{-14} cm^2.

For the species N, O, N_2, O_2, NO, there are ten possible different charge-exchange reactions involving unlike particles (each reaction is two-way). The largest $|\Delta E|$ is 6eV, for (NO^+, N_2) or (NO, N_2^+), and the smallest $|\Delta E|$ is 0.65 eV, for (O^+, N_2) or (O, N_2^+). Thus the smallest resonance-velocity V_{res} is that for 0.65 eV, which is 1.2×10^7 cm/sec. We consider only velocities of at most several km/sec, which by (7) lead to σ_c several orders of magnitude lower than σ_m, for unlike particles.

For charge-exchange interaction between an ion and a parent molecule, $V_{res} = 0$. The only such interaction we need consider is (O, O^+), since they are the only like-pair in which the ion and molecule are both dominant in the total number density of ions and molecules respectively, this occurring

above roughly 180 km.[7] The experimental measurements of Stebbings, Smith and Erhardt[9] indicate that the following empirical formula holds from about 0.1 eV to 10^{3} eV:

$$\sigma_c^{1/2} = \left[5.95 \times 10^{-8} - 0.63 \times 10^{-8} \log_{10} \mathcal{E}\right] \text{ cm} \qquad (8)$$

where $\mathcal{E}$ is the energy of the primary particle in eV. For $V = 10^5$ cm/sec (0.08 eV), $\sigma_c \approx 4 \times 10^{-15}$ cm^2 (to within probably a factor of 3).

For the sample calculations, which are performed for the vicinity of 200 km, we therefore take

$$\begin{aligned} \nu_i &\leq \times 10^{-10} n_a \\ &\leq \text{sec}^{-1}. \end{aligned} \qquad (9)$$

Electron-neutral momentum exchange cross sections may be obtained from the tables of Ref. 5 which indicate that the cross sections at relevant energies are all of the order 10^{-15} cm^2. Thus ν_e is of the order $(m_i/m_e)^{1/2}\ \nu_i$ for equilibrium and $\nu_e \sim \nu_i$ for cold electrons and ions moving relative to the neutrals. The same result is obtained if one employs the model of Moiseiwitsch[10], which is equivalent to Eqs. (1) to (3) for the low energies under consideration. Again we obtain, independently of considerations of temperature or relative velocities:

$$\nu_{en} \simeq (m_i/2m_e)^{1/2} \nu_i \qquad (10)$$

or

$$\begin{aligned} \nu_{en} &\simeq 10^{-6} n_a \\ &= 10^{3} \text{ sec}^{-1} \text{ at 200km}. \end{aligned}$$

1. Chapman, S., and T. Cowling, Mathematical Theory of Nonuniform Gases, Cambridge University Press, 1939.

2. Dalgarno, A., in Atomic and Molecular Processes, (Bates, ed.) Academic Press, 1962 (p. 622).

3. Zhdanov, V. M., PMM 26, 280 (1962), English translation: Appl. Math. and Mech. 26, 401 (1962).

4. Spitzer, L., Jr, Physics of Fully Ionized Gases, Interscience, 1956.

5. Hochstim, A. R., Institute for Defense Analyses, Research Paper P-124, Feb. 1965 (see data in Table III).

6. Morse, P. M., and H. Feshbach, Methods of Theoretical Physics, McGraw-Hill Book Co., 1953 (p. 530).

7. Johnson, F. S., Satellite Environment Handbook, Stanford University Press, 1961 (Chapters 1 and 2).

8. Hasted, J. B., in Atomic and Molecular Processes, (Bates, ed.), Academic Press, 1962 (p. 696).

9. Stebbings, Smith, Erhardt, in Atomic Collision Processes (McDowell, ed.) J. Wiley and Sons, 1964 (p. 814).

10. Moiseiwitsch, B. L., in Atomic and Molecular Processes, (Bates, ed.), Academic Press, 1962 (p. 281).

11. Kemp, N., and H. Petschek, J. Fluid Mech. 4, 553 (1958).

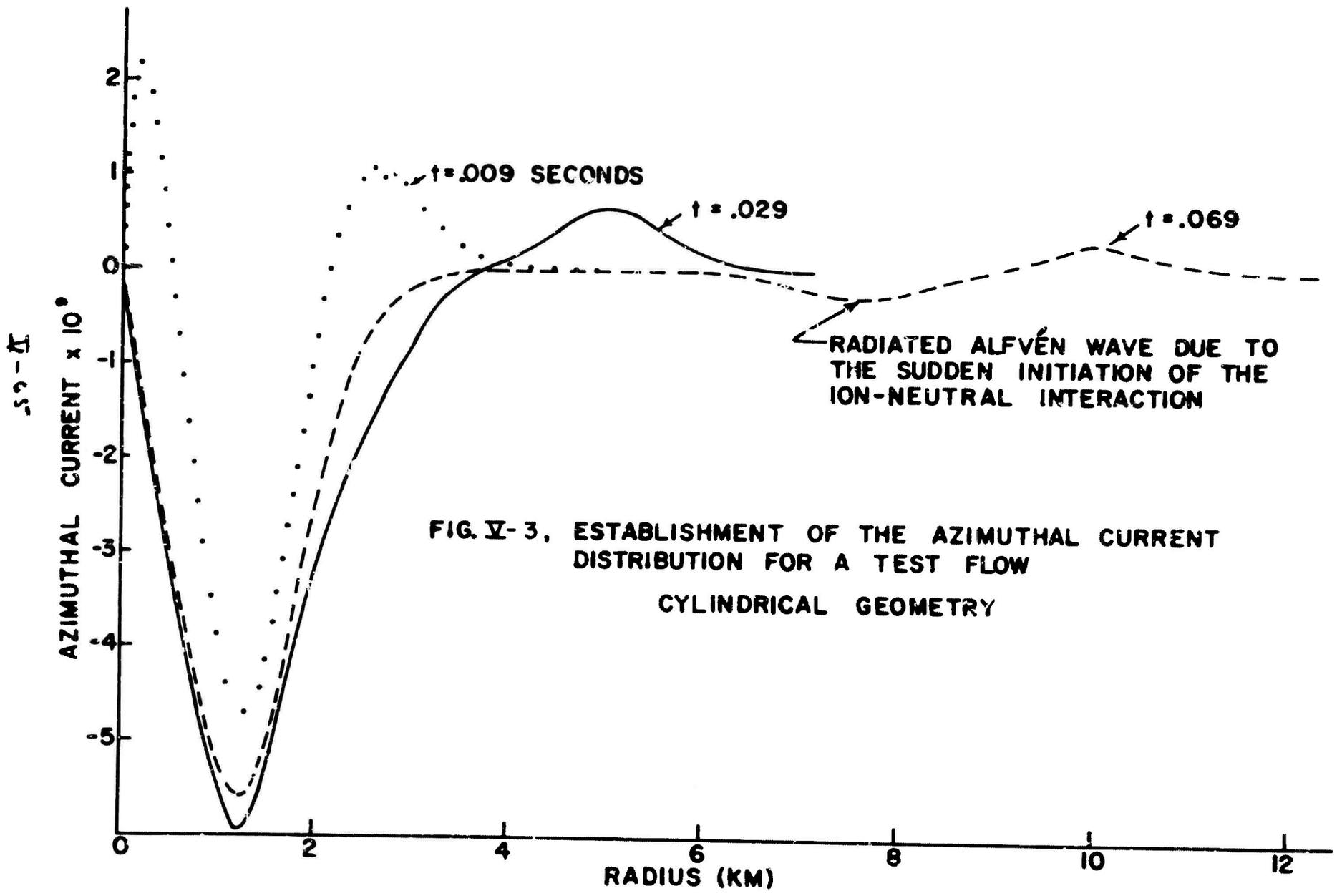

FIG. V-3, ESTABLISHMENT OF THE AZIMUTHAL CURRENT DISTRIBUTION FOR A TEST FLOW

CYLINDRICAL GEOMETRY

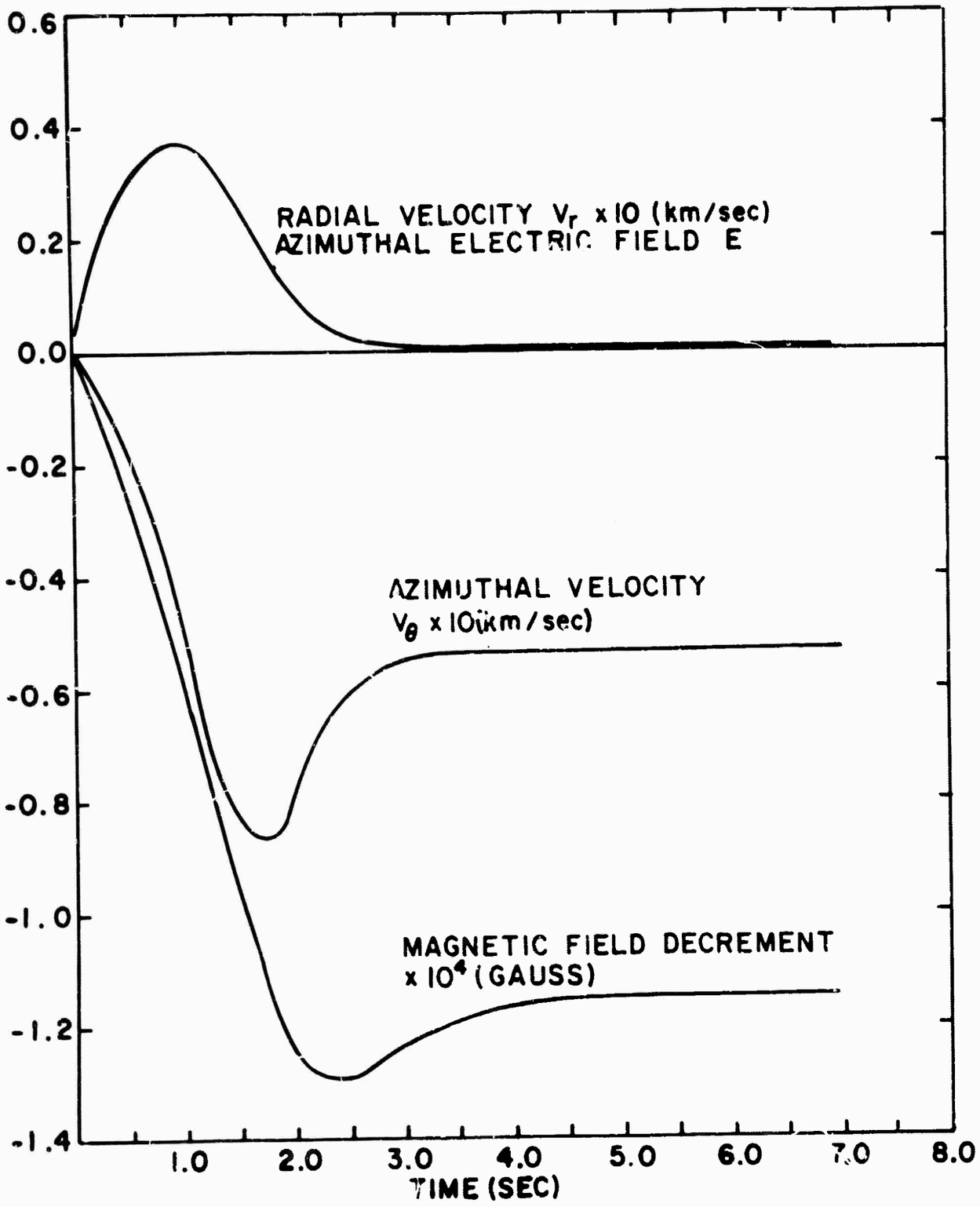

FIG. V-4, TIME HISTORIES AT R = 1 km

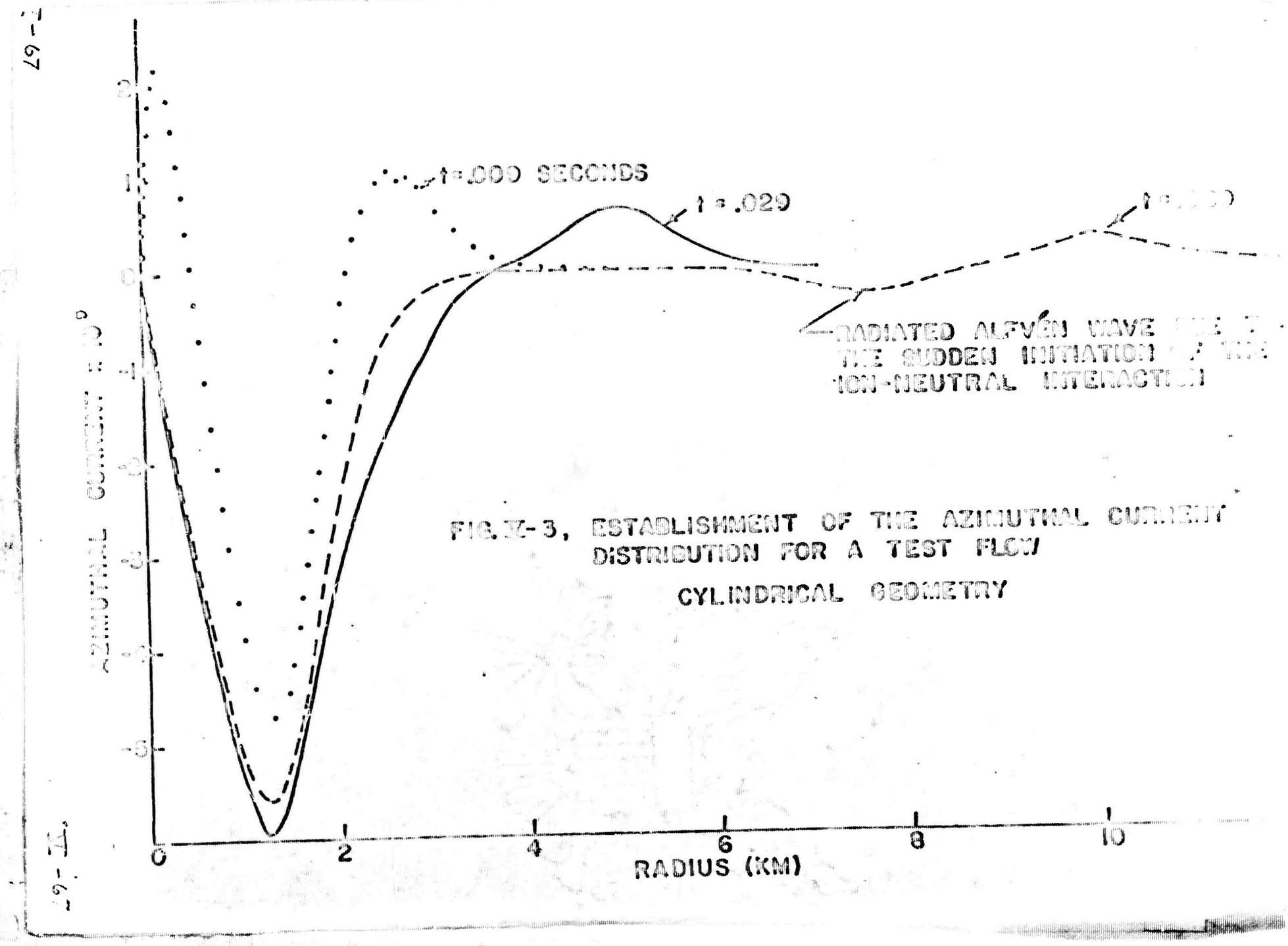

FIG. IV-3, ESTABLISHMENT OF THE AZIMUTHAL CURRENT DISTRIBUTION FOR A TEST FLOW

CYLINDRICAL GEOMETRY

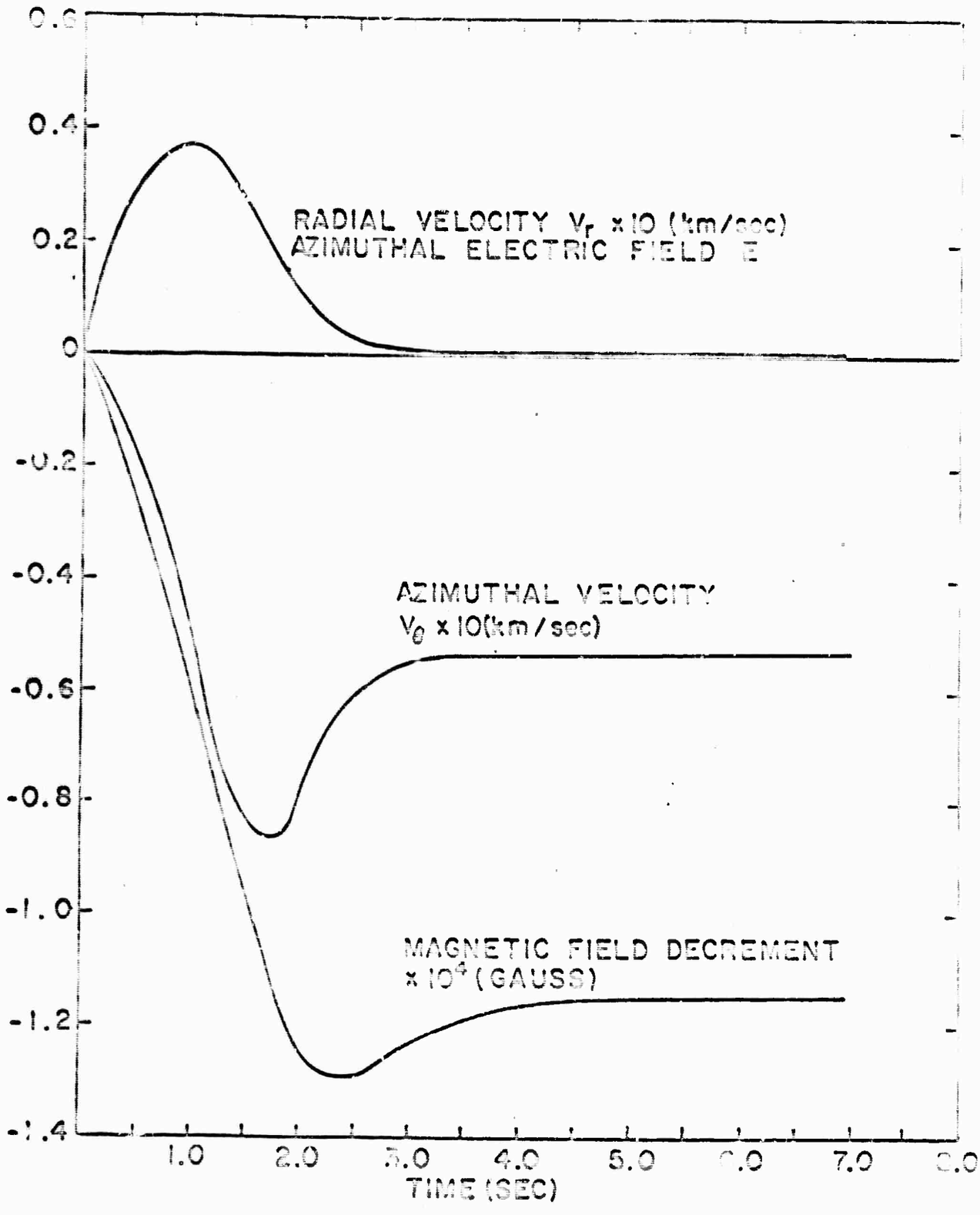

FIG. IV-4 TIME HISTORIES AT R = 1 km

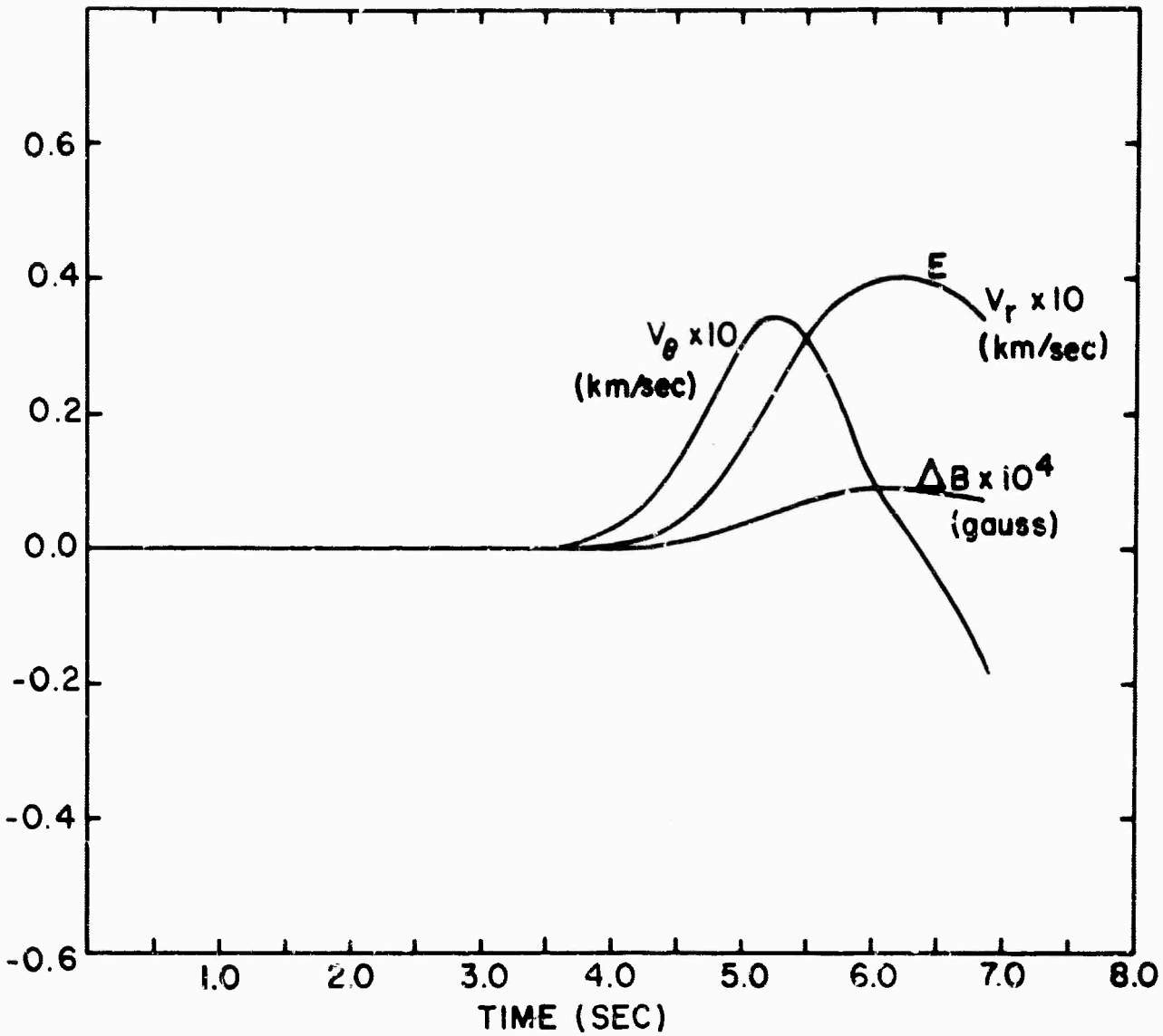

FIG. V-6 TIME HISTORIES AT R = 8 km

END